Fakultät für Informatik
Technische Universität München

Deep Learning for Fast and Robust Multiparametric Magnetic Resonance Imaging

Carolin Martha Anna Pirkl

Vollständiger Abdruck der von der Fakultät für Informatik der Technischen Universität München zur Erlangung des akademischen Grades einer

Doktorin der Naturwissenschaften (Dr. rer. nat.)

genehmigten Dissertation.

Vorsitzende:
Prof. Dr. Julia Schnabel

Prüfende der Dissertation:
1. Prof. Dr. Bjoern H. Menze
2. Priv.-Doz. Dr. Marion I. Menzel
3. Prof. Dr. Jan S. Kirschke

Die Dissertation wurde am 22.06.2021 bei der Technischen Universität München eingereicht und durch die Fakultät für Informatik am 13.09.2021 angenommen.

DEEP LEARNING FOR FAST AND ROBUST MULTIPARAMETRIC MAGNETIC RESONANCE IMAGING

CAROLIN MARTHA ANNA PIRKL

Meiner Familie

ABSTRACT

Magnetic Resonance Imaging (MRI) has become one of the prevailing imaging modalities in modern radiology. As it is capable of non-invasively providing a multitude of comprehensive anatomical and physiological information, MRI is essential for diagnosis, guides treatment planning and is the method of choice for therapy follow-up. Despite its great versatility, MRI is an inherently slow technique - a problem that scales in quantitative methods, where multiple MRI acquisitions are required for parameter encoding. Although these techniques have great potential for comprehensive tissue and hence disease characterization, the long scan times are the main challenge that prevents them from being widely adopted into clinical routine. Also, with prolonged acquisitions, MRI scans become more susceptible to motion artifacts, which constitutes another major problem of clinical MRI.

This work aims at developing Deep Learning (DL) methods for fast and robust multiparametric MRI. It builds on the recent breakthrough of Machine Learning (ML) in general and DL in particular to meet the practical needs on the way to a broad clinical deployment of quantitative MRI biomarkers. Taking advantage of physics-informed Neural Network (NN) concepts, the core of this thesis is to present methodological advances all along the MRI pipeline. To this end, a highly accelerated MRI acquisition that simultaneously encodes for multiple physiological parameters is combined with advanced image reconstruction and multiparameter inference to solve the underlying multivariate regression task. With the goal to improve clinical acceptance of quantitative MRI techniques, feasibility and potential benefits of the proposed multiparametric acquisition and reconstruction frameworks are validated and initial clinical experience with glioma and multiple sclerosis patients is demonstrated.

ZUSAMMENFASSUNG

Die Magnetresonanztomographie (MRT) hat sich zu einer der vorherrschenden Bildgebungsmodalitäten in der modernen Radiologie entwickelt. Da sie auf nicht-invasive Weise eine Vielzahl aussagekräftiger anatomischer und physiologischer Informationen zur Verfügung stellen kann, ist die MRT für die Diagnostik unverzichtbar, ist Grundlage für die Behandlungsplanung und ist die Methode der Wahl zur Therapiekontrolle. Trotz ihrer enormen Vielseitigkeit ist die MRT allerdings auch eine von Natur aus langsame Technik - ein Problem, das sich bei quantitativen Methoden, bei denen mehrere MRT-Akquisitionen für die Parameterkodierung erforderlich sind, verstärkt. Die langen Akquisitionszeiten sind die größte Herausforderung, die verhindert, dass diese Techniken trotz ihres großen Potenzials für eine umfassende Charakterisierung von Gewebe und somit auch von Krankheitsbildern breitflächig in die klinische Routine übernommen werden. Außerdem werden die MRT Aufnahmen bei längeren Akquisitionen anfälliger für Bewegungsartefakte, was ein weiteres schwerwiegendes Problem der klinischen MRT darstellt.

Ziel dieser Arbeit ist es Deep Learning (DL) Methoden für schnelle und robuste multiparametrischen MRT zu entwickeln. Die vorliegende Dissertation baut auf dem jüngsten Durchbruch des Maschinellen Lernens (ML) im Allgemeinen und des DLs im Besonderen auf, um die praktischen Anforderungen auf dem Weg zu einer breiten klinischen Anwendung von quantitativen MRT-Biomarkern zu erfüllen. Unter Nutzung der Vorteile von Physik-informierten Konzepten Neuronaler Netzwerke besteht der Kern dieser Arbeit darin, methodische Fortschritte entlang des gesamten MRT Bildgebungsprozesses zu präsentieren. Zu diesem Zweck wird eine hochbeschleunigte MRT-Akquisition, die mehrere physiologische Parameter gleichzeitig kodiert, mit einer leistungsstarken Bildrekonstruktion und Multiparameter-Schätzung kombiniert, um die zugrunde liegende multivariate Regression zu lösen. Mit dem Ziel, die klinische Akzeptanz quantitativer MRT-Techniken zu verbessern, werden Machbarkeit und potenzielle Vorteile der vorgeschlagenen multiparametrischen Ansätze für Akquisition und Rekonstruktion validiert und erste klinische Erfahrungen mit Gliom- und Multiple Sklerose-Patienten demonstriert.

PUBLICATIONS

This publication-based thesis is based on the following relevant first-author publications, which are included in their original form.

PEER-REVIEWED JOURNAL AND CONFERENCE PAPERS

1. **CM. Pirkl***, PA. Gómez*, I. Lipp, G. Buonincontri, M. Molina-Romero, A. Sekuboyina, D. Waldmannstetter, J. Dannenberg, S. Endt, A. Merola, JR. Whittaker, V. Tomassini, M. Tosetti, DK. Jones, BH. Menze†, MI. Menzel†. "Deep learning-based parameter mapping for joint relaxation and diffusion tensor MR Fingerprinting". In: *Proceedings of the Third Conference on Medical Imaging with Deep Learning*. PMLR, Vol. 121, Sept. 2020, pp.638–654. [1]

2. **CM. Pirkl**, L. Nunez-Gonzalez, F. Kofler, S. Endt, L. Grundl, M. Golbabaee, PA. Gómez, M. Cencini, G. Buonincontri, RF. Schulte, M. Smits, B. Wiestler, BH. Menze†, MI. Menzel†, JA. Hernandez-Tamames†. "Accelerated 3D whole-brain T1, T2 and proton density mapping: feasibility for clinical glioma MR imaging". In: *Neuroradiology* (Apr.2021). [2]

3. **CM. Pirkl**, M. Cencini, JW. Kurzawski, D. Waldmannstetter, H. Li, A. Sekuboyina, S. Endt, L. Peretti, G. Donatelli, R. Pasquariello, M. Costagli, G. Buonincontri, M. Tosetti, MI. Menzel†, BH. Menze†. "Residual learning for 3D motion corrected quantitative MRI: Robust clinical T1, T2 and proton density mapping". In press: *Proceedings of the Forth Conference on Medical Imaging with Deep Learning*. PMLR. [3]

*Contributed equally
†Contributed equally

In addition to these relevant first-author journal and conference papers, the appendix of this thesis includes the following peer-reviewed first-author conference abstracts.

PEER-REVIEWED CONFERENCE ABSTRACTS

1. **CM. Pirkl**, I. Lipp, G. Buonincontri, M. Molina-Romero, A. Sekuboyina, D. Waldmannstetter, J. Dannenberg, V. Tomassini, M. Tosetti, DK. Jones, MI. Menzel, BH. Menze, PA. Gómez. "Deep

learning-enabled diffusion tensor MR Fingerprinting". In: *Proceedings of the 27th Annual Meeting of the International Society for Magnetic Resonance in Medicine (ISMRM)*. Montréal, QC, Canada, 2019. [4]

2. **CM. Pirkl**, L. Nuñez-Gonzalez, S. Endt, G. Buonincontri, RF. Schulte, PA. Gómez, M. Smits, BH. Menze, MI. Menzel, JA. Hernandez-Tamames. "Accelerated 3D multiparametric MRI in glioma patients - Initial clinical experience". In: *Proceedings of the 28th Annual Meeting of the International Society for Magnetic Resonance in Medicine (ISMRM)*. 2020. [5]

3. **CM. Pirkl**, I. Horvath, S. Endt, G. Buonincontri, MI. Menzel, PA. Gómez, BH. Menze. "Synchronizing dimension reduction and parameter inference in 3D multiparametric MRI: A hybrid neural network approach". In: *Proceedings of the 28th Annual Meeting of the International Society for Magnetic Resonance in Medicine (ISMRM)*. 2020. [6]

Besides the first-author publications listed above, the following peer-reviewed journal papers and conference abstracts have been published during the course of this doctoral thesis but are not included in this dissertation.

PEER-REVIEWED JOURNAL PAPERS

1. PA. Gómez, M. Cencini, M. Golbabaee, RF. Schulte, **C. Pirkl**, I. Horvath, G. Fallo, L. Peretti, M. Tosetti, BH. Menze, G. Buonincontri. "Rapid three-dimensional multiparametric MRI with quantitative transient-state imaging". In: *Scientific Reports* 10.1 (Aug. 2020), p.13769. [7]

2. M. Golbabaee, G. Buonincontri, **CM. Pirkl**, MI. Menzel, BH. Menze, M. Davis, PA. Gómez. "Compressive MRI quantification using convex spatiotemporal priors and deep encoder-decoder networks". In: *Medical Image Analysis* 69 (Apr. 2021), p. 101945. [8]

PEER-REVIEWED CONFERENCE ABSTRACTS

1. M. Golbabaee, **CM. Pirkl**, MI. Menzel, G. Buonincontri, PA. Gómez. "Deep MR Fingerprinting with total-variation and low-rank subspace priors". In: *Proceedings of the 27th Annual Meeting of the International Society for Magnetic Resonance in Medi-cine (ISMRM)*. Montréal, QC, Canada, 2019. [9]

2. C. Hecking-Veltman, **CM. Pirkl**, J. Dannenberg, RF. Schulte, T. Sprenger, BH. Menze, MI. Menzel. "Estimation and Correction of Image Phase in diffusion weighted MRI using Deep Learning". In: *Proceedings of the 27th Annual Meeting of the International Society for Magnetic Resonance in Medicine (ISMRM)*. Montréal, QC, Canada, 2019. [10]

3. N. Andriamanga, **CM. Pirkl**, A. Sekuboyina, G. Buonincontri, MI. Menzel, PA. Gómez, M. Piraud, BH. Menze. "Long Short Term Memory Recurrent Neural Network for MR Fingerprinting parameter estimation". In: *Proceedings of the 36th Annual Scientific Meeting of the European Society for Magnetic Resonance in Medicine and Biology (ESMRMB)*. Rotterdam, Netherlands, 2019. [11]

4. I. Horvath, **CM. Pirkl**, G. Buonincontri, MI. Menzel, PA. Gómez, BH. Menze. "Deep learning for 3D MR fingerprinting: a dual pathway parameter mapping and reconstruction approach". In: *Proceedings of the 36th Annual Scientific Meeting of the European Society for Magnetic Resonance in Medicine and Biology (ESMRMB)*. Rotterdam, Netherlands, 2019. [12]

5. S. Endt, **CM. Pirkl**, CM. Verdun, BH. Menze, MI. Menzel. "A deep-learning approach to accelerated T1-T2-relaxation-correlation imaging". In: *Proceedings of the 37th Annual Scientific Meeting of the European Society for Magnetic Resonance in Medicine and Biology (ESMRMB)*. 2020. [13]

6. F. Wiesinger, G. McKinnon, S. Kaushik, AB. Solana, E. Ljungberg, M. Vogel, N. Takei, R. Schulte, **C. Pirkl**, C. Cozzini, L. Nuñez-Gonzalez, JA. Hernandez Tamames, M. Engström. "3D Silent Parameter Mapping: Further refinements & quantitative assessment". In: *Proceedings of the 29th Annual Meeting of the International Society for Magnetic Resonance in Medicine (ISMRM)*. 2021. [14]

ACKNOWLEDGMENTS

I am deeply thankful to all who have contributed to the success of this thesis and supported me over the past years.

First, I want to express my sincere gratitude to my first supervisor Prof. Dr. Bjoern Menze. Thank you for all your inspiration, guidance and all the freedom that made me go beyond my limits. In the same way, I am sincerely grateful to my second supervisor Priv.-Doz. Dr. Marion Menzel. You have been an exceptional and passionate Doktormutter, guiding me to grow not only scientifically but also personally. To Dr. Timo Schirmer, thank you for being a true mentor, for all your feedback, guidance and support. I thank Prof. Dr. Jan Kirschke who guided me over the past years in his role as project team leader of the RadioTumor project and is now acting as an examiner of this dissertation. I also thank Prof. Dr. Julia Schnabel for acting as a chairman during the thesis defense.

A huge thank you goes to all my (post-) doctoral fellows - from **A**mir, Anjany, Bea, Bran, Cadgas, Claudio, Dhritiman, Diana, Eduardo, Fernando, Florian, Giles, Ivan, Izabela, Jana, Johannes, John, Jonathan, Judith, Lina, Marie, Markus, Miguel, Oliver, Pedro, Rami, Rami, Sandeep, Sebastian, Supro, Teresa, Timo, Xiaobin, Yu to **Y**usuf. Thank you for the great work atmosphere in this multicultural environment, for making the last years an unforgettable experience and for becoming great friends. A special thanks to all of you who accompanied me through all the fascinations and challenges of MRI and/or helped me kicking off my exciting dive into the field of DL. To Carolin, Izabela and Niry for giving me the opportunity to supervise their Bachelor and Master theses. Thanks for your great work and the wonderful experience along the way.

To my colleagues at GE, thank you for all your support, the stimulating discussions and for sharing your experience but also your enthusiasm for MRI with me. I am very grateful to be a part of your team, for the opportunity to work with and to learn from you.

Also, I would like express my sincere acknowledgement to all my coauthors and collaborators in Munich, Italy, the Netherlands, the UK and the US who made this truly interdisciplinary work possible. I also acknowledge my funding sources: the Deutsche Forschungsgemeinschaft (DFG) through TUM International Graduate School of Science and Engineering (IGSSE), GSC 81, and the European Union's Horizon 2020 research and innovation programme under grant agreement number 952172.

Finally, to my family, for all your unconditional and unwavering support and trust. This thesis is dedicated to you.

CONTENTS

ACRONYMS

ANN	Artificial Neural Network
AD	Axial Diffusivity
ADC	Apparent Diffusion Coefficient
CNN	Convolutional Neural Network
CS	Compressed Sensing
CT	X-ray computed tomography
DL	Deep Learning
EPI	Echo-planar Imaging
EPG	Extended Phase Graphs
FID	Free Induction Decay
FFT	Fast Fourier Transform
FLAIR	Fluid-Attenuated Inversion Recovery
FA	Fractional Anisotropy
GRAPPA	Generalized Autocalibrating Partial Parallel Acquisition
MRI	Magnetic Resonance Imaging
MRF	Magnetic Resonance Fingerprinting
ML	Maximum Likelihood
MLP	Multi-Layer Perceptron
MD	Mean Diffusivity
MR-STAT	Magnetic Resonance Spin TomogrAphy in Time-domain
ML	Machine Learning
MR	Magnetic Resonance
NMR	Nuclear Magnetic Resonance
NN	Neural Network
NUFFT	Non-uniform Fast Fourier Transform
PI	Parallel Imaging
PD	Proton Density
PET	Positron Emission Tomography
QTI	Quantitative Transient-state Imaging
RD	Radial Diffusivity
ReLU	Rectified Linear Unit

RF	Radiofrequency
SENSE	Sensitivity Encoding
SNR	Signal to Noise Ratio
SSFP	Steady-state Free Precession
SPECT	Single-Photon Emission Computed Tomography
TI	Inversion Time
TE	Echo Time
TR	Repetition Time

Part I

INTRODUCTION AND SUMMARY OF CONTRIBUTIONS

1 INTRODUCTION

Since Lauterbur [15], Mansfield [16], Damadian [17] and Ernst [18] laid the basis for MRI in the early 1970s, it has emerged as a powerful imaging modality and now plays a major role in the detection and diagnosis of a wide variety of medical conditions in modern radiology [19]. In contrast to X-ray computed tomography (CT) [20, 21], Single-Photon Emission Computed Tomography (SPECT) [22] or Positron Emission Tomography (PET) [23], MRI does not involve ionizing radiation, but exploits the Nuclear Magnetic Resonance (NMR) effect. This makes it the diagnostic method of choice in many clinical applications - from diagnosis, treatment planning to monitoring of therapy response [24]. The great versatility of MRI is in turn attributed to the intrinsic sensitivity of the NMR signal to the wide range of physico-chemical interactions, including relaxation [25, 26], motion such as perfusion [27] or self-diffusion [28, 29], or chemical exchange [30, 31]. Therefore, MRI does not only provide comprehensive anatomical information but also enables imaging of various physiological processes of tissue function that goes beyond morphological imaging alone. As such, MRI represents a mainstay of personalized medicine, a concept that aims to tailor medical therapy decisions to each individual patient [32, 33].

Although in theory the fundamental concept of NMR allows for measuring any of these physico-chemical tissue properties in a *quantitative* sense [34], modern clinical practice is dominated by *qualitative* MRI. The basic principle of qualitative or contrast-weighted MRI is to generate images that are weighted by NMR relaxation times, Proton Density (PD) or other tissue properties, creating contrast differences between individual tissue types [35]. This gives rise to the generation of a multitude of differential contrast-weighted acquisitions.

Despite its superior soft-tissue contrast that is instrumental in the widespread usage of MRI, the potential of quantitative MRI for tissue and hence disease characterization is underutilized in state-of-the-art routine imaging practice. The predominantly qualitative nature of current clinical MRI protocols - not only in terms of MRI image generation, but also with respect to interpretation and analysis - limits its reliability and reproducibility due to dependence on a variety of confounds, e.g. the specific set of acquisition parameters. This is in clear contradiction to the overall strive for precision medicine and personalized treatment. Aiming for objective disease detection and characterization, e.g. to reveal spatial heterogeneity in tumors, quantitative MRI is therefore a previously not fully exhausted opportunity on the

way to accurate, reproducible and standardized imaging biomarkers for clinical decision making as well as for valid comparison across multiple time-points, subjects or sites [36].

The main challenge that prevents quantitative MRI techniques from being widely adopted into clinical routine is that MRI image acquisition is an inherently slow process. For quantitative tissue property mapping, this drawback is particularly problematic as multiple MRI acquisitions are required for encoding the parameters of interest in addition to the spatial encoding. The resulting long scan times of quantitative MRI techniques are a main barrier for routine clinical practice [37]. Also, with prolonged acquisitions, these techniques become more susceptible to voluntary and involuntary motion. This further complicates clinical application especially in children, elderly and severely ill patients who have difficulty lying still.

With the goal of accelerating MRI, significant technical advances on both hardware and computation side have entered the field over the recent years. Key technologies such as Parallel Imaging (PI) [38], sparsity-based reconstruction techniques [39], including Compressed Sensing (CS) [40], and more recently also the breakthrough of ML and specifically DL methods [41] made MRI to evolve towards shorter scan times, whilst simultaneously targeting higher image qualities. As such, these advancements have great potential to also pave the way towards quantitative MRI that is feasible for widespread use in clinical routine [42].

Still, the high degree of acceleration, which can now be achieved, usually comes at the expense of spatially undersampled k-space information. Although advanced reconstruction and parameter estimation algorithms have proven capable of compensating for this in a variety of applications, they are computationally intensive and oftentimes result in clinically infeasible reconstruction times. In spite of the ongoing research efforts to progress from single parameter to more efficient multiparameter encoding strategies, state-of-the-art quantitative MRI methods are still confined to only a small number of parameters, e.g. T_1 and T_2 relaxation times. In addition, susceptibility to motion artifacts remains a complex and only partially solved problem for MRI in general and for quantitative mapping methods in particular. Despite its great diagnostic potential, these practical limitations, which have not been adequately resolved yet, have hampered broad clinical adoption to date. In view of the tremendous success that DL methods have demonstrated in various fields, including medical imaging and specifically MRI, they can significantly contribute to address these practical limitations of quantitative MRI research to eventually bring its broad clinical translation forward.

Therefore, the main objective of this thesis is to develop fast and robust multiparametric MRI by taking advantage of DL concepts. In particular, this thesis presents DL-driven methodological contributions

starting with an efficient quantification of T_1, T_2 and PD, which in turn enables the synthesis of contrast-weighted MRI images, through the extension of multiparametric encoding beyond T_1 and T_2 to diffusion tensor information to a motion correction for fast 3D multiparametric MRI.

This dissertation is structured as follows. Part I gives an introduction to the theoretical background in Chapter 2 and the key concepts and methodology that are used in the works relevant to this dissertation in Chapter 3. Chapter 4 summarizes the main contributions of this thesis.

Part II is composed of three peer-reviewed publications [1–3], constituting the main contribution of this thesis, in Chapter 5. Each of these journal and conference papers is presented in a self-contained section, starting with a summary of the publication.

In Part III of this thesis, Chapter 6 provides a discussion of the presented work. In Chapter 7, conclusions are drawn and an outlook to future research directions is given.

Appendix A comprises three peer-reviewed conference abstracts that are not relevant to the evaluation of this thesis but complement the main publications thematically, either presenting initial results or relevant side projects.

2 THEORETICAL BACKGROUND

To set the theoretical background and to provide a concise summary of the key methodologies that this thesis builds on, this chapter gives an introduction to the concepts of NMR, MRI and DL. However, it is not intended to be a complete review of the respective research fields.

2.1 NUCLEAR MAGNETIC RESONANCE

In the following, the theoretical concepts of MRI are introduced. For a more comprehensive description of MRI physics that goes beyond this high-level review, the reader may be referred to Levitt [43] and Haacke [44].

2.1.1 *Nuclear spin and macroscopic magnetization*

Clinical MRI primarily relies on NMR of the hydrogen nucleus ^{1}H, i.e. a single proton, that is omnipresent in water (H_2O) and lipid (CH_2) molecules in the human body.

The fundamental principle of NMR is the interaction of the nuclear angular momentum $\mathbf{I}$, termed nuclear spin, and external static and dynamic magnetic fields $\mathbf{B}$. Protons (with $I = \frac{1}{2}$) and all other nuclei with a non-zero quantum number $I \neq 0$ possess a nuclear angular momentum or *spin* $\mathbf{I}$ with an associated non-vanishing magnetic moment $\boldsymbol{\mu}$

$$\boldsymbol{\mu} = \gamma \mathbf{I}, \tag{1}$$

where γ is the gyromagnetic ratio with $\gamma = 2.675 \times 10^8 s^{-1} T^{-1}$ for protons.

Although nuclear spin is a quantum mechanical property, the macroscopic behaviour of a large number of nuclei, so-called spin isochromates, that is actually measured in NMR, can be described by classical mechanics [45].

In the absence of a magnetic field $\mathbf{B}$, the individual spins do not precess and are oriented randomly, with a uniform distribution of their directions in space. This results in a near zero macroscopic magnetization $\mathbf{M} = \sum_i \boldsymbol{\mu}_i$. However, when exposed to a static magnetic field $\mathbf{B}_0$, the individual spins start to precess around its direction with a frequency ω_0, referred to as Larmor frequency, proportional to the magnetic field strength B_0

$$\omega_0 = \gamma B_0. \tag{2}$$

Without loss of generality, $\mathbf{B}_0$ is assumed to point in the positive z-direction, i.e. $\mathbf{B}_0 = B_0\hat{\mathbf{e}}_z$.

At the same time, a macroscopic equilibrium magnetization $\mathbf{M}_0 = M_0\hat{\mathbf{e}}_z$ builds up gradually as individual spins have a tendency to align with $\mathbf{B}_0$. However, at body temperature and the commonly applied magnetic field strengths, thermal energy has a significantly stronger effect on the nuclear spins than the applied magnetic field. For this reason, only a weak alignment sets in. The high natural abundance of hydrogen nuclei in the human body is what makes the net magnetization still measurable.

2.1.2 *Radiofrequency excitation*

In order to actually detect the net magnetization $\mathbf{M}$ in the vicinity of the large external magnetic field $\mathbf{B}_0$, it is flipped out of its equilibrium state into the perpendicular plane to $\mathbf{B}_0$. To do so, an additional Radiofrequency (RF) field $\mathbf{B}_1(t)$ ($B_1 << B_0$) is applied orthogonal to $\mathbf{B}_0$ causing the net magnetization to precess around both of the magnetic fields. Exploiting the magnetic resonance phenomenon, the oscillation frequency of $\mathbf{B}_1(t)$ is tuned to the Larmor frequency $\omega_1 = \omega_0$ to perturb the magnetization out of its initial equilibrium state aligned with $\mathbf{B}_0$.

The amount of *excitation* that is achieved by a temporary RF-field $\mathbf{B}_1(t)$, commonly referred to as RF-pulse, over a time interval Δt is described by the flip angle α

$$\alpha = \gamma B_1 \Delta t. \tag{3}$$

The dynamics of the net magnetization $\mathbf{M} = (M_x, M_y, M_z)^\top$ when exposed to an external magnetic field $\mathbf{B}(t) = \mathbf{B}_0 + \mathbf{B}_1(t)$ is described by the Bloch equations

$$\frac{d\mathbf{M}(t)}{dt} = \gamma\mathbf{M}(t) \times (\mathbf{B}_0 + \mathbf{B}_1(t)) = \gamma\mathbf{M}(t) \times \begin{pmatrix} B_1 \cos(\omega_1 t) \\ B_1 \sin(\omega_1 t) \\ B_0 \end{pmatrix}. \tag{4}$$

The relation in Equation 4 is commonly appreciated via a transformation from the stationary (x, y, z) to a rotating frame of reference (x', y', z') that rotates around $\mathbf{B}_0$ with a frequency ω. For the resonance condition $\omega = \omega_1 = \omega_0$, Equation 4 simplifies to

$$\begin{aligned} \frac{d\mathbf{M}(t)}{dt} &\overset{\omega=\omega_1}{=} \gamma\mathbf{M}(t) \times \begin{pmatrix} B_1 \\ 0 \\ B_0 - \frac{\omega_1}{\gamma} \end{pmatrix} \\ &\overset{\omega_1=\omega_0}{=} \gamma\mathbf{M}(t) \times \begin{pmatrix} B_1 \\ 0 \\ 0 \end{pmatrix} = \gamma\mathbf{M}(t) \times \mathbf{B}_{eff}. \end{aligned} \tag{5}$$

The resulting transverse magnetization $M_\perp(t) = M_x(t) + iM_y(t)$ rotates around $\mathbf{B}_0$ with the Larmor frequency ω_0 and can be expressed as

$$M_\perp(t) = M_\perp(0)e^{i\omega_0 t}. \tag{6}$$

2.1.3 *Relaxation mechanisms*

After excitation, interactions of the spins among each other (spin-spin) and with their surrounding (spin-lattice) cause the net magnetization $\mathbf{M}$ to eventually return to its equilibrium state $\mathbf{M}_0$. This process is described by two fundamental *relaxation* mechanisms.

The longitudinal or spin-lattice relaxation describes the recovery of the longitudinal magnetization M_z along the axis of $\mathbf{B}_0$. This exponential restoration of M_z to its thermal equilibrium is characterized by the longitudinal relaxation time T_1.

The transverse or spin-spin relaxation time T_2 characterizes the decay of the transverse magnetization $M_\perp$ due to a loss of phase coherence of the precessing spins. The individual spins within the isochromate interact with each other through their own oscillating magnetic fields. This causes the spins to gradually dephase and ultimately results in a decaying transverse magnetization $M_\perp$.

Taking both longitudinal and transverse relaxation into account, the Bloch equations from Equation 4 become

$$\begin{aligned}
\frac{dM_x(t)}{dt} &= \gamma\left(\mathbf{M}(t) \times \mathbf{B}(t)\right)_x - \frac{M_x(t)}{T_2} \\
\frac{dM_y(t)}{dt} &= \gamma\left(\mathbf{M}(t) \times \mathbf{B}(t)\right)_y - \frac{M_y(t)}{T_2} \\
\frac{dM_z(t)}{dt} &= \gamma\left(\mathbf{M}(t) \times \mathbf{B}(t)\right)_z - \frac{M_z(t) - M_0}{T_1}.
\end{aligned} \tag{7}$$

The relationships in Equation 7 can also be expressed in matrix form:

$$\frac{d\mathbf{M}(t)}{dt} = \gamma\mathbf{M}(t) \times \mathbf{B}(t) - \begin{pmatrix} \frac{1}{T_2} & 0 & 0 \\ 0 & \frac{1}{T_2} & 0 \\ 0 & 0 & \frac{1}{T_1} \end{pmatrix} \left(\mathbf{M}(t) - \mathbf{M}_0\right). \tag{8}$$

After RF-excitation via $\mathbf{B}_1(t)$, the analytical solution for the Bloch equations for a constant, homogeneous magnetic field $\mathbf{B}_0$ is given by

$$\begin{aligned}
M_z(t) &= M_0 - (M_0 - M_z(0))e^{-\frac{t}{T_1}} \\
M_\perp(t) &= M_\perp(0)e^{i\omega_0 t}e^{-\frac{t}{T_2}}.
\end{aligned} \tag{9}$$

This evolution of the magnetization $\mathbf{M}(t)$ is referred to as Free Induction Decay (FID): The transverse magnetization $M_\perp$ decays exponentially with the time constant T_2 while precessing around $\mathbf{B}_0$ with the

Larmor frequency ω_0. The longitudinal magnetization M_z recovers exponentially with the time constant T_1.

Measuring the current that the rotating transverse magnetization $M_\perp$ induces via receiver coils is the basic principle of NMR experiments. Generally, a series of RF-pulses, commonly referred to as pulse sequence, is played out to generate NMR signals that are a function of the underlying physico-chemical tissue parameters, such as T_1, T_2 or PD.

2.2 MAGNETIC RESONANCE IMAGING

2.2.1 *Spatial encoding via imaging gradients*

To ultimately form MRI images, the NMR signal needs to be spatially encoded. This is achieved by superimposing a linear magnetic field gradient $\mathbf{g}(t) = (g_x, g_y, g_z)^\top$ onto the static magnetic field $\mathbf{B}_0 = B_0\hat{\mathbf{e}}_z$ such that

$$B(\mathbf{r}, t)\hat{\mathbf{e}}_z = (B_0 + \mathbf{r}\cdot\mathbf{g}(t))\hat{\mathbf{e}}_z. \tag{10}$$

Consequently, a spatial dependency of the Larmor frequency ω is introduced

$$\omega(\mathbf{r}, t) = \gamma B(\mathbf{r}, t) = \gamma B_0 + \gamma\mathbf{r}\cdot\mathbf{g}(t) = \omega_0 + \gamma\mathbf{r}\cdot\mathbf{g}(t). \tag{11}$$

This in turn causes transverse magnetization $M_\perp$ to accumulate a spatially dependent phase $\phi(\mathbf{r}, t)$ over time

$$\phi(\mathbf{r}, t) = \int_0^t \omega(\mathbf{r}, t')dt' = \omega_0 t + \gamma\mathbf{r}\cdot\int_0^t \mathbf{g}(t')dt' = \omega_0 t + \mathbf{r}\cdot\mathbf{k}(t), \tag{12}$$

where the spatial frequency vector $\mathbf{k}(t)$ is given by

$$\mathbf{k}(t) = \gamma\int_0^t \mathbf{g}(t')dt'. \tag{13}$$

Taking the spatial dependency of the magnetic field into account, the solution of the Bloch equations from Equation 9 becomes

$$\begin{aligned} M_z(\mathbf{r}, t) &= M_0(\mathbf{r}) - (M_0(\mathbf{r}) - M_z(\mathbf{r}, 0))\, e^{-\frac{t}{T_1}} \\ M_\perp(\mathbf{r}, t) &= M_\perp(\mathbf{r}, 0)e^{-i\phi(\mathbf{r},t)}e^{-\frac{t}{T_2}}. \end{aligned} \tag{14}$$

Assuming a spatially varying spin density $\rho(\mathbf{r})$

$$M = \int_V \rho(\mathbf{r})d^3\mathbf{r}, \tag{15}$$

the measured signal $\tilde{S}(t)$ is derived by integrating the expression for the transverse magnetization $M_\perp(\mathbf{r}, t)$ from Equation 14 over the imaging volume V

$$\begin{aligned}\tilde{S}(t) &= \int_V M_\perp(\mathbf{r}, t) d^3\mathbf{r} \\ &= \int_V M_\perp(\mathbf{r}, 0) e^{-i\phi(\mathbf{r},t)} d^3\mathbf{r} \\ &= \int_V \rho(\mathbf{r}) e^{-i\omega_0 t} e^{-i\mathbf{r}\cdot\mathbf{k}(t)} d^3\mathbf{r} \\ &= e^{i\omega_0 t} \int_V \rho(\mathbf{r}) e^{-i\mathbf{r}\cdot\mathbf{k}(t)} d^3\mathbf{r},\end{aligned} \tag{16}$$

where T_2 relaxation effects are neglected for simplicity. Also neglecting the high frequency phase modulation $e^{-i\omega_0 t}$, the signal $S(t)$ becomes

$$S(t) = \tilde{S}(t) e^{-i\omega_0 t} = \int_V \rho(\mathbf{r}) e^{-i\mathbf{r}\cdot\mathbf{k}(t)} d^3\mathbf{r}. \tag{17}$$

From the above relationship, it becomes clear that the measured signal $S(t) = S(\mathbf{k}(t))$ is the Fourier transform of the spatial spin density $\rho(\mathbf{r})$. In turn, an approximation of $\rho(\mathbf{r})$ can be reconstructed via the inverse Fourier transform of the acquired signal

$$\rho(\mathbf{r}) = \int_k S(\mathbf{k}(t)) e^{i\mathbf{r}\cdot\mathbf{k}(t)} d^3\mathbf{k}. \tag{18}$$

The above Fourier relationship between the spatially-encoded NMR signal and the spatial spin density, established by magnetic gradient fields, constitutes the fundamental principle of MRI.

2.2.2 *Slice selection*

Spatial encoding of the NMR signal as described before is realized after the initial RF-excitation. That is, the RF-pulse excites all spins in a given 3D volume that have a Larmor frequency equal to the frequency of the oscillating $\mathbf{B}_1$ field. This is therefore commonly referred to as *non-selective* excitation. To achieve *slice-selective* excitation, a magnetic field gradient, e.g. along the z direction, is already applied during the initial RF-pulse. Due to the spatial varying Larmor frequency $\omega(z) = \gamma(B_0 + z g_z)$, only the spins in a plane perpendicular to the direction of the gradient field meet the resonance condition $\omega_1 = \omega(z)$. In this case, Equation 16 reduces to

$$S(k_x(t), k_y(t)) = \int_V \rho(x, y) e^{-i(k_x x + k_y y)} dx dy. \tag{19}$$

The thickness Δz of the xy-plane that is excited depends on the bandwidth of the RF-pulse $\Delta\omega$ and the strength of the gradient field g_z

$$\Delta z = \frac{\Delta\omega}{\gamma g_z}. \tag{20}$$

2.3 DIFFUSION IN MRI

2.3.1 *Diffusion*

Diffusion refers to random interactions of particles due to thermal motion. Free diffusion, i.e. the movement of particles from regions with high concentration to regions with low concentration, are described by Fick's laws [46].

In an isotropic medium, the diffusion flux vector $\mathbf{j}$ and the concentration gradient $\nabla c(\mathbf{r}, t)$ are related via the diffusion coefficient D, as given by Fick's first law

$$\mathbf{j}(\mathbf{r}, t) = -D\nabla c(\mathbf{r}, t). \tag{21}$$

Together with the principle of mass conservation

$$\nabla \mathbf{j}(\mathbf{r}, t) = -\frac{\partial c(\mathbf{r}, t)}{\partial t}, \tag{22}$$

Equation 21 yields Fick's second law

$$D\nabla^2 c(\mathbf{r}, t) = \frac{\partial c(\mathbf{r}, t)}{\partial t}. \tag{23}$$

With diffusion being a random process, the probability density function for free isotropic diffusion is given by a three-dimensional Gaussian distribution

$$P(\mathbf{r} \mid \mathbf{r_0}, t) = (4\pi D t)^{-\frac{3}{2}} \exp\left(-\frac{1}{4Dt}(\mathbf{r} - \mathbf{r_0})^2\right), \tag{24}$$

where $\Delta\mathbf{r} = \mathbf{r}_0 - \mathbf{r}$ is the displacement in a time t [47]. The mean-squared displacement $\langle \Delta r^2 \rangle$ is given by the variance σ^2 of the Gaussian distribution

$$\langle \Delta \mathbf{r}^2 \rangle = \sigma^2 = 2NDt, \tag{25}$$

with $N = 1, 2, 3$ being the dimensionality of the diffusion process.

2.3.2 *Bloch-Torrey equations*

The Bloch equations from Equation 7 and Equation 8, respectively, can be extended to also include the effect of diffusion on the temporal evolution of the magnetization in addition to the relaxation effects. For isotropic diffusion, the resulting Bloch-Torrey equations [48] are given by

$$\frac{d\mathbf{M}(t)}{dt} = \gamma \mathbf{M}(t) \times \mathbf{B}(t) - \begin{pmatrix} \frac{1}{T_2} & 0 & 0 \\ 0 & \frac{1}{T_2} & 0 \\ 0 & 0 & \frac{1}{T_1} \end{pmatrix} (\mathbf{M}(t) - \mathbf{M}_0) + D\nabla^2 \mathbf{M}(t). \tag{26}$$

To measure diffusive motion, again magnetic field gradients are applied to introduce spatially varying Larmor frequencies. In the presence of a diffusion-encoding magnetic field gradient $\mathbf{g}(t)$, the time evolution of the transverse magnetization $M_\perp(\mathbf{r}, t)$ in the rotating frame of reference is described by an additional diffusion term

$$\frac{dM_\perp(\mathbf{r}, t)}{dt} = -i\gamma(B_0 + \mathbf{r} \cdot \mathbf{g}(t))M_\perp(\mathbf{r}, t) - \frac{M_\perp(\mathbf{r}, t)}{T_2} + D\nabla^2 M_\perp(\mathbf{r}, t). \tag{27}$$

Assuming

$$M_\perp(\mathbf{r}, t) = A(t) \exp\left(-i\gamma\left(B_0 t + \mathbf{r} \cdot \int_0^t \mathbf{g}(t')dt'\right) - \frac{t}{T_2}\right), \tag{28}$$

where $A(t)$ is the diffusion-induced change of the amplitude over time, Equation 27 yields

$$\frac{dA(t)}{dt} = -D\gamma^2 \left(\int_0^t \mathbf{g}(t')dt'\right)^2 A(t). \tag{29}$$

This differential equation can be solved by

$$A(t) = A(0)e^{-Db}, \tag{30}$$

where the b-value is given by

$$b = \gamma^2 \int_0^t \left(\int_0^{t'} \mathbf{g}(t'')dt''\right)^2 dt'. \tag{31}$$

For unrestricted isotropic diffusion, the measured diffusion-weighted signal intensity is therefore given by

$$S(b, D) = S(b = 0)e^{-bD}, \tag{32}$$

where $S(b = 0)$ is the signal intensity without diffusion-encoding gradients.

2.3.3 *Diffusion tensor model*

Going beyond the specific case of isotropic diffusion, characterized by a single diffusion coefficient D, anisotropic diffusion behavior can be described by the diffusion tensor $\mathbf{D}$

$$\mathbf{D} = \begin{pmatrix} D_{xx} & D_{xy} & D_{xz} \\ D_{yx} & D_{yy} & D_{yz} \\ D_{zx} & D_{zy} & D_{zz} \end{pmatrix}, \tag{33}$$

where the three diagonal elements (D_{ii}) refer to the diffusion coefficients measured along the principal x-, y- and z-axes [49]. The six

off-diagonal terms ($D_{ij} = D_{ji}$) are the covariance terms. For the special case of isotropic diffusion, $\mathbf{D}$ becomes

$$\mathbf{D} = \begin{pmatrix} D_{xx} & 0 & 0 \\ 0 & D_{yy} & 0 \\ 0 & 0 & D_{zz} \end{pmatrix}, \tag{34}$$

with $D_{xx} = D_{yy} = D_{zz} = D$.

For the general case of anisotropic diffusion, the expression for the measured signal intensity in Equation 32 can be rewritten as

$$S(b, \mathbf{n}, \mathbf{D}) = S(b = 0)e^{-b\mathbf{n}\mathbf{D}\mathbf{n}^\top}, \tag{35}$$

where the unit vector $\mathbf{n}$ refers to the respective diffusion-encoding direction.

Diagonalization of $\mathbf{D}$ such that $\mathbf{D} = \mathbf{E}\boldsymbol{\Lambda}\mathbf{E}^\top$ yields the eigenvalues $\lambda_{1,2,3} = \mathrm{diag}(\boldsymbol{\Lambda})$ with $\lambda_1 \geqslant \lambda_2 \geqslant \lambda_3$ and the corresponding eigenvectors $\boldsymbol{\epsilon}_{1,2,3}$, representing the matrix columns of $\mathbf{E} = (\boldsymbol{\epsilon}_1 \mid \boldsymbol{\epsilon}_2 \mid \boldsymbol{\epsilon}_3)$. The principal diffusion orientation is given by the principal eigenvector $\boldsymbol{\epsilon}_1$.

From the derived eigenvalues $\lambda_{1,2,3}$, scalar diffusion metrics can be calculated, including the Mean Diffusivity (MD) or Apparent Diffusion Coefficient (ADC)

$$MD = \langle D \rangle = \langle \lambda \rangle = \frac{1}{3}\sum_{i=1}^{3} \lambda_i, \tag{36}$$

the Axial Diffusivity (AD)

$$AD = D_{\parallel} = \lambda_{\parallel} = \lambda_1, \tag{37}$$

the Radial Diffusivity (RD)

$$RD = D_{\perp} = \lambda_{\perp} = \frac{\lambda_2 + \lambda_3}{2}, \tag{38}$$

and the Fractional Anisotropy (FA)

$$FA = \sqrt{\frac{3\sum_{i=1}^{3}(\lambda_i - \langle\lambda\rangle)^2}{2\sum_{i=1}^{3}\lambda_i^2}}. \tag{39}$$

2.4 DEEP LEARNING-BASED INFORMATION PROCESSING

This section gives a brief introduction to the concept of DL-based information processing - from the theoretical foundation of artificial neurons to the formation of an Artificial Neural Network (ANN) and Convolutional Neural Network (CNN) entities. For a deeper insight into the field of DL, the reader is referred to the relevant literature, e.g. [50–52].

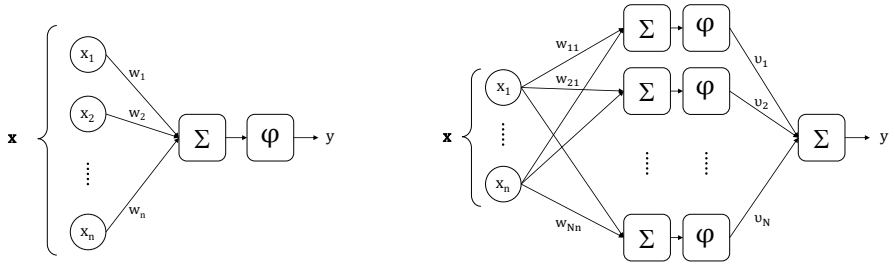

Figure 1: Artificial neural networks. The mathematical concept of an artificial neuron (left) constitutes the basic building block for ANNs. A Perceptron (right) is the simplest architecture of ANNs.

2.4.1 *Artificial neurons*

The fundamental concept of DL is the formulation of an artificial neuron as a mathematical construct. In analogy to the information processing in biological neurons, an artificial neuron combines the information or activation received from other neurons in a weighted sum, which is then processed by a non-linear activation function φ as illustrated in Figure 1. Mimicking excitatory and inhibitory transmission, commonly used activation functions are the sigmoid function $\sigma(x) = \frac{1}{1+e^{-x}}$, the tangens hyperbolicus $\tanh(x) = \frac{e^x - e^{-x}}{e^x + e^{-x}}$ or the Rectified Linear Unit (ReLU) function $\mathrm{ReLU}(x) = \max(0, x)$. The incorporation of such activation functions makes artificial neurons capable of approximating not only linear but also non-linear relationships. As such, the output of an artificial neuron $f(\mathbf{x})$ given the input $\mathbf{x} = (x_1, ..., x_n)$ is defined by

$$f(\mathbf{x}) = \varphi(\mathbf{w}^\top \mathbf{x} + w_0), \tag{40}$$

where $\mathbf{w} = (w_1, ..., w_n)$ is a weight vector and w_0 is a bias term [53].

2.4.2 *Types of Neural Networks*

Building on this basic concept of artificial neurons, the two different types of NNs in DL that are relevant to this thesis, are the concepts of ANNs and CNNs.

(ARTIFICIAL) NEURAL NETWORKS To increase modeling capacities, individual artificial neurons are combined to form an ANN. The most common type of ANNs is a fully-connected structure. Here, the individual neurons are arranged in layers with fully pairwise connections of all neurons between two adjacent layers and no connections within a layer. Given a sufficiently large number of neurons N, any continuous function $f(\mathbf{x})$ can in principle be approximated by a single layer ANN

$$f(\mathbf{x}) = \sum_{i=0}^{N-1} v_i \varphi(\mathbf{w}_i^\top \mathbf{x} + w_{0,i}), \tag{41}$$

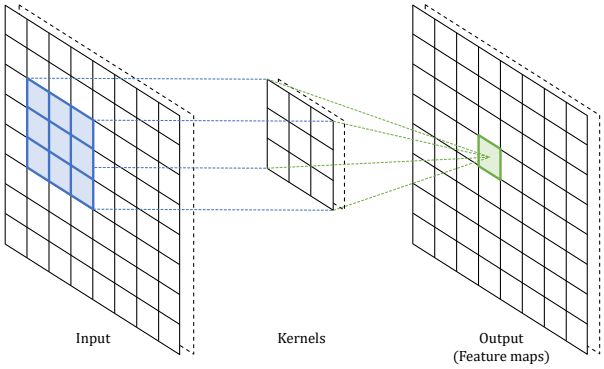

Figure 2: Convolutional neural networks. A CNN is based on convolving the input with a weight matrix, the convolutional kernel. This concept can be extended to further feature dimensions, the so-called channels.

where v_i are the combination weights. The simplest structure of an ANN is the so-called Perceptron, consisting of an input layer, i.e. the first layer, one hidden layer and an output layer, i.e. the last layer (Figure 1). ANN architectures with more than one hidden layer are therefore referred to as Multi-Layer Perceptrons (MLPs) or deep ANNs.

CONVOLUTIONAL NEURAL NETWORKS Just like fully-connected ANNs, CNNs are comprised of neurons that are connected via weights and biases with a subsequent non-linear activation. However, in contrast to MLPs, CNNs are constructed by convolution and pooling layers that precede a fully-connected output layer. With these two core building blocks, CNNs account for local connectivity and preserve spatial relationships when progressing from one dimensional to two or higher dimensional problems. Convolutional layers are linear operations that rely on matrix multiplication to convolve its input with a weight matrix, referred to as kernel or filter. As such, convolutional layers connect each neuron to only a local region of the input and all neurons within one layer share the same weights (Figure 2). This results in a drastically reduced number of model parameters compared to fully-connected layers. The output of the linear convolution operations, called feature maps, is then passed through a nonlinear activation function. Along with convolutional layers, pooling layers are introduced in-between successive convolutional layers to progressively reduce the dimension of the feature representations. That is, a pooling layer constitutes a downsampling operation, which can also be expressed as a matrix operation with fixed weights, typically employing average or maximum pooling.

2.4.3 *Neural Network training*

Independent of the actual topology of NNs, the overall goal is to optimize the trainable weight and bias parameters to approximate the non-linear relationship between its input and the desired output. How well the targeted relationship is modelled by the NN with its particular set of parameters θ is determined by a loss function $L(\theta)$. Therefore, the fundamental aim of NN training is to minimize the loss function by adjusting the model parameters via gradient descent. To use gradient descent (or variants thereof) for training deep NNs, backpropagation constitutes a key concept as it enables the efficient computation of gradients based on the chain rule [54].

To minimize $L(\theta)$, the trainable parameters $\theta = (\theta_1, ..., \theta_N)$ are gradually adjusted via gradient descent

$$\begin{aligned} \theta^{j+1} &= \theta^j - \lambda \nabla L(\theta^j), \\ \theta_n^{j+1} &= \theta_n^j - \lambda \frac{\partial L}{\partial \theta_n^j}, \end{aligned} \tag{42}$$

where λ is the learning rate and j indicates the j^{th} iteration. The partial derivative of the loss function with respect to a parameter $\frac{\partial L}{\partial \theta_n}$ is calculated by iteratively applying the chain rule. To do so, the non-linear activation function of the artificial neurons needs to be differentiable.

3

METHODOLOGY

3.1 FROM QUALITATIVE TO QUANTITATIVE MRI

Traditional contrast-weighted MRI relies on the sensitivity of the NMR signal to various tissue properties. Alongside this purely qualitative perspective, quantitative MRI techniques aim for an actual measurement of these parameters to ultimately produce quantitative maps instead of / in addition to qualitative anatomical images. Just like qualitative MRI, quantitative techniques also rely on the principle of image formation in the Fourier domain as introduced in Section 2.1. However, while qualitative MRI contrasts are sensitive to the various physico-chemical tissue properties, quantitative MRI aims at encoding for these in order to measure the underlying tissue parameters. To do so, NMR signals are not only encoded spatially, but the sequence design has to be expanded to additional parameter-encoding dimensions, e.g. by introducing a signal variation over time. To describe the resulting signal evolution in the k-t domain, Equation 17 can be generalized to

$$y(\mathbf{k}(t), t) := S(\mathbf{k}(t), t) = \int_V \rho(\mathbf{r}) f_t(\mathbf{r}) e^{-i\mathbf{k}(t)\mathbf{r}} d^3\mathbf{r}. \tag{43}$$

The k-t-space signal is now denoted as $y(\mathbf{k}(t), t) := S(\mathbf{k}(t), t)$ following the convention in [55]. The additional parameter encoding dimension in Equation 43 is accounted for by introducing a temporal dependence to the k-space signal via $f_t(\mathbf{r})$

$$f_t(\mathbf{r}) = f_t\left(\boldsymbol{\eta}(t), \boldsymbol{\theta}(\mathbf{r})\right) \tag{44}$$

that links the set of time-dependent acquisition parameters $\boldsymbol{\eta}(t)$, including flip angle α, Repetition Time (TR) or Echo Time (TE), and the spatially-varying tissue parameters $\boldsymbol{\theta}(\mathbf{r})$, such as T_1 and T_2 relaxation times or the diffusion tensor $\mathbf{D}$.

The image-space signal $x(\mathbf{r}, t = \tau)$ after the τth RF excitation at voxel location $\mathbf{r}$ can therefore be written as

$$x(\mathbf{r}, \tau) = \rho(\mathbf{r}) f_\tau(\mathbf{r}) = \rho(\mathbf{r}) f_\tau\left(\boldsymbol{\eta}(\tau), \boldsymbol{\theta}(\mathbf{r})\right), \tag{45}$$

where the full signal evolution at voxel location $\mathbf{r}$ along T time points is given by $\mathbf{x}(\mathbf{r}, t) = (x(\mathbf{r}, \tau = 1), x(\mathbf{r}, \tau = 2), ..., x(\mathbf{r}, \tau = T))^\top \in \mathbb{C}^T$.

To describe the full spatio-temporal image evolution $\mathbf{X} \in \mathbb{C}^{N \times T}$ for N voxels, a formal encoding operator $\mathbf{E}$ that comprises both spatial Fourier and parameter encoding can be introduced

$$\mathbf{E} = \mathbf{UFS}. \tag{46}$$

The encoding operator $\mathbf{E}$ itself is composed of the operators $\mathbf{U}$ that describes the undersampled k-space acquisition, $\mathbf{F}$ that is the Fourier Transform, and $\mathbf{S}$ that refers to the coil sensitivity profiles.

With the formulation of the encoding operator in Equation 46, the reconstructed image time-series $\mathbf{X}$ can be written as a function of the acquired raw k-t data $\mathbf{Y} \in \mathbb{C}^{M \times T}$ with M sampled k-space locations per time point

$$\mathbf{Y} = \mathbf{E}\mathbf{X}. \tag{47}$$

Although the large variety of quantitative MRI methods results in different formulations of the encoding operator, they all share the common goal to quantify the tissue parameters of interest θ. In general, this is achieved by enforcing voxelwise consistency between a biophysical signal model and the acquired image time-series, e.g. by means of model fitting or dictionary grid search techniques (see Section 3.5).

Despite their great capabilities, quantitative MRI techniques also share a common drawback, the additional parameter-encoding dimensions result in (clinically impractically) long scan times compared to conventional contrast-weighted MRI. Also, quantitative MRI techniques are generally limited to probing only one or a few parameters at a time, which additionally prolongs MRI protocols if multiparametric information is required and sequential quantitative MRI acquisitions have to be performed.

For broad clinical deployment, quantitative MRI therefore has to achieve scan times that meet the tight clinical time constraints. Recent technical developments to accelerate quantitative MRI address this requirement by presenting

1. Novel multiparametric encoding and signal modeling motives,
2. Accelerated acquisition schemes,
3. Advanced image reconstruction algorithms,
4. Efficient parameter estimation,

and often a combination of the above.

In the following, a brief introduction of these concepts in the particular context of fast multiparametric mapping are given. This section has a particular focus on transient-state methods such as Magnetic Resonance Fingerprinting (MRF) schemes as they build the core techniques of this thesis. For more comprehensive insights into the respective methodologies and related research activities, the reader is referred to the relevant literature.

3.2 MULTIPARAMETRIC ENCODING AND SIGNAL MODELING

As the MRI signal depends on the various physico-chemical tissue properties θ (T_1, T_2, M_0, etc.), the respective acquisition parameters

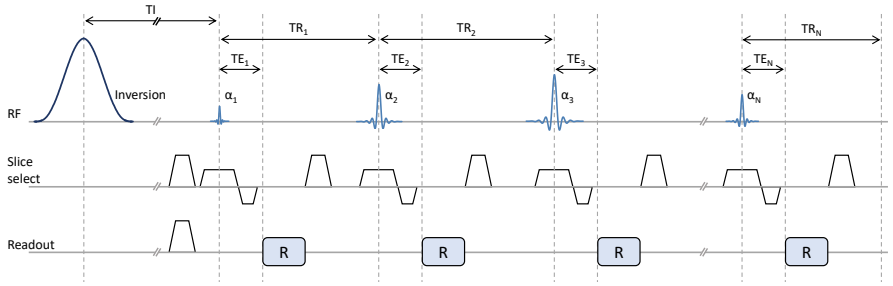

Figure 3: Pulse sequence diagram of a 2D SSFP-based MRF scheme. An initial inversion pulse (with Inversion Time (TI)) is followed by a variable flip angle train $\alpha_{1,2,\ldots,N}$ to jointly encode T_1 and T_2 relaxation times in the transient state: while the beginning of the sequence is mainly sensitized to T_1 due to the inversion recovery, T_2 information is primarily encoded via the formation of stimulated echoes. As the signal response evolves over time, one interleaf of an undersampled spiral trajectory is acquired in each repetition. To achieve spatial incoherence, k-space undersampling is generally randomized by rotating the spiral waveforms from one repetition to the next, e.g. with golden angles.

$\boldsymbol{\eta}$ (TR, TE, α, etc.) and hardware properties (B_0, B_1, etc.), a comprehensive understanding of these relationships and their mathematical formulation into an appropriate signal model is a key requisite for any quantitative MRI technique. Compared to single parameter mapping, multiparametric MRI techniques exploit this inherent dependency of the MRI signal to simultaneously encode for multiple parameters within a single scan. For joint T_1-T_2-relaxometry [56], this is generally accomplished by either multicontrast steady-state MRI or through variations of balanced or unbalanced Steady-state Free Precession (SSFP) readouts [57–61]. Although being grounded on an inversion recovery SSFP scheme, the seminal work on MRF [62, 63] gave rise to a conceptionally novel type of fast multiparametric MRI. In MRF [64] and other newly emerged techniques such as Quantitative Transient-state Imaging (QTI) [7, 65] or Magnetic Resonance Spin TomogrAphy in Time-domain (MR-STAT) [66, 67], the signal is acquired in the transient state. Instead of enforcing a steady state, parameter encoding in the transient state is driven by continuous variation of acquisition parameters as schematically shown in Figure 3. This way, these techniques present highly efficient strategies to simultaneously encode for spatial and multiparameter information in the k-t-space. While MRF was initially implemented using a pseudo-random variation of acquisition parameters, sequence design is now more and more optimized for increasing parameter encoding efficiency, e.g. by means of Bayesian methods [65, 68] or Crámer-Rao Lower Bounds [69, 70].

While for the steady-state signal response, the time-dependent encoding function $f_t(\mathbf{r})$ simplifies to an analytical time-invariant expression $f(\mathbf{r})$, signal modeling in the transient state is more complex as the magnetization evolves dynamically in time. The transient signal response to RF excitation or gradient dephasing can be recursively modeled via Bloch simulation or using the Extended Phase Graphs (EPG) formalism [71]. In EPG theory, the temporally evolving magnetization vector $\mathbf{M} = (M_x, M_y, M_z)^\top$ is described by a change into the reference system of complex magnetization components $(M_+, M_-, M_z)^\top$ that are expressed as Fourier states

$$\begin{aligned} M_\pm(\mathbf{r}) = M_x(\mathbf{r}) \pm iM_y(\mathbf{r}) &= \int_V \tilde{F}_k^\pm e^{i\mathbf{kr}} d^3\mathbf{k} \\ M_z(\mathbf{r}) &= \int_V \tilde{Z}_k e^{i\mathbf{kr}} d^3\mathbf{k} \end{aligned} \tag{48}$$

so that

$$\begin{aligned} \tilde{F}_k^\pm &= \int_V M_\pm(\mathbf{r}) e^{-i\mathbf{kr}} d^3\mathbf{r} \\ \tilde{Z}_k &= \int_V M_z(\mathbf{r}) e^{-i\mathbf{kr}} d^3\mathbf{r}. \end{aligned} \tag{49}$$

Here k is the dephasing order and the complex conjugate operation * relates the magnetization $M_- = M_+^*$ as well as the de- and rephasing configuration states $\left(\tilde{F}_k^+\right)^* = \tilde{F}_k^-$, $\left(\tilde{Z}_k\right)^* = \tilde{Z}_{-k}$. The Fourier configuration states are efficiently comprised in a state matrix $\mathbf{\Omega}$

$$\mathbf{\Omega} = \begin{pmatrix} \tilde{F}_0^+ & \tilde{F}_1^+ & \tilde{F}_2^+ & \cdots \\ \tilde{F}_0^- & \tilde{F}_1^- & \tilde{F}_2^- & \cdots \\ \tilde{Z}_0 & \tilde{Z}_1 & \tilde{Z}_2 & \cdots \end{pmatrix}. \tag{50}$$

As such, the temporal evolution of the magnetization is efficiently modelled by linear operators acting on the state matrix Ω. The state matrix Ω_t at time t is consequently described in a recursive form

$$\Omega_t = f_t(\boldsymbol{\eta}, \boldsymbol{\theta})\Omega_{t-1}. \tag{51}$$

Neglecting effects such as magnetization transfer or coherent and incoherent motion, the encoding operator $f_t(\boldsymbol{\eta}, \boldsymbol{\theta})$ is composed of the linear operators $\mathbf{T}_\theta(\alpha)$, $\mathbf{S}(\Delta k)$ and $\mathbf{E}(\Delta t, T_1, T_2)$ that account for RF excitation, gradient dephasing due to unbalanced gradient waveforms and tissue relaxation, respectively [65]. The encoding function $f_t(\boldsymbol{\eta}, \boldsymbol{\theta})$ can therefore be expressed as

$$f_t(\boldsymbol{\eta}, \boldsymbol{\theta}) = \mathbf{E}(\Delta t, T_1, T_2)\mathbf{S}(\Delta k)\mathbf{T}_\theta(\alpha), \tag{52}$$

where $\boldsymbol{\eta}$ comprises the time-dependent acquisition parameters, i.e. flip angle α and phase ϕ of the RF excitation, the timings of the pulse sequence Δt in terms of TE and TR as well as an indirect measure

of the gradient moments via Δk. θ are the tissue-specific parameters, typically T_1 and T_2. In theory the EPG formalism can also be extended to motion phenomena, e.g. flow or diffusion. Although the theoretical framework is in principle capable of incorporating physiological effects such as anisotropic diffusion through the diffusion tensor $\mathbf{D}$, such calculations become computationally infeasible in practice [72].

3.3 ACCELERATED ACQUISITION

To achieve acceptable scan times, MRI acquisitions oftentimes rely on fast alternatives to traditional spin-warp imaging, which fills the k-space row by row based on sequential phase encodings with subsequent frequency encoding steps. Common alternatives to spin-warp-based acquisition techniques can be divided into Cartesian imaging strategies, such as Echo-planar Imaging (EPI), and non-Cartesian techniques, such as but not limited to spiral or radial trajectories [73].

Independent of the actual sampling trajectory, the aim of speeding up the inherently slow MRI process has triggered the development of two major classes of acceleration strategies: PI and CS. PI relies on the simultaneous acquisition of multi-coil data and therefore requires less k-space data to be acquired, ultimately shortening MRI scan times without causing artifacts in the reconstructed images [74]. To achieve acceleration beyond the Nyquist limit, CS and other sparse sampling methods rely on incoherent undersampling in the spatial and / or the parametric domain with a subsequent transformation of the original signal into a sparse representation for image reconstruction [40, 75].

3.4 ADVANCED IMAGE RECONSTRUCTION ALGORITHMS

Non-Cartesian trajectories offer several advantages over Cartesian sampling schemes, including faster readout times, higher robustness to subject motion, better Signal to Noise Ratio (SNR). Image reconstruction of the non-uniformly sampled k-space, however, constitutes the main drawback of non-Cartesian sampling schemes as it is more complex and therefore computationally more expensive. Also, as non-Cartesian gradient waveforms do not have unique frequency- and phase-encoding directions, artifacts appear as rather diffuse image blurring instead of coherent ghosting or geometric distortions as in case of Cartesian sampling and are therefore more difficult to correct for. The uniformly sampled k-space from spin-warp techniques can be efficiently reconstructed by means of a Fast Fourier Transform (FFT). In contrast, non-Cartesian raw data is commonly reconstructed by resampling the acquired k-space to a Cartesian grid, which is commonly referred to as (re-) gridding. In general, this involves a density compensation of the k-space data, convolution with a (re-) gridding kernel and inverse FFT. All reconstructions of 2D or 3D spiral

trajectories performed in the works relevant to this thesis, employ Non-uniform Fast Fourier Transform (NUFFT) operations, i.e. fast, generalized implementations of the above k-space processing steps that can be applied to any non-Cartesian sampling scheme [76]. To take advantage of the benefits of non-Cartesian over Cartesian acquisitions, which are still predominant in clinical routine imaging, there has been significant advance in addressing its inherent practical concerns on both hardware and software side. This includes the development of efficient NUFFT implementations [77] or the transfer of Cartesian PI algorithms, such as Generalized Autocalibrating Partial Parallel Acquisition (GRAPPA) or Sensitivity Encoding (SENSE) [78], to non-Cartesian sampling [73].

Independent of the underlying sampling scheme, i.e. Cartesian or non-Cartesian, undersampled k-space acquisitions are an effective measure to reduce scan time. This however comes at the cost of aliasing artifacts in the reconstructed images. Therefore, significant research effort has been put into developing advanced reconstruction techniques to resolve these corruptions and to reconstruct aliasing-free image data from highly undersampled k-space measurements. In this context, sparsity-driven methods, including CS reconstructions, gained a lot of popularity. Sparse reconstruction methods generally rely on the assumption that there is redundancy in the MRI data. This can be exploited to undersample the k-space in an incoherent way to generate noise-like aliasing artifacts as touched upon in Section 3.3. To eventually reconstruct high quality MRI data from k-space data sampled below the Nyquist limit, these algorithms take advantage of the existence of a sparse representation. Although sparse reconstruction methods are generally based on this basic assumption, there is large variety of how this is reflected in the actual reconstruction process. In case of CS reconstruction, the core assumption is that although the MRI data is not per se an intrinsically sparse domain, it can be transferred into a sparse representation by means of a sparsifying transform $\mathbf{\Psi}$. Here total variation or wavelet transforms are two popular representatives for k-space. In the spirit of a model-constraint optimization, the a priori ill-posed image reconstruction problem can be formulated as a minimization problem [75]

$$\arg\min_{\mathbf{X}} \|\mathbf{E}\mathbf{X} - \mathbf{Y}\|_2^2 + \lambda\|\mathbf{\Psi}\mathbf{X}\|_1, \tag{53}$$

where the first data fidelity term enforces consistency between the reconstructed image and the acquired k-space via the formal encoding operator $\mathbf{E}$. The second regularization term ensures a sparse representation, e.g. via L_1 regularization in terms of CS.

CS and other sparsity-driven reconstruction algorithms have proven to be powerful methods for reconstructing high fidelity MRI images from massively undersampled k-space data [79]. In the context of this thesis, a CS reconstruction with efficient spatiotemporal regular-

isations [8] is employed to suppress the aliasing artifacts due to the highly undersampled k-space acquisition [2] (Section 5.1).

Although achieving convincing image reconstruction quality in a multitude of MRI reconstruction scenarios, the iterative optimization makes them an inherently slow reconstruction. Here, recent achievements in the context of DL-based image reconstruction have demonstrated great potential in achieving similar performances as conventional methods or even outperforming the current state of the art in terms of image qualities, reconstruction speed or computational efficiency [80, 81]. In general, most of the recently proposed DL-based reconstruction approaches for accelerated MRI acquisitions rely on one of the following strategies [82]: image quality enhancement / denoising in the image [83, 84] or k-space domain [82], cascaded NN architectures with data consistency measures between k-space and image domain via (inverse) Fourier Transform [85, 86] and end-to-end k-space to image-space learning [87]. While most of these recent DL techniques were initially developed for image quality enhancement, they are now more and more transferred from the pure image reconstruction task to related fields of application along the MRI pipeline. For example, in Section 5.3, a CNN, which falls into the first category of DL-strategies, is employed to resolve motion-induced artifacts in the context of fast multiparametric mapping via QTI [3].

3.5 EFFICIENT PARAMETER ESTIMATION

Independent of the parameter encoding and acquisition strategies, the overarching goal of all single- and multiparametric MRI techniques is the voxelwise quantification of the respective parameter(s) of interest. This is commonly achieved by formulating the parameter estimation as a voxelwise optimization problem

$$\hat{\theta}(\mathbf{r}) = \arg\min_{\rho,\theta} \|\mathbf{x}(\mathbf{r},t) - \rho(\mathbf{r}) f_t(\boldsymbol{\eta}(t), \theta(\mathbf{r}))\|_2^2. \tag{54}$$

However, for complex signal models $f_t(\boldsymbol{\eta}(t), \theta(\mathbf{r}))$ that may not have an analytical solution like in case of the recursive formulation via EPGs, conventional optimization techniques become computationally expensive. Also, in case of non-convex objective functions Non-Linear Least Square algorithms might converge to a local minimum, causing parameter estimation errors as a consequence.

To circumvent these drawbacks, MRF-based multiparameter estimation relies on a brute force dictionary matching technique. Following an orthogonal matching pursuit [88], the measured signal $\mathbf{x}(\mathbf{r},t)$ is matched to a dictionary of pre-computed signal responses $\tilde{\mathbf{x}}_i(t)$ obtained from Bloch simulations

$$\hat{i}(\mathbf{r}) = \arg\max_i \frac{\langle \mathbf{x}(\mathbf{r},t), \tilde{\mathbf{x}}_i(t) \rangle}{\|\mathbf{x}(\mathbf{r},t)\|_2 \|\tilde{\mathbf{x}}_i(t)\|_2} \tag{55}$$

in a voxelwise manner. The dictionary entry $\hat{\imath}$ with the highest correlation in terms of the complex inner product is retained and the associated set of parameters $\theta_{\hat{\imath}}$ yields the parameter estimates $\hat{\theta}(\mathbf{r}) = \theta_{\hat{\imath}}$ for the voxel $\mathbf{r}$. A relative density estimate $\hat{\rho}(\mathbf{r})$ is determined as the scaling factor between $\mathbf{x}(\mathbf{r}, t)$ and $\tilde{\mathbf{x}}_{\hat{\imath}}(t)$.

Although this grid search approach has proven to allow for robust parameter mapping, it is an intrinsically slow method. Also, dictionary matching does not yield continues estimates but is restricted to the preset parameter grid. The goodness of the parameter estimates is therefore dependent on the discretization of the dictionary. To achieve sufficiently high precision of the the parameter estimates, dictionaries are typically computed with fine granularity over the entire range of feasible values. As dictionary size increases exponentially with the number of parameters, the resulting memory and computational requirements, however, make a broad application of the dictionary matching impracticable. Recent methodological advances address these inherent drawbacks of pattern matching, e.g. by proposing compressing techniques for dimensionality reduction along the temporal dimension [89, 90], and thereby increasing computational efficiency of the matching procedure.

More recently, DL-based approaches have emerged as an efficient alternative to expensive dictionary matching by learning the nonlinear mapping between the measured signal evolutions and the targeted multiparametric output [91]. The underlying multivariate regression task has either been approached as a voxelwise inference by means of a fully-connected NN model [92–95], or by spatially-constrained implementations [96, 97]. Independent of the potential strengths and weaknesses of the specific model implementations, DL-based parameter mapping has been demonstrated to offer fast parameter inference with high accuracy without being bound by finite grid sizes [91]. In the course of this thesis, NN-based inference of T_1 and T_2 relaxation times was extended to also estimate PD, e.g. when integrated in to 3D QTI scheme [7]. In particular, Section 5.1 and Section A.2 demonstrate that the proposed NN is an efficient and clinically feasible alternative to expensive dictionary matching [2, 5]. Section 5.2 and Section A.1 show that DL-based parameter inference constitutes a promising tool for expanding multiparametric MRI to higher dimensional parameter spaces, where conventional approaches become infeasible because the underlying biophysical signal model is too complex or inaccurate [1, 4].

4 CONTRIBUTION OF THIS THESIS

To contribute to the integration of quantitative MRI into clinical routine, this thesis proposes methodological advances towards fast and robust multiparametric mapping. Building on the concept of physics-informed DL [98], it addresses aspects along the entire imaging pipeline, i.e. covering the aspects of image reconstruction and parameter inference when combined with highly accelerated transient-state acquisitions. Complementing the ongoing research efforts to unlock the great potential of quantitative MRI for comprehensive disease detection and characterization for clinical practice, this thesis presets the following three contributions:

EFFICIENT QUANTIFICATION OF T_1, T_2 AND PD On the way to fast multiparametric MRI, highly accelerated acquisition schemes, including transient-state imaging techniques such as MRF [62, 63], have recently been proposed to address the clinical time constraints. To achieve clinically feasible image qualities despite the massive spatial undersampling that usually makes such short scan times possible, advanced reconstruction algorithms are employed. Also, in contrast to the initially proposed dictionary matching for MRF-based parameter mapping, recent works aimed at learning the non-linear relationship between the complex MRI signal and the encoded parameters of interest [92–94]. Voxelwise parameter inference via NNs, which can be trained on purely simulated signal dynamics, has thus emerged as an efficient mean to circumvent the memory and runtime expensive grid search method. Still, the aforementioned approaches only comprise regression of T_1 and T_2 without providing a relative PD estimate so far and therefore cannot completely replace dictionary matching.

Building on these previous works, a fully-connected NN was developed in the course of this thesis that also infers a relative PD estimate together with T_1 and T_2. Only by incorporating the quantification of the relative PD within the NN framework, it can be considered a full replacement of the dictionary matching pursuit. As an alternative to synthetic MRI methods, the joint inference of T_1, T_2 and PD now enables the subsequent synthesis of clinically relevant image contrasts [99–101] with the potential to eliminate the need for additional contrast-weighted scans.

With a mainly technical focus, the NN-based T_1, T_2 and relative PD quantification was initially presented in Gómez *et al.* [7] as an integral feature of the 3D QTI acquisition and reconstruction scheme. With a particular emphasis on its clinical practicability, Section 5.1

presents an initial assessment of its feasibility for the clinical setting of routine glioma imaging and its potential for providing quantitative MRI biomarkers.

JOINT RELAXATION TIMES AND DIFFUSION TENSOR QUANTIFICATION Despite the significant technical advances, most of the novel multiparametric mapping techniques are still incapable of estimating more than two parameters at once [102]. In the context of dictionary-based parameter estimation with MRF, a potential expansion beyond the quantification of T_1, T_2 and PD generally comes along with high computational and memory burdens due to the exponential scaling of the dictionary size with the dimensionality of the parameter space. Due to its transient nature, sensitizing the signal encoding and acquisition scheme to physiological effects, such as diffusion, will also increase susceptibility to motion-induced artifacts. These reasons pose significant challenges for joint relaxation and diffusion quantification, limiting previous work to the estimation of the ADC only [103–107].

To overcome these difficulties, the underlying sequence design and the subsequent parameter inference were approached as a joint problem in Section 5.2 [1]: A MRF-type sequence was extended beyond the encoding of T_1 and T_2 to also accumulate sensitization to orientational diffusion information along the excitation train. Combining this acquisition scheme with a CNN-based multivariate regression, enables a high degree of acceleration by deliberately going against established imaging paradigms of diffusion MRI at the expense of image quality. While established (model-based) parameter mapping methods break down in such high-parametric and artifact-prone domains, the proposed CNN proved capable of recovering the implicit physical relationships between the spatiotemporal MRF data and the scalar and tensorial parameters. Finally, to demonstrate its feasibility and generalizability, parameter mapping results were reported for a cohort of healthy volunteers and multiple sclerosis patients who are expected to have significant alterations of the tissue microstructure in white matter lesions.

As such, this work constitutes a proof of concept of how DL methods can bridge the gap towards higher parametric domains that were previously out of scope with conventional parameter inference approaches. Providing multiparametric information that are naturally obtained in the same image space, facilitates data analysis immensely and is an important step towards lowering the practical barriers for comprehensive clinical diagnostics.

RETROSPECTIVE 3D MOTION CORRECTION FOR FAST MULTIPARAMETRIC MRI The recent research efforts towards faster acquisition schemes also constitute crucial advances to reduce the susceptibility to motion artifacts compared to the lengthy scan protocols of state-

of-the-art quantitative MRI exams. Nevertheless, (in-) voluntary body movements are still an omnipresent challenge in current radiological practice because motion artifacts make MRI images unusable and scans have to be repeated frequently [108]. This problem is amplified in quantitative MRI techniques in general and transient-state methods in particular. Here not only a single image but the entire temporal signal evolution is affected and eventually causes parameter misquantification. To address this problem, previous works have demonstrated motion correction approaches for MRF-type parameter mapping techniques. However, they focused almost exclusively on 2D acquisition schemes [109–111].

Going beyond the specific scenario of 2D scanning, Section 5.3 addresses the problem of subject motion for 3D fast multiparametric MRI [3]. Using 3D QTI as an example, a navigator-based realignment [112] is combined with a 3D multiscale CNN for retrospective motion correction. The CNN was trained to learn the error between the high-quality motion-free reference and the motion-affected parameter maps with remaining artifacts that could not be resolved by an initial registration-based correction due to the limited temporal resolution of the navigators. Taking advantage of the sparsity in the residual maps, the proposed two-stage correction substantially enhanced the quality of T_1, T_2 and PD maps in case of healthy volunteers as well as pediatric and adult patients with pathological findings.

Enabling fast multiparametric mapping with high immunity to subject motion is an important step to facilitate clinical routine scanning with quantitative MRI.

The use of DL methods to tailor efficient (multi-) parameter encoding and advanced reconstruction algorithms has great potential to advance the establishment of quantitative MRI for broad clinical application. With the above research at the interface of Magnetic Resonance (MR) physics and computer science, this doctoral thesis aims to contribute to the paradigm chance on the way to the ultimate goal of precision medicine and, as a first step, to make quantitative imaging biomarkers more suitable and hence more attractive for clinical practice.

Part II

PUBLICATIONS

5

PEER-REVIEWED JOURNAL AND CONFERENCE PAPERS

This chapter comprises three publications that propose DL-based improvements on the way to fast and robust multiparametric MRI. Building on the work of Gómez *et al.* [7], Accelerated 3D whole-brain T1, T2 and proton density mapping: feasibility for clinical glioma MR imaging reports clinical experience of fast, whole-brain multiparameter quantification with QTI for routine glioma imaging. In Deep learning-based parameter mapping for joint relaxation and diffusion tensor MR Fingerprinting, a novel acquisition and CNN-based parameter inference for jointly mapping T_1, T_2 and the full diffusion tensor are presented and validated. Based on these initial results in terms of clinical feasibility, a DL-based motion correction is proposed to increase robustness of the QTI framework in Residual learning for 3D motion corrected quantitative MRI: Robust clinical T1, T2 and proton density mapping.

5.1 ACCELERATED 3D WHOLE-BRAIN T1, T2 AND PROTON DENSITY MAPPING: FEASIBILITY FOR CLINICAL GLIOMA MR IMAGING

Peer-reviewed journal paper

Authors: CM. Pirkl, L. Nunez-Gonzalez, F. Kofler, S. Endt, L. Grundl, M. Golbabaee, PA. Gómez, M. Cencini, G. Buonincontri, RF. Schulte, M. Smits, B. Wiestler, BH. Menze†, MI. Menzel†, JA. Hernandez-Tamames†.

†Contributed equally

In: *Neuroradiology* (Apr. 2021). [2]

Abstract: "*Purpose* Advanced MRI-based biomarkers offer comprehensive and quantitative information for the evaluation and characterization of brain tumors. In this study, we report initial clinical experience in routine glioma imaging with a novel, fully 3D multiparametric quantitative transient-state imaging (QTI) method for tissue characterization based on T_1 and T_2 values.

Methods To demonstrate the viability of the proposed 3D QTI technique, nine glioma patients (grade II–IV), with a variety of disease states and treatment histories, were included in this study. First, we investigated the feasibility of 3D QTI ($6:25\ \mathrm{min}$ scan time) for its use in clinical routine imaging, focusing on image reconstruction, parameter estimation, and contrast-weighted image synthesis. Second, for an initial assessment of 3D QTI-based quantitative MR biomarkers, we performed a ROI-based analysis to characterize T_1 and T_2 components in tumor and peritumoral tissue.

Results The 3D acquisition combined with a compressed sensing reconstruction and neural network-based parameter inference produced parametric maps with high isotropic resolution ($1.125 \times 1.125 \times 1.125\ \mathrm{mm}^3$ voxel size) and whole-brain coverage ($22.5 \times 22.5 \times 22.5\ \mathrm{cm}^3$ FOV), enabling the synthesis of clinically relevant T_1-weighted, T_2-weighted, and Fluid-Attenuated Inversion Recovery (FLAIR) contrasts without any extra scan time. Our study revealed increased T_1 and T_2 values in tumor and peritumoral regions compared to contralateral white matter, good agreement with healthy volunteer data, and high inter-subject consistency.

Conclusion 3D QTI demonstrated comprehensive tissue assessment of tumor substructures captured in T_1 and T_2 parameters. Aiming for fast acquisition of quantitative MR biomarkers, 3D QTI has potential

to improve disease characterization in brain tumor patients under tight clinical time-constraints."

Contribution of thesis author: Conceptualization, algorithmic development and implementation, experimental design, data analysis, manuscript preparation and editing.

Neuroradiology
https://doi.org/10.1007/s00234-021-02703-0

DIAGNOSTIC NEURORADIOLOGY

Accelerated 3D whole-brain T1, T2, and proton density mapping: feasibility for clinical glioma MR imaging

Carolin M. Pirkl[1,2] · Laura Nunez-Gonzalez[3] · Florian Kofler[1] · Sebastian Endt[1,2] · Lioba Grundl[4] · Mohammad Golbabaee[5] · Pedro A. Gómez[1] · Matteo Cencini[6,7] · Guido Buonincontri[6,7] · Rolf F. Schulte[2] · Marion Smits[3] · Benedikt Wiestler[4,8] · Bjoern H. Menze[1,9] · Marion I. Menzel[2,10] · Juan A. Hernandez-Tamames[3]

Received: 1 February 2021 / Accepted: 28 March 2021

Abstract

Purpose Advanced MRI-based biomarkers offer comprehensive and quantitative information for the evaluation and characterization of brain tumors. In this study, we report initial clinical experience in routine glioma imaging with a novel, fully 3D multiparametric quantitative transient-state imaging (QTI) method for tissue characterization based on T1 and T2 values.

Methods To demonstrate the viability of the proposed 3D QTI technique, nine glioma patients (grade II–IV), with a variety of disease states and treatment histories, were included in this study. First, we investigated the feasibility of 3D QTI (6:25 min scan time) for its use in clinical routine imaging, focusing on image reconstruction, parameter estimation, and contrast-weighted image synthesis. Second, for an initial assessment of 3D QTI-based quantitative MR biomarkers, we performed a ROI-based analysis to characterize T1 and T2 components in tumor and peritumoral tissue.

Results The 3D acquisition combined with a compressed sensing reconstruction and neural network-based parameter inference produced parametric maps with high isotropic resolution ($1.125 \times 1.125 \times 1.125$ mm^3 voxel size) and whole-brain coverage ($22.5 \times 22.5 \times 22.5$ cm^3 FOV), enabling the synthesis of clinically relevant T1-weighted, T2-weighted, and FLAIR contrasts without any extra scan time. Our study revealed increased T1 and T2 values in tumor and peritumoral regions compared to contralateral white matter, good agreement with healthy volunteer data, and high inter-subject consistency.

Conclusion 3D QTI demonstrated comprehensive tissue assessment of tumor substructures captured in T1 and T2 parameters. Aiming for fast acquisition of quantitative MR biomarkers, 3D QTI has potential to improve disease characterization in brain tumor patients under tight clinical time-constraints.

Keywords MRI · Image-based biomarkers · Multiparametric imaging · Glioma imaging · Neural networks

Bjoern H. Menze, Marion I. Menzel and Juan A. Hernandez-Tamames contributed equally to this work.

✉ Carolin M. Pirkl
carolin.pirkl@tum.de

[1] Department of Computer Science, Technical University of Munich, Munich, Germany

[2] GE Healthcare, Munich, Germany

[3] Radiology & Nuclear Medicine, Erasmus MC, University Medical Center, Rotterdam, Netherlands

[4] Department of Neuroradiology, Klinikum rechts der Isar, Munich, Germany

[5] Department of Computer Science, University of Bath, Bath, UK

[6] Fondazione Imago7, Pisa, Italy

[7] IRCCS Fondazione Stella Maris, Pisa, Italy

[8] TranslaTUM - Central Institute for Translational Cancer Research, Munich, Germany

[9] Department of Quantitative Biomedicine, University of Zurich, Zurich, Switzerland

[10] Department of Physics, Technical University of Munich, Munich, Germany

Published online: 09 April 2021

Introduction

Gliomas are the most frequent primary brain tumors in adults. This diverse group of brain tumors comprises glioblastomas, astrocytomas, oligodendrogliomas, and ependymomas [1]. Although there have been great advances in glioma research, and treatment continues to evolve with new methods and strategies, gliomas remain a disease with poor prognosis [2]. State-of-the-art glioma treatment includes a multi-disciplinary approach, combining surgical resection, chemotherapy, and radiation therapy [3]. Treatment strategy and prognosis for each individual case depend on tumor grade, which is defined upon histopathologic appearance and molecular features according to the 2016 WHO criteria [4]. High-grade gliomas (grade IV), so called glioblastomas, are aggressive, fast-growing tumor types that require immediate treatment. For lower-grade gliomas (grades II, III), including various types of astrocytic, oligodendroglial, and ependymal tumors, extensive treatment is often delayed as long as possible [5].

For all types of gliomas, comprehensive multimodal neuroimaging is fundamental for disease characterization [6, 7]. It also guides the individualized therapy planning and is required to monitor treatment response and progression of the disease. Here, MRI has become the key diagnostic measure for the evaluation and characterization of brain tumors: while the multitude of image contrasts of conventional structural MRI allows for better detection of tumor-infiltrated areas, advanced image-based physiologic and molecular biomarkers have been demonstrated to offer comprehensive and quantitative information about the biological characteristics of tumor types and tumor substructures [8]. For the ultimate goal of an as-precise-as-possible therapy [9], quantitative MRI can therefore provide versatile tissue characterization [10]. This in turn is essential to better comprehend the complex proliferative and invasive behavior, to identify and describe structures of interest, such as enhancing tumor structures, or critical thresholds in a reliable and reproducible way to better predict therapy response and treatment outcomes.

Usually, long acquisition times of such conventional quantitative MR techniques, however, hinder their adoption into clinical practice. Routine imaging protocols therefore rely on mainly qualitative information so far. Also, visual inspection and qualitative interpretation are dominating clinical MRI-based diagnosis because the analysis of complex multi-parametric, multimodal, and even multi-temporal image data sets remains a major challenge. These issues, together with the lack of MRI protocol standardization [11], hamper a reliable identification of tumor substructures, render an exact quantification of infiltration patterns impossible, and complicate monitoring of treatment response in follow-up examinations.

To meet the clinical need for fast acquisition of quantitative MR biomarkers, advanced multiparametric MRI schemes have been proposed, offering reproducible and accurate diagnostic information, which is less affected by system and interpretation biases [12–16]. They all share the common goal of revealing clinically relevant tissue characteristics, which are not appropriately captured in standard qualitative MRI, with clinically practicable scan times.

Aiming for joint T1 and T2 mapping, different acquisition and data processing strategies based on (undersampled) k-space data are used to achieve optimal multiparametric estimation [12–15, 17]. In this work, we present the feasibility of a novel, fully 3D multiparametric quantitative transient-state imaging (QTI) technique [18] for simultaneous mapping of T1 and T2 relaxation times and relative proton density (PD) for use in clinical routine glioma imaging. With 3D QTI, we demonstrate a 3D acquisition with high isotropic resolution that allows us to go beyond the resolution of other recently presented quantitative MRI methods based on 2D (multi-)-slice acquisitions. We pursue a conceptionally different approach compared to steady-state magnetization techniques and acquire the signal evolution in the transient state. In

Table 1 Patient demographics, diagnoses, and treatment histories

Patient ID	Age	Gender	Diagnosis	Treatment
1	69 y	f	Giant cell glioblastoma, IDH wild type	Resection, radiation therapy, chemotherapy
2	63 y	m	Anaplastic astrocytoma (WHO grade III)	Chemotherapy
3	49 y	m	Glioblastoma, IDH wild type	Chemotherapy
4	69 y	m	Glioblastoma	Resection, chemotherapy
5	63 y	m	Transitional cell oligodendroglioma (WHO grade II)	Resection, radiation therapy
6	52 y	f	Glioblastoma	Resection, radiation therapy, chemotherapy
7	50 y	m	Oligodendroglioma (WHO grade II)	Resection, radiation therapy, chemotherapy
8	58 y	f	Anaplastic oligodendroglioma, IDH mutant and 1p/19q co-deleted	Resection, chemotherapy
9	25 y	f	Low-grade astrocytoma	Resection, chemotherapy

Table 2 MR sequence parameters

	3D QTI	T1-weighted FSPGR (T1w)	Gd-enhanced T1-weighted FSPGR (T1c)	T2-weighted PROPELLER (T2w)	CUBE FLAIR (FLAIR)
Acquisition	3D	3D	3D	2D	3D
Native resolution (mm^3)	1.125 × 1.125 × 1.125	0.47 × 0.47 × 0.8	0.47 × 0.47 × 0.8	0.5 × 0.5 × 3.3	0.8 × 0.47 × 0.47
Matrix size	200 × 200 × 200	512 × 512 × 212	512 × 512 × 212	512 × 512 × 46	192 × 512 × 512
Field of view (mm^3)	225 × 225 × 225	240 × 240 × 170	240 × 240 × 170	260 × 260 × 152	154 × 240 × 240
Slices	-	-	-	46	-
Native slice thickness (mm)	-	-	-	3.0	-
TE (ms)	1.8	2.1	2.1	120.7	92
TR (ms)	7.8	4.6	7.1	5751	5002
TI (ms)	18	-	-	-	1701
a (°)	$0.8 \leq a \leq 70$	12	12	160	90
Acquisition time (min)	6:25	1:54	4:43	5:15	4:48

contrast to Cartesian readout schemes, the combination of efficient spiral k-space (under-)sampling with transient-state imaging in 3D QTI constitutes an attractive candidate for fast multiparametric MRI under tight clinical time constraints.

As a form of clinical stress test for 3D QTI, we chose a variety of glioma patients (grades II–IV) with heterogenous disease states and treatment histories to demonstrate the viability of this technique. In this study, we focus on two main aspects:

I. Initial clinical experience with 3D QTI: We demonstrate the feasibility of this fast, multiparametric sequence with whole-brain coverage and high isotropic resolution for being used in routine brain tumor imaging protocols. We examine the applicability of 3D QTI with its clinically relevant scan time of 6:25 min, focusing on its image reconstruction and parameter estimation approaches. Based on the quantitative parameter maps, we synthesize qualitative image contrasts and explore their clinical relevance. We also assess the behavior of the 3D QTI scheme in the presence of patient movement, i.e., rigid head motion and non-rigid physiological motion.
II. Application to quantitative characterization of tumor substructures: We identify tumor tissue heterogeneity that is captured by T1 and T2 values to offer comprehensive tissue assessment of tumor substructures and quantifiable differentiation of healthy tissue. We therefore characterize T1 and T2 components in a variety of glioma patients with different disease stages and treatment histories. We aim to gain insights into potential benefits of 3D QTI in cases where pseudo-regression, pseudo-therapy response, or radiation-induced necrosis complicate follow-up assessments [19].

Materials and methods

Subjects

Within the course of this study, we collected MR data and respective demographic and clinical data from nine glioma patients who had been scheduled for follow-up clinical imaging (Table 1). The study included a variety of patients who were initially diagnosed with glioblastoma (anaplastic and low-grade), astrocytoma (transitional cell and anaplastic), or oligodendroglioma. Prior treatment strategies cover surgical resection, chemotherapy, radiation therapy, or a combination thereof.

MR imaging

Clinical contrast-weighted MRI

All MRI data were acquired on a 3T MR750 system (GE Healthcare, Milwaukee, WI) using a 16-channel head, neck, and spine array coil. The multimodal MRI protocol included a pre-contrast T1-weighted fast spoiled gradient echo (FSPGR) sequence (T1w), a T2-weighted PROPELLER sequence (T2w), and a fluid-attenuated inversion recovery (FLAIR) sequence which were followed by a gadolinium (Gd)-enhanced T1-weighted FSPGR sequence (T1c). All imaging parameters are shown in Table 2.

3D QTI acquisition and reconstruction

In addition to the clinical sequences, and before contrast agent administration, the patients were scanned with the proposed 3D QTI acquisition with an inversion time TI = 18 ms, repetition time TR = 7.8 ms, and echo time TE = 1.8 ms. Flip angles ($0.8° \leq a \leq 70°$) follow a ramp-up/ramp-down pattern,

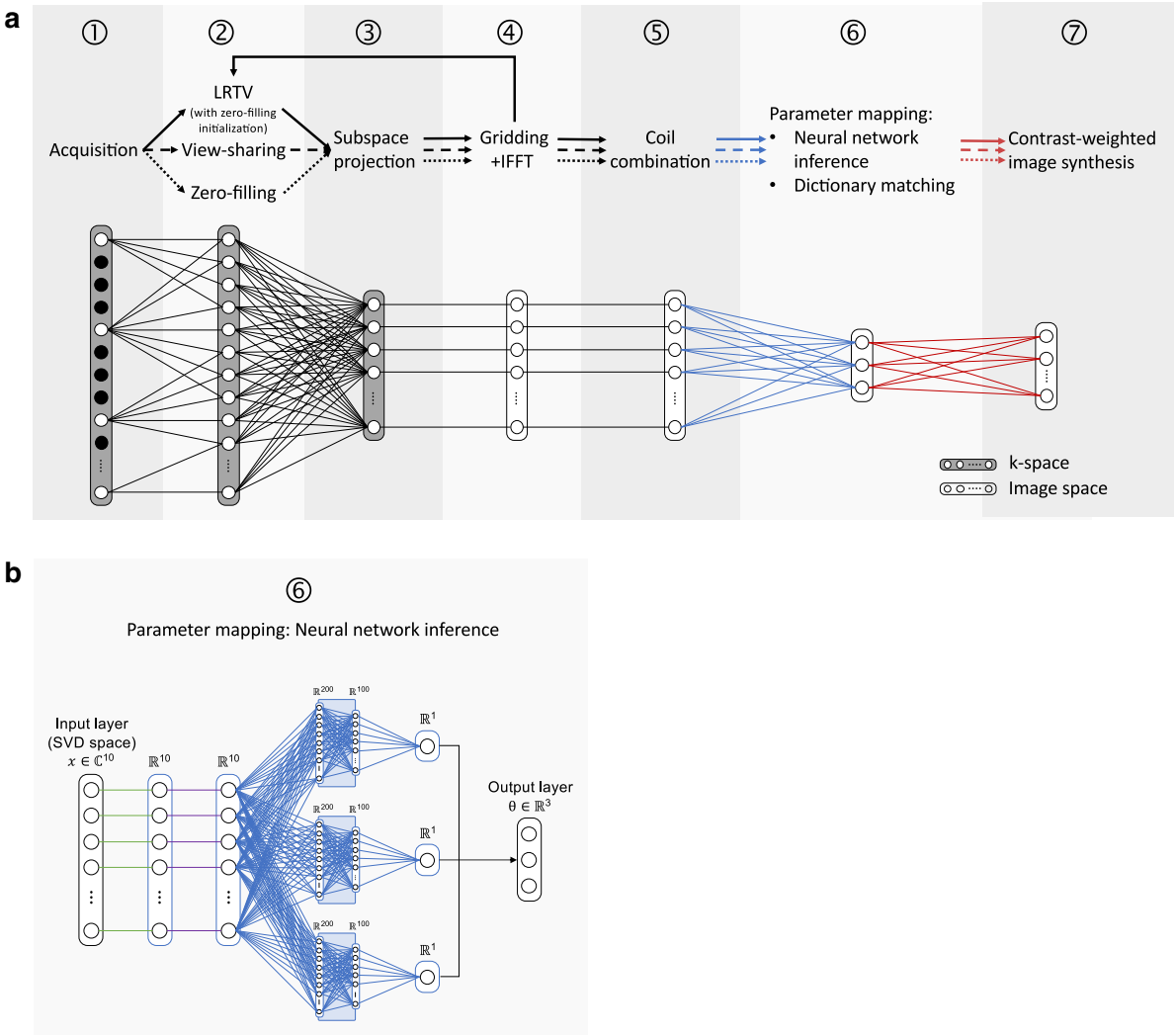

Fig. 1 3D QTI data processing. **a** Reconstruction and processing. After acquisition (①), raw k-space data is processed via naïve zero-filling (dotted line), k-space weighted view-sharing (dashed line), or a compressed sensing LRTV technique (solid line). All methods in ② are followed by dimensionality reduction via SVD subspace projection in the time domain (③), gridding onto a Cartesian grid followed by a 3D IFFT (④), and coil sensitivity estimation and combination (⑤). The reconstructed image series are then fed into a neural network or are matched to a precomputed dictionary to output parametric maps of T1, T2 and PD (⑥). We then synthesize clinical image contrasts using the parametric maps (⑦). **b** Neural network architecture for parameter inference. The model receives the complex, voxel-wise signal in SVD subspace x and infers the underlying tissue parameter vector $\boldsymbol{\theta}$ with T1, T2, and a PD-related scaling factor. The input signal $\boldsymbol{x}$ is phase-aligned (green lines) to transfer the complex into real-valued signal, followed by a normalization layer (purple lines). The model then divides into separate pathways, each with three ReLU-activated hidden layers and 200, 100, and one node, to eventually yield the concatenated parametric output vector $\boldsymbol{\theta}$

comprising 880 repetitions. Highly undersampled k-space data (undersampling factor of 628 for each of the 880 3D k-space volumes) is acquired in the transient state [16, 20] using a spiral readout ($22.5 \times 22.5 \times 22.5$ cm^3 FOV, $1.125 \times 1.125 \times 1.125$ mm^3 isotropic voxel size) with in-plane and spherical rotations to achieve full 3D coverage. The total scan time of the 3D QTI acquisition was 6:25 min.

3D QTI data was reconstructed using a compressed sensing (CS) approach with joint spatial and temporal regularizations, referred to as low-rank and total-variation (LRTV) method [21]. To demonstrate the anti-aliasing that is achieved by this iterative k-space processing, we compared this reconstruction to naïve zero-filling and k-space weighted view-sharing [22]. Figure 1 a schematically shows the 3D QTI reconstruction pipeline with these three k-space processing alternatives in step ②. In all cases, we applied dimensionality reduction via SVD subspace projection (step ③) to compress the full temporal signal evolution to its first

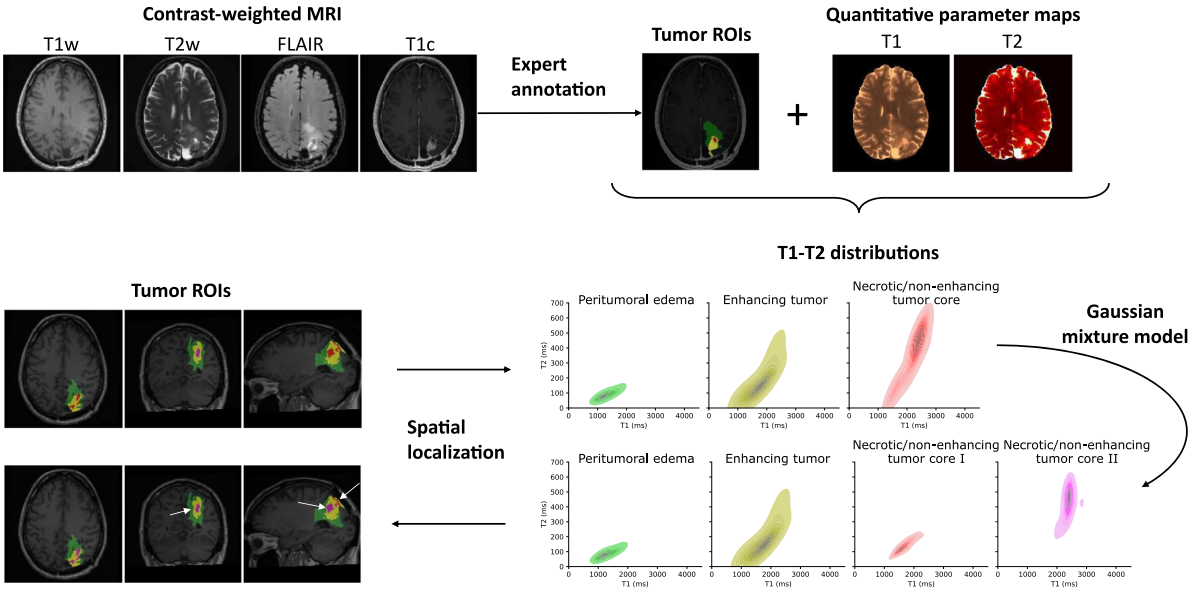

Fig. 2 Application to quantitative characterization of tumor substructures. For quantitative analysis of tumor substructures, intratumoral structures, i.e., peritumoral edema, necrotic/non-enhancing tumor core, and enhancing tumor, were annotated by a trained expert based on the clinical contrast-weighted MR data. Voxel-wise T1-T2 distributions were then derived for the individual ROIs. Using a Gaussian mixture model, we explored whether we can identify the two voxel classes that are apparent in the T1-T2 space in necrotic/non-enhancing tumor areas, which were then mapped back to the image space

ten singular images. SVD projection was followed by gridding onto a Cartesian grid using gpuNUFFT [23] and 3D inverse fast Fourier transform (IFFT, step ④). In step ⑤, coil sensitivity maps were computed using adaptive coil combination [24].

For parameter mapping in step ⑥, the reconstructed, complex SVD images were fed into a compact multi-path neural network for voxel-wise T1, T2, and PD inference, which has shown to be a time and memory-efficient alternative to conventional dictionary matching [25, 26]. Note that neural network inference and dictionary matching can be applied independent of the previously performed k-space processing.

The proposed neural network architecture, as depicted in Fig. 1b, receives the first ten singular components of the SVD compressed QTI signal $\mathbf{x}$ as input and outputs the underlying tissue parameters T1, T2, and a PD-related scaling factor, comprised in the output vector $\boldsymbol{\theta}$, with the final PD estimate $\mathrm{PD} = \frac{\|\mathbf{x}\|_2}{\theta_3}$. The latent-space input signal is phase-aligned [18], transferring the complex into a real-valued signal, and normalized in the subsequent layer. The model then splits into separate pathways, each consisting of three hidden layers with rectified linear unit (ReLU) activations and 200, 100, and one node, to eventually form the concatenated parametric output $\boldsymbol{\theta}$.

To train the neural network, we generated a dataset of synthetic QTI signals for 10 ms ≤ T1 ≤ 5000 ms and 10 ms ≤ T2 ≤ 2000 ms using the extended phase graphs formalism [27]. T1 values were sampled in steps of 10 ms for 10 ms ≤ T1 ≤ 2000 ms and in steps of 100 ms for 2100 ms ≤ T1 ≤ 5000 ms. T2 values were increased in steps of 5 ms for 10 ms ≤ T2 ≤ 300 ms and in steps of 10 ms for 310 ms ≤ T2 ≤ 2000 ms. The dataset was also used to obtain a dictionary matching reference. For model training, we used 80% of the samples in the simulated dataset and added white complex Gaussian noise to the generated signal time-series. The network was trained for a maximum of 1000 epochs with mean absolute percentage error loss and stochastic gradient descent optimization with a learning rate of 1e-4 and a dropout rate of 0.8. We kept the model state that achieved the best validation loss for the remaining 20% of the signals.

With the obtained T1, T2, and PD estimates, we generated synthetic T1-weighted, T2-weighted, and T2-weighted FLAIR image contrasts by applying the respective voxel-wise signal equations to the estimated parameter maps, as motivated by [18, 28]. To assess the quality of the synthetic images, we evaluated them against the corresponding acquisitions in the clinical protocol.

Annotation and quantitative analysis of tumor substructures

For quantitative analysis of tumor substructures in terms of T1 and T2 parameter values, as schematically shown in Fig. 2, intra-tumoral structures—peritumoral edema, necrotic/non-enhancing tumor core, and enhancing tumor core—were annotated by a trained radiologist using ITK SNAP [29] in each

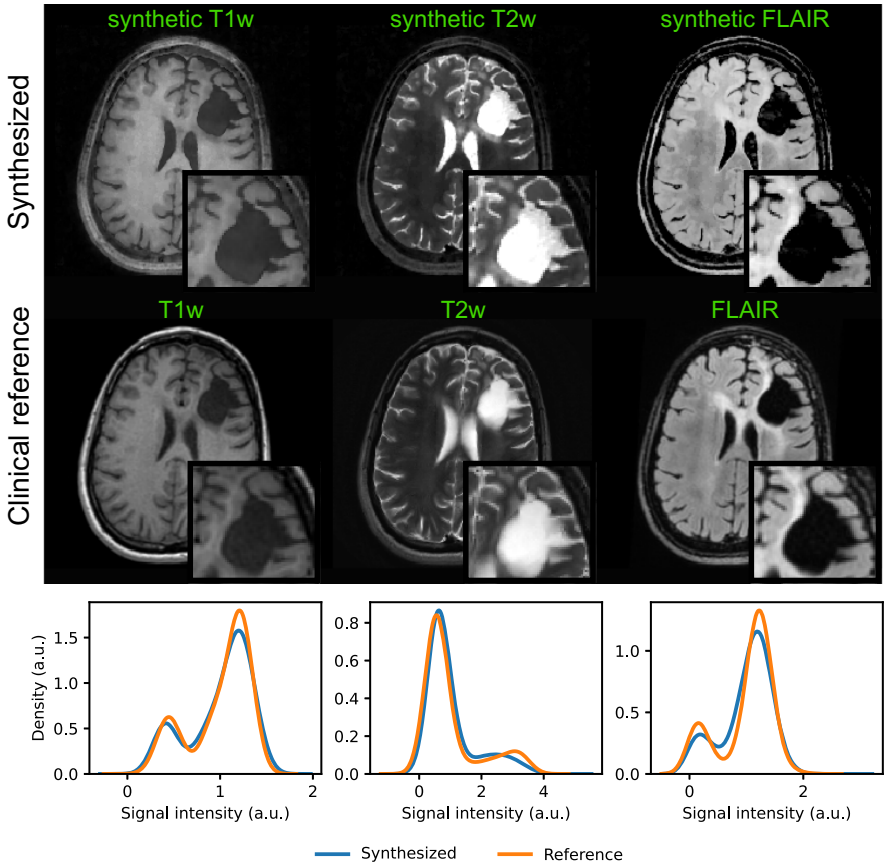

Fig. 3 Contrast-weighted image synthesis for a representative patient case. From the T1, T2, and PD maps, we produce clinically relevant, fully 3D qualitative image information with high isotropic resolution and without additional scan time. As seen from the axial views and the histogram-based comparison considering the whole image volumes, synthetic T1-weighted, T2-weighted, and FLAIR MRI contrasts correspond to the clinical reference acquisitions. Corresponding sagittal and coronal views are shown in Fig. 11

patient dataset based on the clinical contrast-weighted MRI data. The T1-weighted, T2-weighted, FLAIR, and Gd-enhanced T1-weighted images were therefore transformed into the 3D QTI image space using ANTs [30].

In addition to the tumor annotations, we obtained white matter (WM) and gray matter (GM) tissue segmentations using the FSL FAST algorithm [31], which we applied to the synthesized T1-weighted image data. For the glioma patients, we only considered contralateral WM and GM. If the tumor or its peritumoral tissue affected both hemispheres, normal-appearing WM and GM regions were delineated in the hemisphere with less tumor-affected volume.

Voxel-wise T1-T2 distributions were then identified for individual ROIs. We also compared ROI-based mean T1 and T2 among individual patients. For an initial attempt to explore whether the obtained T1 and T2 information allows us to go beyond the manual segmentation, we fitted a Gaussian mixture model to the T1-T2 space of all necrotic/non-enhancing voxels in the cohort to understand whether we can identify the two apparent tissue types, which we attribute to solid tumor (necrotic/non-enhancing tumor core I) and fluidic tissue voxels (necrotic/non-enhancing tumor core II) therein. The fitted model was then applied to the individual patient datasets to disentangle the voxels in the necrotic/non-enhancing ROI into two classes. The thereby obtained subclassification of necrotic/non-enhancing voxels was then mapped back to the anatomical context to complement the clinical baseline labeling based on qualitative visual MRI contrasts

Results

We first present and evaluate the 3D QTI method with its modular data processing pipeline. Accuracy and precision of acquisition and reconstruction elements of 3D QTI were evaluated in [18, 21, 32]. Focus of the work presented here is to assess the applicability of 3D QTI for clinical routine imaging in terms of reconstruction performance and image quality of the multiparametric maps. We then use the multiparametric output of 3D QTI to identify tumor tissue heterogeneity and to understand whether this allows a quantifiable differentiation of tumor substructures and healthy tissue in cancer patients.

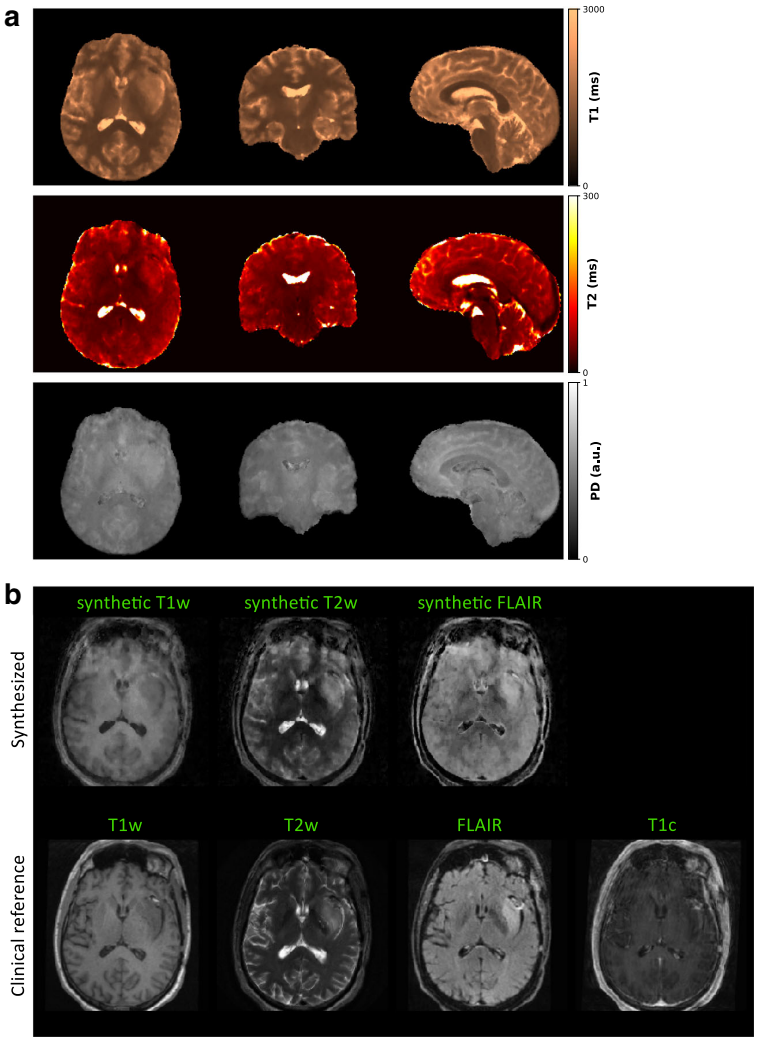

Fig. 4 Sensitivity to rigid head motion. Profuse head motion can affect image acquisition in the transient-state, which leads to image degradation in the parametric maps (**a**) and the synthetic image contrasts (**b**) compared to the clinical contrast-weighted acquisitions. The post-contrast T1-weighted MRI indicates that state-of-the-art conventional MRI cannot fully recoup the pronounced head motion in this case. Corresponding sagittal and coronal views are shown in Fig. 12

Initial clinical experience with 3D QTI

Figure 9 illustrates the isotropic 3D maps of T1, T2, and PD that we obtained from the three reconstruction modules with subsequent dictionary matching for a representative patient case and a healthy volunteer. All subsequent results in this study rely on LRTV-based image reconstruction. Figure 10 shows parameter quantification results obtained via neural network-based inference and conventional dictionary matching for a representative patient dataset and a healthy volunteer. From the estimated T1, T2, and PD maps, we synthesized common MRI contrasts using the respective MR signal equations. In Fig. 3 and Fig. 11, we compare the synthetic images for T1-weighted, T2-weighted, and FLAIR image contrasts to the images that were acquired as part of the clinical protocols. As part of the sensitivity analysis towards rigid head movements and physiological motion, Fig. 4 and Fig. 12 show an exemplary case of pronounced patient movement, where motion-related artifacts degrade the image quality in the parametric maps and therefore affect the synthesized MRI contrasts. From Fig. 5 and Fig. 12, we observe how physiological motion, such as blood flow and CSF pulsation effects, impact parameter quantification and subsequent contrast-weighted image synthesis.

Application to quantitative characterization of tumor substructures

Figure 6 gives an overview of the tumor ROI annotations together with the clinical contrast-weighted MRIs and the obtained T1 and T2 maps for all patients. In all cases, tumor core (red annotation) and peritumoral edema regions (green

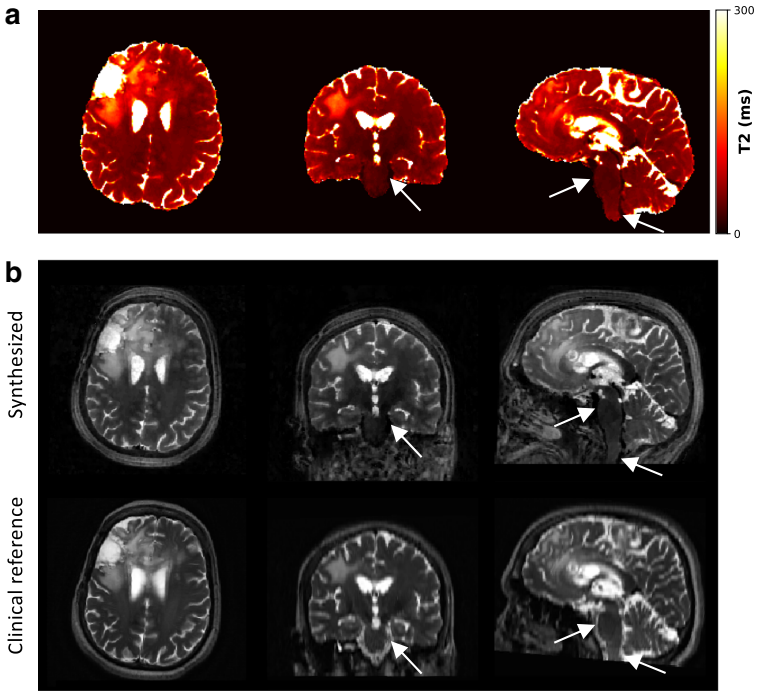

Fig. 5 Sensitivity to physiological motion. Pulsating blood flow and thereby induced pulsation of the cerebrospinal fluid (CSF) can impact the T2 estimation (**a**) and subsequent synthesis of T2-weighted image contrasts (**b**) as observed in large vessels and in regions with high CSF pulsation, e.g., along the brainstem (white arrows)

annotation) appear hyperintense on the conventional T2-weighted and FLAIR images and hypointense on T1-weighted images, relative to normal appearing tissue. T1 and T2 values obtained in these regions are higher compared to healthy tissue areas. Post-contrast T1-weighted images of patients 1 to 4 and 6 additionally identify areas with Gd enhancement (yellow annotation). Patients 3, 4, and 6 are cases with clearly visible gross tumor volumes. For patients 1 and 8, contrast-weighted MRIs do not indicate tumor relapse around the resection cavities. In case of patient 8, there are small tumor-suspected findings in the corpus callosum and the left anterior horn of the lateral ventricle without hyperintensities in the post-contrast T1-weighted MRI. In case of patient 1, the post-contrast MRI reveals small findings that are positive for Gd enhancement. For patient 2, there are small, discrete areas of Gd enhancement, which might indicate diffuse tumor growth, surrounded by edema. For patient case 5, 7, and 9, there is no clear sign for tumor reoccurrence after resection. In these cases, tumor ROIs only comprise areas of peritumoral edema and gliosis.

Figure 7 illustrates exemplary results for patient case 4 and 6 that we obtained from the Gaussian mixture model, when trained on all voxels in the patients' dataset labeled as necrotic/non-enhancing tumor tissue. The two voxel types, i.e., necrotic/non-enhancing tumor I (red) and necrotic/non-enhancing tumor core II (magenta) that are identified in the T1-T2 parameter space were projected back into the anatomical context to complement the manual ROI segmentation. Figure 8 and Table 3 quantitatively summarize the ROI-based analysis of tumor substructures. Quantitative T1 and T2 mapping results obtained in a healthy volunteer are reported in Table 4.

Discussion

This study aimed to evaluate the feasibility of 3D quantitative transient-state imaging (QTI) for clinical imaging of glioma patients. First, we demonstrated a feasibility analysis of QTI-based, fully 3D multiparametric MRI for integration into state-of-the-art clinical routine brain tumor protocols with strict requirements regarding acquisition times and robustness. Second, we showed that 3D QTI offers comprehensive characterization of both healthy and diseased tissue in a variety of brain tumor patients. Despite the heterogeneity of the patient cohort, this approach captures tissue heterogeneity in tumor substructures based on quantifiable T1 and T2 parameters.

Initial clinical experience with 3D QTI

Multiparametric mapping

Initial experience with 3D QTI in glioma patients demonstrated fully quantitative, multiparametric MR mapping with high isotropic resolution and an acquisition time of 6:25 min that make it feasible for use under tight clinical time

constraints. We observed that parameter quantification is consistent across the different reconstruction approaches provided by the 3D QTI pipeline, i.e., zero-filling, view-sharing, and LRTV methods (Fig. 9). This is in correspondence with previous study results [18, 21]. View-sharing and LRTV reconstruction can improve spatial consistency in the reconstructed SVD image series compared to naïve zero-filling as reflected in an increased image quality of the inferred parameter maps. The iterative LRTV reconstruction with joint spatio-temporal regularization achieves best suppression of aliasing artifacts. It provides best image quality and maintains clinically important tissue changes and critical tissue interfaces within tumor and peritumoral regions. That is, complementing the fast 3D QTI acquisition with a compressed sensing reconstruction with joint spatio-temporal regularization has demonstrated convincing capacities to suppress aliasing artifacts, producing high-quality parametric maps. In 3D QTI, acquisition and reconstruction are well aligned, allowing to successfully mitigate inherent practical concerns of spiral sampling such as gradient imperfections or spiral artifacts due to a massively undersampled k-space. As such, we take advantage of the high scanning efficiency of spiral trajectories and use it in clinical routine imaging, as an alternative to the prevalent Cartesian readout schemes. Based on the initial results presented here, we are confident that we can further advance 3D QTI, e.g., to smaller voxel sizes or faster scanning times.

Comparison of neural network-based inference and dictionary matching (Fig. 10) showed that both approaches produce T1, T2, and PD maps that are largely consistent in terms of quantification accuracy and image quality as previously shown by Gómez et al. [18]. As such, the neural network provides high-resolution maps with quantification accuracy and image quality comparable to dictionary matching. This is observed for healthy tissue, i.e., of the volunteer scan and normal-appearing tissue regions in glioma patients, as well as in tumor regions with alterations of the tissue microstructure.

With the combination of the CS-based LRTV reconstruction and the neural network-based parameter inference, we therefore present a memory-efficient, dictionary-free reconstruction pipeline.

Synthetic MRI

Given the premise of an as-short-as-possible imaging protocol, we have shown that contrast-weighted image synthesis based on the multiparametric 3D QTI output can produce fully 3D, high-quality, and clinically relevant qualitative information without prolonging the scan session (Fig. 3). As such, it offers an attractive feature with the potential to replace conventional contrast-weighted acquisitions, including T1-weighted, T2-weighted, and FLAIR contrasts, to potentially reduce the required scan times of routine brain imaging protocols (Table 2). Note that the synthetic contrast-weighted MRIs are naturally obtained in the same image space. That is, expensive processing, i.e., co-registration and resampling of image volumes, which is generally a key requirement in multimodal studies in order to homogenize the individual datasets, becomes redundant. So far, image synthesis based on T1, T2, and PD estimates is confined to native, i.e., pre-contrast image contrasts, and can therefore not replace Gd-enhanced acquisitions yet. In light of the ongoing research efforts to reduce the use of contrast agents to an absolute minimum, there have been initial studies suggesting that T1-relaxometry can potentially provide equivalent insights into tissue characteristics as qualitative post-contrast information [33]. However, based on our results, we cannot draw such conclusions solely based on native T1 and T2 parameters, i.e., without the inclusion of diffusion information which is also part of recent research works [34–37].

Motion sensitivity

Subject motion is known to affect the quality of the reconstructed transient-state image time-series, which then propagates to the estimation of tissue parameters [38, 39]. 3D QTI was found to be tolerant to marginal head movements so that we achieved image qualities of the parametric maps comparable to qualitative, state-of-the-art protocols. We attribute this to the fast acquisition based on undersampled spiral readouts, which repeatedly sample the k-space center and are therefore more robust to motion already in the first place. This is particularly advantageous for severely diseased patients with difficulties to lie still during lengthy scanning sessions. However, initial experience also revealed that more pronounced patient motion can degrade the image quality of reconstructed image time-series and biases estimated parameter maps (Fig. 4). The axial, sagittal, and coronal views showcase that depending on the actual motion pattern, image quality is not homogeneously degraded in all spatial directions. For instance, despite the motion-caused image blurring, image quality in the sagittal direction of the motion-affected synthetic T2-weighted image is still comparable to the clinical T2-weighted PROPELLER acquisition with a native slice thickness of 3 mm and thus lower spatial resolution in this direction. Further, from the image artifacts that are apparent in the post-contrast T1-weighted MRI, it becomes clear that patient motion is also a major challenge in state-of-the-art conventional MRI. While patient motion manifests as diffuse image blurring in case of the spiral 3D QTI readout, we observe typical ghosting artifacts for the Cartesian readout scheme of the clinical post-contrast T1-weighted scan due to the unique frequency- and phase-encoding directions. Combining the 3D QTI

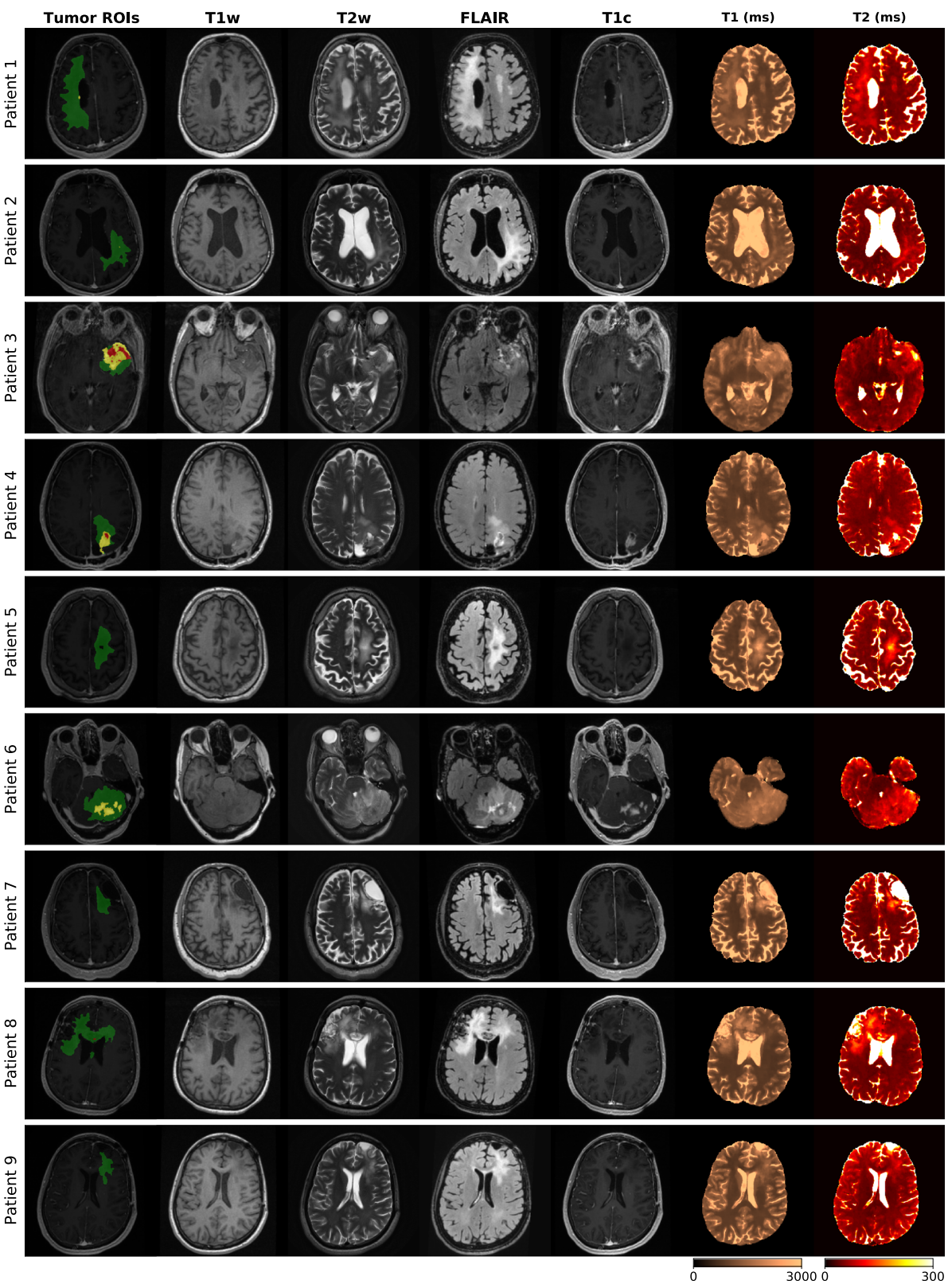
Tumor ROIs
T1w
T2w
FLAIR
T1c
T1 (ms)
T2 (ms)
Patient 1
Patient 2
Patient 3
Patient 4
Patient 5
Patient 6
Patient 7
Patient 8
Patient 9
0
3000
0
300

◀ **Fig. 6** Qualitative comparison of tumor patient cases. Expert ROIs (green: peritumoral edema, red: necrotic core/non-enhancing tumor, yellow: enhancing tumor) are shown together with clinical T1-weighted FSPGR, T2-weighted, FLAIR, Gd-enhanced T1-weighted FSPGR images and quantitative T1 and T2 maps

framework with a motion correction algorithm was previously shown to improve its robustness and can correct for patient motion [38]. Currently, this method can only correct for movements on a 7-s timescale, which could not sufficiently resolve the image degradation for the motion-affected patient case in our study.

In the same fashion as rigid head motion, the pulsating blood flow and the thereby induced pulsation of the cerebrospinal fluid (CSF) impact parameter estimation (Fig. 5). This is particularly seen in large vessels and in regions with high CSF pulsation, e.g., along the brainstem. Here, T2 values in the flowing blood are underestimated, which then reflects in lower signal intensities in the synthesized T2-weighted MRI compared to the clinical acquisition.

Given these findings, it is subject to our current and future work to also resolve motion on a faster scale, such as continuous rigid head motion, and to reduce sensitivity to physiological motion due to blood flow and/or brain pulsation.

Application to quantitative characterization of tumor substructures

Current state-of-the-art

Combination of advanced quantitative MR techniques together with contrast-weighted MRI has been shown to provide clinically relevant tissue information and is a key feature for precise tumor diagnostics: to date, state-of-the-art clinical routine MRI protocols, with acquisition times ranging from 20 to 60 min, generally comprise pre- and post-contrast T1-weighted, T2-weighted, and FLAIR sequences, which can be extended by T2*-weighted or susceptibility-weighted contrasts. Qualitative imaging is complemented by advanced quantitative MRI [40, 41] to capture tumor morphology and functionality, namely diffusion-weighted imaging and perfusion MRI [10]. Also, MR spectroscopy is used to improve brain tumor diagnostics and grading, although usually not as part of routine imaging. Diffusion tensor imaging and functional MRI provide essential information for surgery planning and guide tumor resection, as they inform the identification of tumor boundaries as well as localization of critical functional areas and neuron tracts.

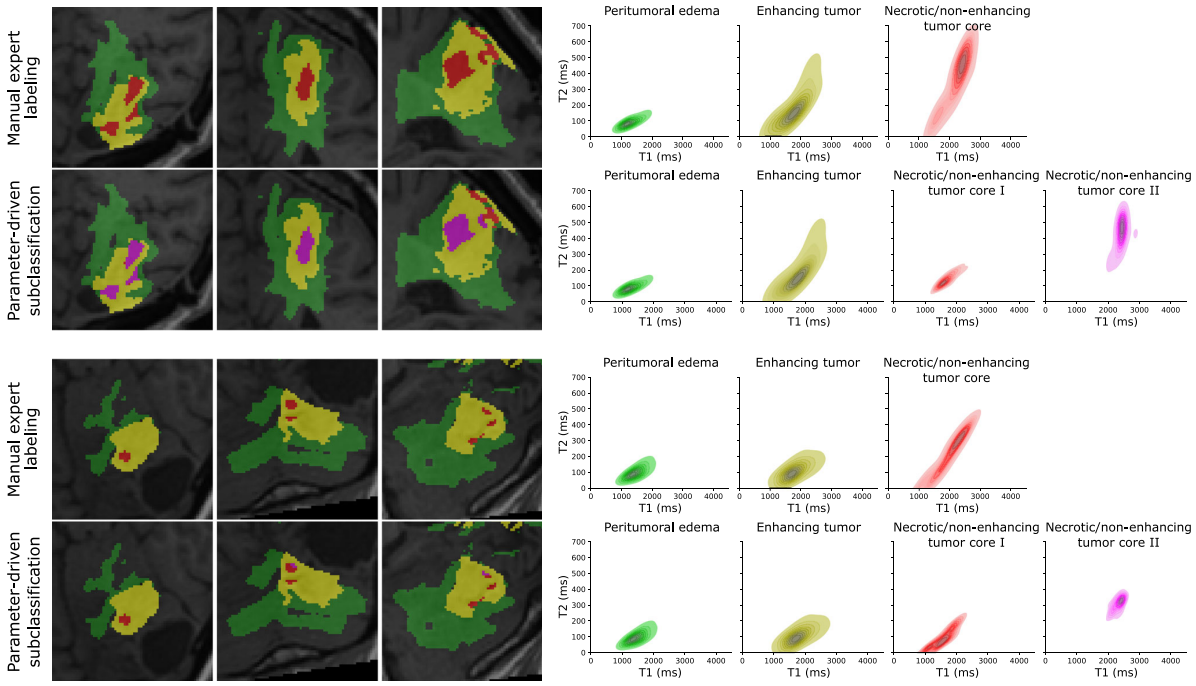

Fig. 7 Qualitative T1-T2-analysis based on manual ROI annotations together with additional explorative parameter-driven tumor subclassification for two representative patient cases. Classification of necrotic/non-enhancing tissue voxels based on quantitative T1 and T2 values can give more insights into the heterogenous structure, which we attribute to fluidic (necrotic/non-enhancing tumor core II, magenta) and solid (necrotic/non-enhancing tumor core I, red) components, within the gross tumor regions (right). Expected spatial correlations of the two subcomponents are maintained as the back-projection of the T1-T2-based classification of necrotic and solid tissue results in connected annotations (left)

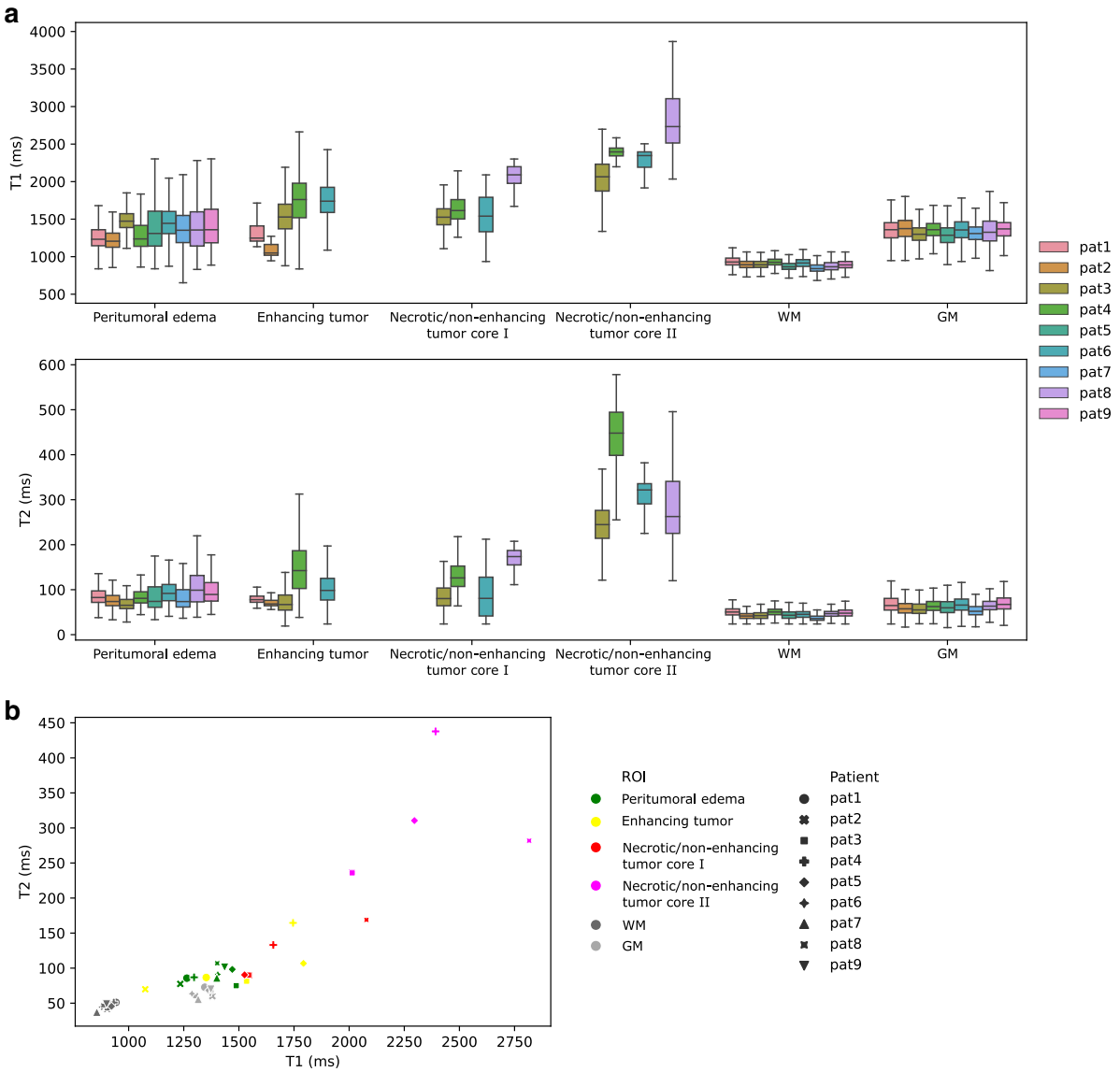

Fig. 8 Quantitative ROI-based parameter analysis. Boxplots of the patient-wise T1 and T2 parameter spaces (**a**) and a scatter plot of the respective mean T1 and T2 values (**b**) indicate increased T1 and T2 values in diseased, tumorous regions compared to healthy, contralateral WM and GM regions with high inter-subject consistency and small variance. Outliers in the boxplots are omitted for clarity

Beyond the mentioned quantitative MRI schemes, which already made their way into clinical routine, several studies have shown that MR relaxometry can provide additional, clinically relevant information about critical tissue changes in gliomas that are not visible in contrast-weighted MRIs [42–44]. Among other findings, quantitative T1 and T2 mapping has been demonstrated to aid earlier detection of tumor progression compared to standard contrast-weighted MR imaging, due to an increase in T1 and T2 values in recurring glioblastoma [45, 46]. It has also been shown that detection of tissue changes in peritumoral regions can benefit from quantitative T1 and T2 mapping due to their earlier sensitivity compared to contrast-weighted MRI [47].

Although above mentioned methods have proven to offer critical measures for disease characterization and prognosis, they often require expensive off-line processing, involve case-specific tuning of sequence settings, or cannot meet the clinical time-constraints that challenge their standard use in clinical brain tumor imaging protocols.

A variety of advanced multiparametric relaxometry techniques [12, 13, 48], including the pioneering work on MR

Table 3 Quantitative summary of T1 and T2 values (mean, standard deviation) of the tumor ROIs and contralateral WM and GM regions

ROI	T1 (ms)		T2 (ms)	
	Mean	Std	Mean	Std
Enhancing tumor	1685	340	111	70
Necrotic/non-enhancing tumor core I	1550	195	92	38
Necrotic/non-enhancing tumor core II	2188	375	297	111
Peritumoral edema	1369	264	91	35
WM	903	76	46	11
GM	1353	184	66	24

fingerprinting (MRF) [14, 28], have been shown to offer fast, robust, and user-friendly quantitative MRI to be easily integrated into radiological practice. Its attractiveness in terms of scan times together with its high degree of repeatability [32, 49, 50] makes these techniques attractive candidates for providing relaxometry-based biomarkers in day-to-day brain tumor diagnosis.

Despite the increasing number of recent works that focus on transient-state-based relaxometry techniques, there is only a modest number of studies to investigate their feasibility in disease-specific setups, such as glioma imaging [51–53]. These works have for example demonstrated the feasibility of MRF for brain tumor characterization. While these studies are based on 2D acquisitions with discrete slices placed in the tumor regions, our results in a patient cohort with a realistic, heterogenous clinical picture in terms of disease and treatment histories (Table 1, Fig. 6) demonstrate a fully 3D whole-brain quantitative analysis of tumor information captured in T1 and T2 estimates.

Qualitative comparison of the tumor cases

Our feasibility study of a variety of glioma patients showed that 3D QTI can be viable for tissue characterization and discrimination. Qualitatively, a ROI-based analysis of voxel-wise T1 and T2 relationships revealed homogenous distributions for peritumoral edema and enhancing tumor regions. In case of necrotic/non-enhancing tumor tissue, T1-T2 parameter spaces seemed to be composed of two classes, which we attributed to fluidic and solid tissue components within the gross tumor. Building on the clinical expert annotation, we aimed to gain more insight into necrotic/non-enhancing tumor tissue and explored whether a Gaussian mixture model can disentangle these two voxel classes (Fig. 7). Linking the thereby identified tissue subclasses to the anatomical space reveal spatially well-connected annotations. In clinical routine tumor annotation, solid and fluidic parts within the necrotic/non-enhancing tumor regions are generally not differentiated and comprised in one overall ROI. That is why we do not have a reference annotation to compare the results of the Gaussian mixture model with. Nevertheless, we believe that our explorative analysis is an illustrative example of how quantitative, multiparametric measures of the underlying relaxation times can complement tumor annotations that are generally based on qualitative, visual abnormalities in contrast-weighted MR image data.

Table 4 Quantitative summary of T1 and T2 values (mean, standard deviation) of WM and GM regions in a healthy volunteer

ROI	T1 (ms)		T2 (ms)	
	Mean	Std	Mean	Std
GM	1331	137	66	12
WM	871	77	45	7

Quantitative analysis of tumor substructures

Quantitative analysis (Fig. 8 and Table 3) substantiated and complemented these qualitative findings. We observed that tumor tissue, i.e., enhancing tumor, necrotic/non-enhancing tumor core I + II, as well as peritumoral edema, exhibit higher T1 and T2 values than healthy contralateral WM, as qualitatively suggested from Fig. 6. These findings are in line with initial clinical outcomes of MR fingerprinting [51], supporting the potential of 3D QTI as an image-based biomarker for glioma diagnosis.

Figure 8 also suggests well-defined parameter spaces for healthy WM and GM regions among the patient cohort with only small inter-subject variations. Also, T1 and T2 mapping in non-diseased tissue was found to agree well with our results for healthy volunteer data, as suggested by Table 3 and Table 4, and is consistent with previously reported values [18, 38, 54, 55]. Furthermore, mean T1 and T2 values of the two gross tumor subclasses are well distinguished. That is, mean T1 and T2 values for necrotic/non-enhancing tumor core II, which we attributed to the fluidic subcomponent, are constantly higher than for necrotic tumor/non-enhancing core I. This finding agrees with the fact that T1 and T2 relaxation times are sensitive to tissue composition and microstructure [56, 57].

Overall, T1 and T2 values suggest a clear distinction between peritumoral edema and contralateral WM (Fig. 8b). Also, mean T2 values in peritumoral edema were higher than for contralateral GM in all patients. Mean T1 values in peritumoral edema were lower compared to necrotic/non-enhancing tumor regions. For mean T2 values, this is only observed in case of patients 4 and 8. As observed from Fig. 8b, enhancing tumor overlays with peritumoral edema and necrotic/non-enhancing tumor core I in the T1-T2 space.

Enhancing tumor is segmented as those regions within the gross tumor that exhibit positive Gd enhancement in the Gd-enhanced T1-weighted MRI. Native pre-contrast T1 maps hence do not necessarily capture this differentiation.

Due to the observed inter-subject consistency and stability of T1 and T2 values of healthy and diseased tissue, which is in line with previously performed repeatability studies [32, 58, 59], we believe that not only diagnosis but also treatment planning and monitoring as well as prognostic, longitudinal assessment might benefit from an integration of 3D QTI into standard clinical imaging.

While conventional contrast-weighted MRI can also capture tissue heterogeneity in tumor texture, it always represents weighted information of a combination of relaxation and tissue parameters. Also, qualitative MRI information is known to depend on the actual scanner settings, which can vary from day to day due to different pre-scan conditions or gain tunings, hampering longitudinal or inter-subject comparisons.

Despite the mentioned benefits of fast multiparametric mapping techniques, we emphasize that both quantitative and qualitative MRI are generally limited to macroscopic voxel sizes. Resulting partial volume effects, e.g., at the border of distinct tissue types, are known to mask the underlying cellular tissue characteristics, only providing an effective voxel value of the respective biomarker. However, aiming for high isotropic resolution with sufficient SNR, as in case of 3D QTI, minimizes partial volume effects in the first place. Comparing the synthetic T2-weighted MRI generated from the 3D QTI scan with the clinical 2D reference with higher slice thickness in Fig. 3 illustrates this resolution benefit, e.g., for tumor delineation.

Nevertheless, with 3D QTI producing reliable, reproducible, quantitative image data, it may be a valuable tool for the harmonization of imaging data with the opportunity to make multi-timepoint, multi-subject, multi-vendor, and multi-center studies easier. As such, it can offer a rich set of standardized, comprehensive image data with the potential to also advance methodological developments along the large spectrum of AI-based decision support, i.e., segmentation algorithms or tumor growth modeling.

Limitations

A clear limitation to this study is the rather small sample size. We aimed to present an initial clinical case study demonstrating the feasibility of 3D QTI for integration into routine glioma imaging protocols. As such, the rather small but heterogenous study cohort, comprising both pre- and post-surgery treatment stages as well as different tumor grades, allowed us to nevertheless cover the bandwidth of patient cases in clinical radiological practice.

Outlook

Given our initial clinical results, we would like to employ 3D QTI also for longitudinal follow-up of glioma patients to evaluate its potential for monitoring and quantifying treatment response in individual subjects to support individualized therapy decisions with the aim of personalized medicine. We also plan to investigate how deep learning-based segmentation and interpretation of images [60, 61] could benefit from complementing or even replacing the to-date mainly qualitative data bases with quantitative imaging biomarkers, e.g., as provided by 3D QTI. Furthermore, we believe that extending the method to jointly encode relaxation and diffusion parameters as proposed in [37] with fully 3D, high isotropic resolution, and whole-brain coverage can further improve its attractiveness for integration into clinical glioma imaging and is hence subject of our current work. We also aim to further increase motion robustness of the transient-state encoding scheme. Building on the previously presented retrospective motion correction [38], we are optimistic that we can further develop this approach to account and correct for head motion on a faster time scale. We might also benefit from recent advances on prospective motion correction [62]. To reduce the sensitivity to non-rigid motion, such as blood flow and/or brain pulsation, in first place, it is subject to our future work to investigate potential refinements in the sequence design. The experience with 3D QTI in neuro applications also motivates us to target potential diagnostic scenarios outside the brain as well as in combination with contrast enhancement [63, 64].

Conclusion

3D QTI demonstrated to reliably identify tissue and hence tumor heterogeneity that is captured in T1 and T2 relaxation times under tight clinical time constraints. As such, it offers comprehensive tissue assessment of tumor substructures with the potential to improve disease characterization in brain tumor patients. This is essential to find the optimal treatment strategy and to monitor treatment response along the course of disease.

Appendix

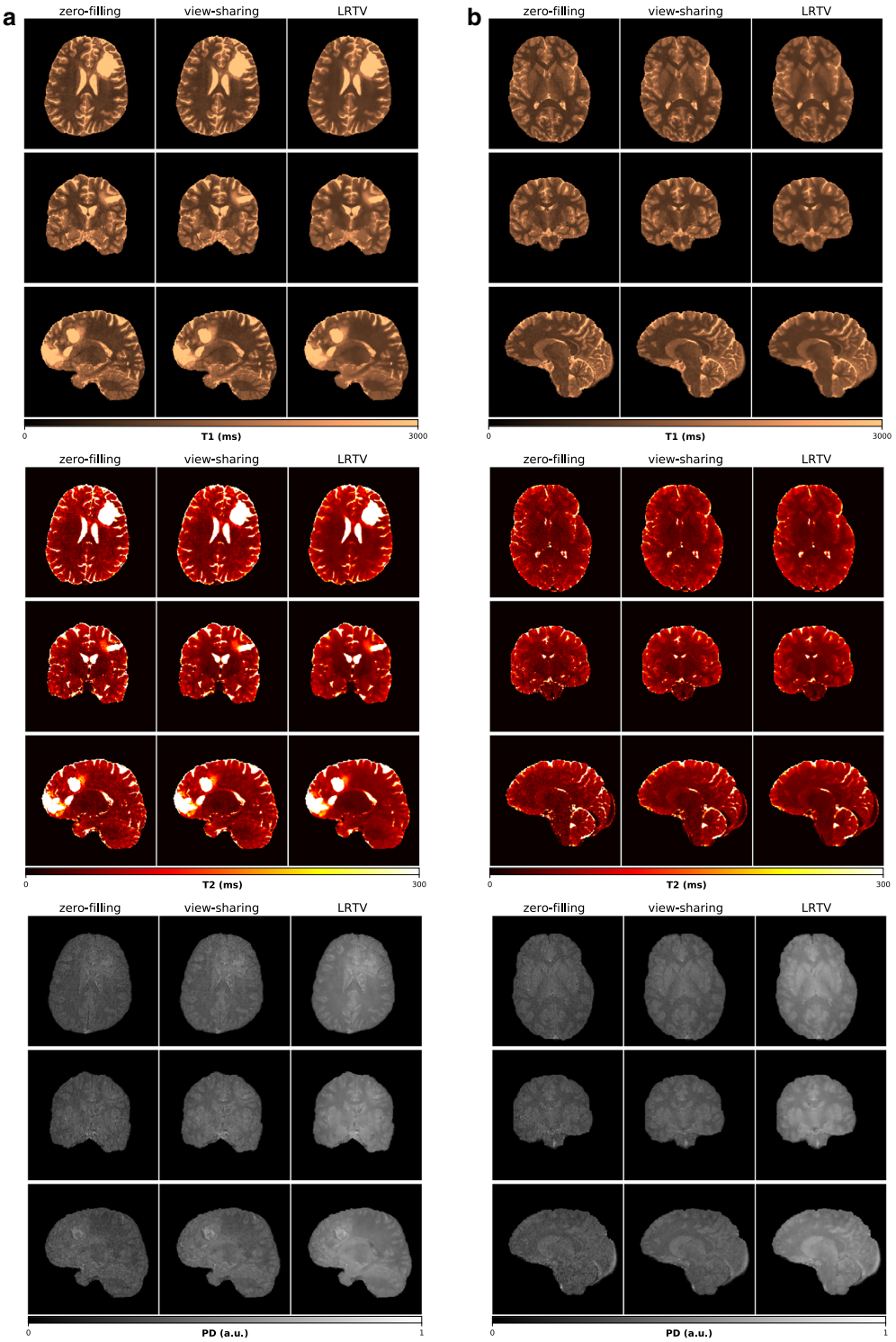

Fig. 9 Parametric maps of T1, T2, and PD obtained with zero-filling, k-space weighted view-sharing, and LRTV reconstructions and subsequent dictionary matching for a representative patient case (**a**) and a healthy volunteer (**b**). Parameter estimation is consistent across all reconstruction approaches. View-sharing reconstruction provides better image quality in the quantitative maps than zero-filling with best reduction of undersampling artifacts obtained with LRTV reconstruction

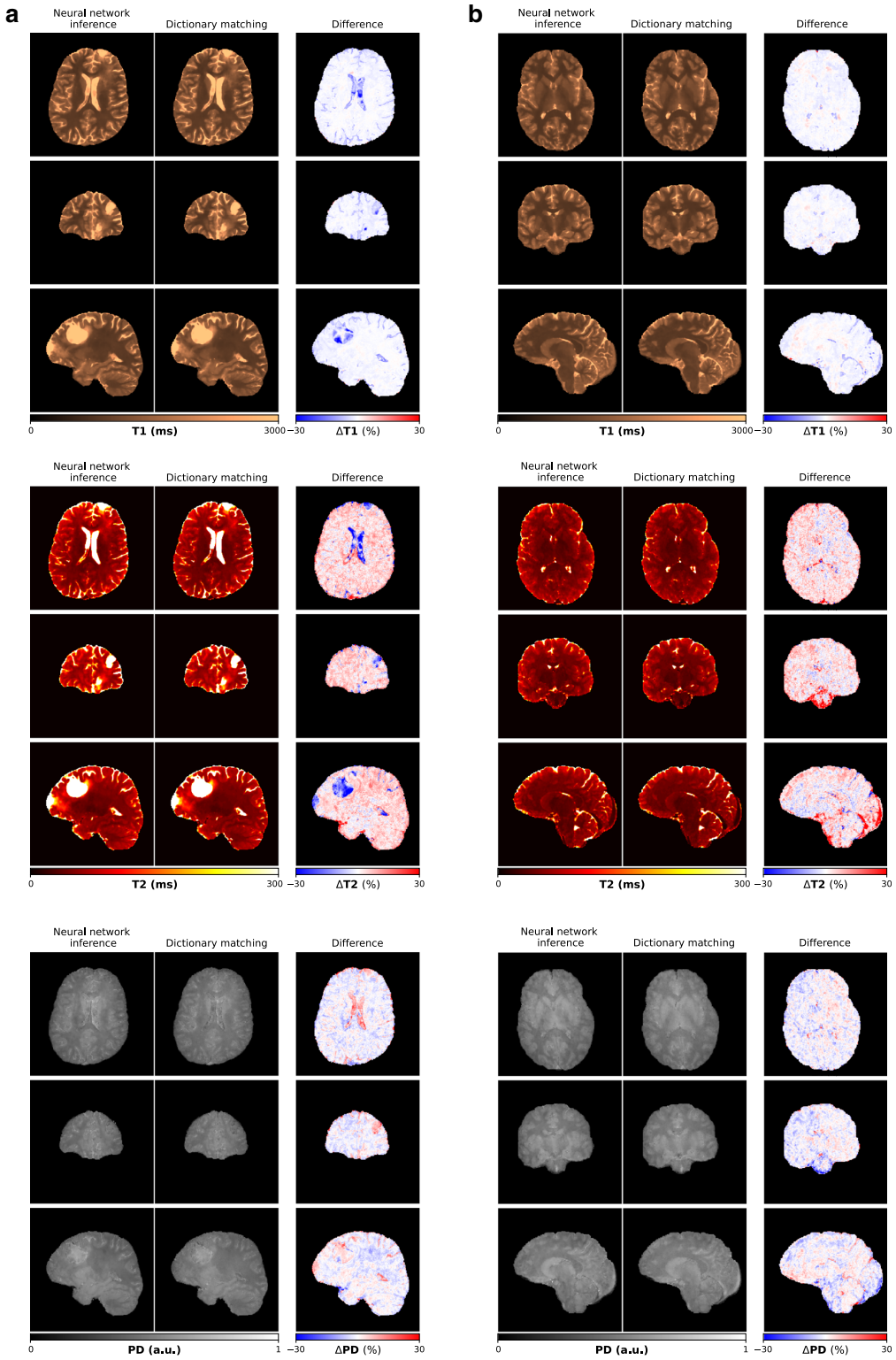
a
b
Neural network inference
Dictionary matching
Difference
0
T1 (ms)
3000
−30
ΔT1 (%)
30
T2 (ms)
300
ΔT2 (%)
PD (a.u.)
1
ΔPD (%)

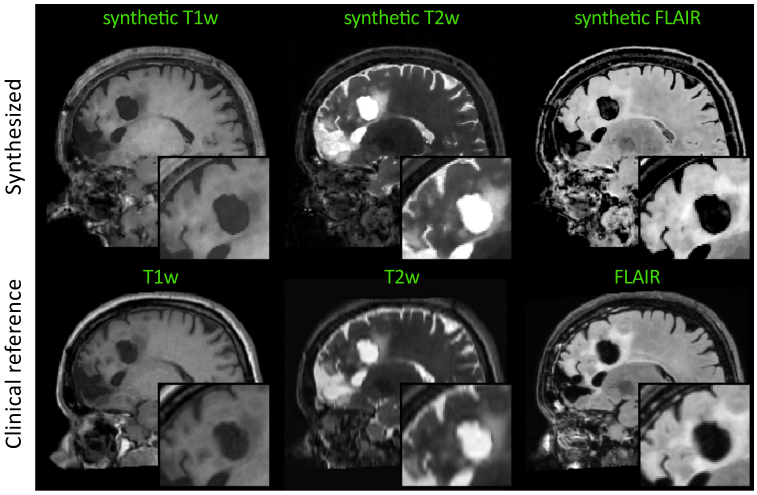

Fig. 11 Contrast-weighted image synthesis for a representative patient case. Sagittal and coronal views in correspondence to the axial views in Fig. 3 are shown

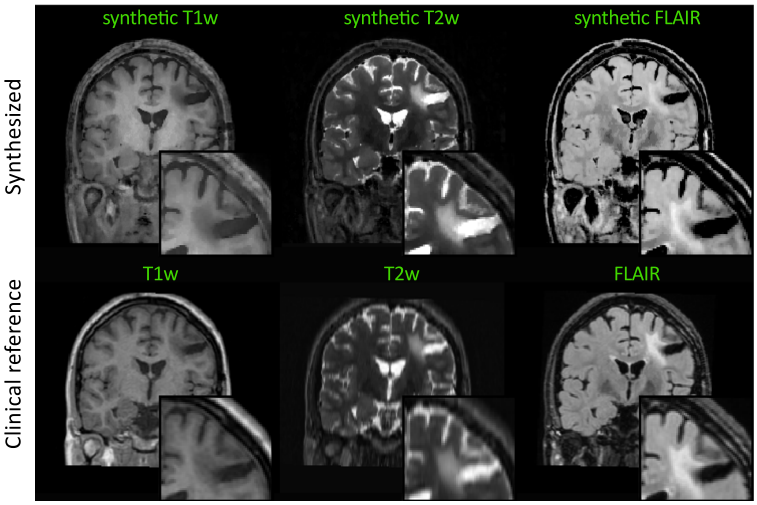

◀ **Fig. 10** Neural network-based parameter estimation for a representative patient case (top) and a healthy volunteer (bottom). T1, T2, and PD maps obtained from voxel-wise neural network inference are consistent with dictionary matching results. The parameter maps are computed from SVD-compressed image-series after LRTV reconstruction

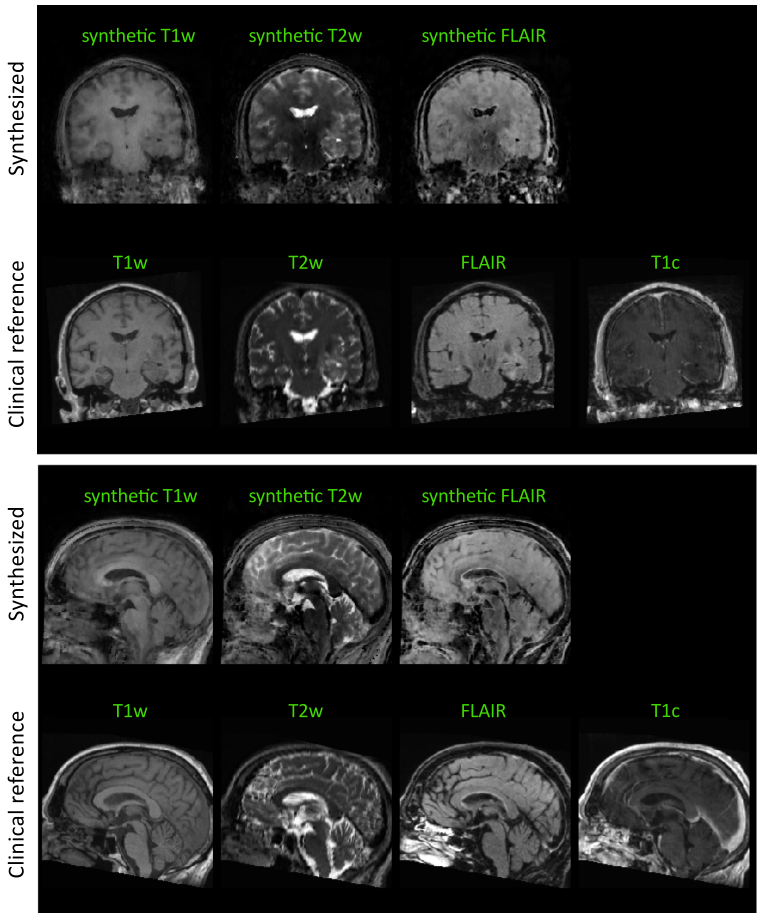

Fig. 12 Sensitivity to rigid head motion. Sagittal and coronal views in correspondence to the axial views in Fig. 4 are shown

Author contribution Conceptualization: C.M.P, M.S., B.H.M, M.I.M., J.A.H.-T.; methodology: C.M.P, M.G., P.A.G., G.B., M.C., R.F.S.; data collection: L.N.-G., M.S., J.A.H.-T.; data analysis: C.M.P, L.N.-G., F.K., S.E., L.G., B.W.; writing–original draft preparation: C.M.P.; writing–review and editing: all authors; supervision: B.H.M., M.I.M., J.A.H.-T.; all authors read and approved the final manuscript.

Funding Open Access funding enabled and organized by Projekt DEAL. C.M.P., S.E., B.H.M., and M.I.M. are supported by Deutsche Forschungsgemeinschaft (DFG) through Research Training Group GRK 2274 and TUM International Graduate School of Science and Engineering (IGSSE), GSC 81. C.M.P., S.E., M.I.M. receive funding from the European Union's Horizon 2020 research and innovation programme under grant agreement No. 952172. Patient data were acquired under the GE Healthcare work statement B-GEHC-05.

Data availability The data presented in this study are available on reasonable request from the corresponding author. The data are not publicly available due to restrictions on the use of confidential data in the written consent provided by participants.

Declarations

Ethics approval This study was in accordance with the ethical standards of the institutional and/or national research committee and with the 1964 Helsinki declaration and its later amendments or comparable ethical standards. Approval was granted by the local ethics board.

Consent to participate All participants included in this study provided written informed consent.

Consent for publication All participants included in this study signed informed consent regarding publishing their MRI data.

Conflict of Interest C.M.P, R.F.S., and M.I.M are employees at GE Healthcare, Munich, Germany. M.S. received an honorarium (paid to institution) from Parexel Ltd. for EORTC-1410 and speaker fees (paid to institution) from GE Healthcare. All other authors declare no competing interests.

References

1. Perry A, Wesseling P (2016) Histologic classification of gliomas. Handb Clin Neurol 134:71–95. https://doi.org/10.1016/B978-0-12-802997-8.00005-0
2. Holland EC (2001) Progenitor cells and glioma formation. Curr Opin Neurol 14:683–688. https://doi.org/10.1097/00019052-200112000-00002
3. Thust SC, Heiland S, Falini A, Jäger HR, Waldman AD, Sundgren PC, Godi C, Katsaros VK, Ramos A, Bargallo N, Vernooij MW, Yousry T, Bendszus M, Smits M (2018) Glioma imaging in Europe: a survey of 220 centres and recommendations for best clinical practice. Eur Radiol 28:3306–3317. https://doi.org/10.1007/s00330-018-5314-5
4. Louis DN, Ohgaki H, Wiestler OD, Cavenee WK (2016) WHO Classification of Tumours of the Central Nervous System, 4th edn. International Agency for Research on Cancer, France
5. van den Bent MJ, Smits M, Kros JM, Chang SM (2017) Diffuse infiltrating oligodendroglioma and astrocytoma. J Clin Oncol 35:2394–2401. https://doi.org/10.1200/JCO.2017.72.6737
6. Fouke SJ, Benzinger T, Gibson D, Ryken TC, Kalkanis SN, Olson JJ (2015) The role of imaging in the management of adults with diffuse low grade glioma: a systematic review and evidence-based clinical practice guideline. J Neuro-Oncol 125:457–479. https://doi.org/10.1007/s11060-015-1908-9
7. Olsen KI, Schroeder P, Corby R, Vucic I, Bardo DME (2005) Advanced magnetic resonance imaging techniques to evaluate CNS glioma. Expert Rev Neurother 5:3–11. https://doi.org/10.1586/14737175.5.6.S3
8. Kao H-W, Chiang S-W, Chung H-W, Tsai FY, Chen CY (2013) Advanced MR imaging of gliomas: an update. Biomed Res Int 2013:2013–2014. https://doi.org/10.1155/2013/970586
9. Wank M, Schilling D, Schmid TE, Meyer B, Gempt J, Barz M, Schlegel J, Liesche F, Kessel K, Wiestler B, Bette S, Zimmer C, Combs S (2018) Human glioma migration and infiltration properties as a target for personalized radiation medicine. Cancers (Basel) 10:10. https://doi.org/10.3390/cancers10110456
10. Kalpathy-Cramer J, Gerstner ER, Emblem KE, Andronesi OC, Rosen B (2014) Advanced magnetic resonance imaging of the physical processes in human glioblastoma. Cancer Res 74:4622–4637. https://doi.org/10.1158/0008-5472.CAN-14-0383
11. Ellingson BM, Bendszus M, Boxerman J et al (2015) Consensus recommendations for a standardized Brain Tumor Imaging Protocol in clinical trials. Neuro-Oncology 17:1188–1198. https://doi.org/10.1093/neuonc/nov095
12. Deoni SCL, Rutt BK, Peters TM (2003) Rapid combined T1 and T2 mapping using gradient recalled acquisition in the steady state. Magn Reson Med 49:515–526. https://doi.org/10.1002/mrm.10407
13. Warntjes JBM, Leinhard OD, West J, Lundberg P (2008) Rapid magnetic resonance quantification on the brain: optimization for clinical usage. Magn Reson Med 60:320–329. https://doi.org/10.1002/mrm.21635
14. Ma D, Gulani V, Seiberlich N, et. al. (2013) Magnetic resonance fingerprinting. Nature 495:187–192. https://doi.org/10.1038/nature11971
15. Sbrizzi A, van der Heide O, Cloos M et al (2018) Fast quantitative MRI as a nonlinear tomography problem. Magn Reson Imaging 46:56–63. https://doi.org/10.1016/j.mri.2017.10.015
16. Gómez PA, Molina-Romero M, Buonincontri G, Menzel MI, Menze BH (2019) Designing contrasts for rapid, simultaneous parameter quantification and flow visualization with quantitative transient-state imaging. Sci Rep 9:8468. https://doi.org/10.1038/s41598-019-44832-w
17. van der Heide O, Sbrizzi A, van den Berg CAT (2020) Accelerated MR-STAT reconstructions using sparse Hessian approximations. IEEE Trans Med Imaging 39:3737–3748. https://doi.org/10.1109/TMI.2020.3003893
18. Gómez PA, Cencini M, Golbabaee M, Schulte RF, Pirkl C, Horvath I, Fallo G, Peretti L, Tosetti M, Menze BH, Buonincontri G (2020) Rapid three-dimensional multiparametric MRI with quantitative transient-state imaging. Sci Rep 10:13769. https://doi.org/10.1038/s41598-020-70789-2
19. da Cruz LCH, Rodriguez I, Domingues RC et al (2011) Pseudoprogression and pseudoresponse: imaging challenges in the assessment of posttreatment glioma. Am J Neuroradiol 32:1978–1985. https://doi.org/10.3174/ajnr.A2397
20. Hargreaves BA, Vasanawala SS, Pauly JM, Nishimura DG (2001) Characterization and reduction of the transient response in steady-state MR imaging. Magn Reson Med 46:149–158. https://doi.org/10.1002/mrm.1170
21. Golbabaee M, Buonincontri G, Pirkl CM, Menzel MI, Menze BH, Davies M, Gómez PA (2021) Compressive MRI quantification using convex spatiotemporal priors and deep encoder-decoder networks. Med Image Anal 69:101945. https://doi.org/10.1016/j.media.2020.101945
22. Cruz G, Schneider T, Bruijnen T, Gaspar AS, Botnar RM, Prieto C (2018) Accelerated magnetic resonance fingerprinting using soft-weighted key-hole (MRF-SOHO). PLoS One 13:e0201808. https://doi.org/10.1371/journal.pone.0201808
23. Knoll F, Schwarzl A, Diwoky C, Sodickson DK (2014) gpuNUFFT – An Open-Source GPU Library for 3D Gridding with Direct Matlab Interface. In: Proceedings of the 22th Annual Meeting of International Society for Magnetic Resonance in Medicine (ISMRM). Milan, Italy
24. Walsh DO, Gmitro AF, Marcellin MW (2000) Adaptive reconstruction of phased array MR imagery. Magn Reson Med 43:682–690. https://doi.org/10.1002/(sici)1522-2594(200005)43:5<682::aid-mrm10>3.0.co;2-g
25. Hoppe E, Körzdörfer G, Würfl T, Wetzl J, Lugauer F, Pfeuffer J, Maier A (2017) Deep learning for magnetic resonance fingerprinting: a new approach for predicting quantitative parameter values from time series. Stud Health Technol Inform 243:202–206
26. Cohen O, Zhu B, Rosen MS (2018) MR fingerprinting Deep RecOnstruction NEtwork (DRONE). Magn Reson Med 80:885–894. https://doi.org/10.1002/mrm.27198
27. Weigel M (2015) Extended phase graphs: dephasing, RF pulses, and echoes - pure and simple. J Magn Reson Imaging 41:266–295. https://doi.org/10.1002/jmri.24619
28. Jiang Y, Ma D, Seiberlich N, Gulani V, Griswold MA (2015) MR fingerprinting using fast imaging with steady state precession (FISP) with spiral readout. Magn Reson Med 74:1621–1631. https://doi.org/10.1002/mrm.25559
29. Yushkevich PA, Piven J, Hazlett HC, Smith RG, Ho S, Gee JC, Gerig G (2006) User-guided 3D active contour segmentation of anatomical structures: significantly improved efficiency and

reliability. Neuroimage 31:1116–1128. https://doi.org/10.1016/j.neuroimage.2006.01.015

30. Avants BB, Tustison NJ, Song G, Cook PA, Klein A, Gee JC (2011) A reproducible evaluation of ANTs similarity metric performance in brain image registration. Neuroimage 54:2033–2044. https://doi.org/10.1016/j.neuroimage.2010.09.025
31. Zhang Y, Brady M, Smith S (2001) Segmentation of brain MR images through a hidden Markov random field model and the expectation-maximization algorithm. IEEE Trans Med Imaging 20:45–57. https://doi.org/10.1109/42.906424
32. Buonincontri G, Kurzawski JW, Kaggie JD, Matys T, Gallagher FA, Cencini M, Donatelli G, Cecchi P, Cosottini M, Martini N, Frijia F, Montanaro D, Gómez PA, Schulte RF, Retico A, Tosetti M (2021) Three dimensional MRF obtains highly repeatable and reproducible multi-parametric estimations in the healthy human brain at 1.5T and 3T. NeuroImage 226:117573. https://doi.org/10.1016/j.neuroimage.2020.117573
33. Hattingen E, Müller A, Jurcoane A et al (2017) Value of quantitative magnetic resonance imaging T1-relaxometry in predicting contrast-enhancement in glioblastoma patients. Oncotarget 8:53542–53551. https://doi.org/10.18632/oncotarget.18612
34. Jiang Y, Hamilton JI, Wright KL, et al (2016) Simultaneous quantification of T1, T2 and diffusion with diffusion-weighted drive-equilibrium prepared magnetic resonance fingerprinting. In: Proceedings of the 24th Annual Meeting of International Society for Magnetic Resonance in Medicine (ISMRM). Singapore
35. Jiang Y, Hamilton JI, Lo W-C, et al (2017) Simultaneous T1, T2 and diffusion quantification using multiple contrast prepared magnetic resonance fingerprinting. In: Proceedings of the 25th Annual Meeting of International Society for Magnetic Resonance in Medicine (ISMRM). Honolulu, HI, USA
36. Rieger B, Akçakaya M, Schad L, Weingärtner S (2018) Simultaneous quantification of T1, T2 and apparent diffusion coefficient using magnetic resonance fingerprinting based on echo planar imaging. In: Proceedings of the 26th Annual Meeting of International Society for Magnetic Resonance in Medicine (ISMRM). Paris, France
37. Pirkl CM, Gomez PA, Lipp I, et al (2020) Deep learning-based parameter mapping for joint relaxation and diffusion tensor MR fingerprinting. In: Third Conference on Medical Imaging with Deep Learning. PMLR, pp 638–654
38. Kurzawski JW, Cencini M, Peretti L, Gómez PA, Schulte RF, Donatelli G, Cosottini M, Cecchi P, Costagli M, Retico A, Tosetti M, Buonincontri G (2020) Retrospective rigid motion correction of three-dimensional magnetic resonance fingerprinting of the human brain. Magn Reson Med 84:2606–2615. https://doi.org/10.1002/mrm.28301
39. Lu L, Chen Y, Shen C, Lian J, Das S, Marks L, Lin W, Zhu T (2020) Initial assessment of 3D magnetic resonance fingerprinting (MRF) towards quantitative brain imaging for radiation therapy. Med Phys 47:1199–1214. https://doi.org/10.1002/mp.13967
40. Seow P, Wong JHD, Ahmad-Annuar A, Mahajan A, Abdullah NA, Ramli N (2018) Quantitative magnetic resonance imaging and radiogenomic biomarkers for glioma characterisation: a systematic review. Br J Radiol 91:20170930. https://doi.org/10.1259/bjr.20170930
41. Guzmán-De-Villoria JA, Mateos-Pérez JM, Fernández-García P et al (2014) Added value of advanced over conventional magnetic resonance imaging in grading gliomas and other primary brain tumors. Cancer Imaging 14:35. https://doi.org/10.1186/s40644-014-0035-8
42. Komiyama M, Yagura H, Baba M, Yasui T, Hakuba A, Nishimura S, Inoue Y (1987) MR imaging: possibility of tissue characterization of brain tumors using T1 and T2 values. AJNR Am J Neuroradiol 8:65–70
43. Just M, Thelen M (1988) Tissue characterization with T1, T2, and proton density values: results in 160 patients with brain tumors. Radiology 169:779–785. https://doi.org/10.1148/radiology.169.3.3187000
44. Newman S, Haughton VM, Yetkin Z, Breger R, Czervionke LF, Williams AL, Ho KC, Papke RA, Rimm AA, Fischer ME, Meyer GA, Asleson R (1993) T1, T2 and proton density measurements in the grading of cerebral gliomas. Eur Radiol 3:49–52. https://doi.org/10.1007/BF00173524
45. Lescher S, Jurcoane A, Veit A, Bähr O, Deichmann R, Hattingen E (2015) Quantitative T1 and T2 mapping in recurrent glioblastomas under bevacizumab: earlier detection of tumor progression compared to conventional MRI. Neuroradiology 57:11–20. https://doi.org/10.1007/s00234-014-1445-9
46. Hattingen E, Jurcoane A, Daneshvar K, Pilatus U, Mittelbronn M, Steinbach JP, Bahr O (2013) Quantitative T2 mapping of recurrent glioblastoma under bevacizumab improves monitoring for non-enhancing tumor progression and predicts overall survival. Neuro-Oncology 15:1395–1404. https://doi.org/10.1093/neuonc/not105
47. Blystad I, Warntjes JBM, Smedby Ö, Lundberg P, Larsson EM, Tisell A (2017) Quantitative MRI for analysis of peritumoral edema in malignant gliomas. PLoS One 12:e0177135. https://doi.org/10.1371/journal.pone.0177135
48. Wang F, Dong Z, Reese TG, Bilgic B, Katherine Manhard M, Chen J, Polimeni JR, Wald LL, Setsompop K (2019) Echo planar time-resolved imaging (EPTI). Magn Reson Med 81:3599–3615. https://doi.org/10.1002/mrm.27673
49. Jiang Y, Ma D, Keenan KE, Stupic KF, Gulani V, Griswold MA (2017) Repeatability of magnetic resonance fingerprinting T1 and T2 estimates assessed using the ISMRM/NIST MRI system phantom. Magn Reson Med 78:1452–1457. https://doi.org/10.1002/mrm.26509
50. Panda A, Chen Y, Ropella-Panagis K, Ghodasara S, Stopchinski M, Seyfried N, Wright K, Seiberlich N, Griswold M, Gulani V (2019) Repeatability and reproducibility of 3D MR fingerprinting relaxometry measurements in normal breast tissue. J Magn Reson Imaging 50:1133–1143. https://doi.org/10.1002/jmri.26717
51. Badve C, Yu A, Dastmalchian S, Rogers M, Ma D, Jiang Y, Margevicius S, Pahwa S, Lu Z, Schluchter M, Sunshine J, Griswold M, Sloan A, Gulani V (2017) Magnetic resonance fingerprinting of adult brain tumors: initial experience. AJNR Am J Neuroradiol 38:492–499. https://doi.org/10.3174/ajnr.A5035
52. Dastmalchian S, Kilinc O, Onyewadume L, Tippareddy C, McGivney D, Ma D, Griswold M, Sunshine J, Gulani V, Barnholtz-Sloan JS, Sloan AE, Badve C (2020) Radiomic analysis of magnetic resonance fingerprinting in adult brain tumors. Eur J Nucl Med Mol Imaging. https://doi.org/10.1007/s00259-020-05037-w
53. Haubold J, Demircioglu A, Gratz M, Glas M, Wrede K, Sure U, Antoch G, Keyvani K, Nittka M, Kannengiesser S, Gulani V, Griswold M, Herrmann K, Forsting M, Nensa F, Umutlu L (2020) Non-invasive tumor decoding and phenotyping of cerebral gliomas utilizing multiparametric 18F-FET PET-MRI and MR Fingerprinting. Eur J Nucl Med Mol Imaging 47:1435–1445. https://doi.org/10.1007/s00259-019-04602-2
54. Ma D, Jiang Y, Chen Y, McGivney D, Mehta B, Gulani V, Griswold M (2018) Fast 3D magnetic resonance fingerprinting for a whole-brain coverage. Magn Reson Med 79:2190–2197. https://doi.org/10.1002/mrm.26886
55. Ma D, Jones SE, Deshmane A, Sakaie K, Pierre EY, Larvie M, McGivney D, Blümcke I, Krishnan B, Lowe M, Gulani V, Najm I, Griswold MA, Wang ZI (2019) Development of high-resolution 3D MR fingerprinting for detection and characterization of epileptic lesions. J Magn Reson Imaging 49:1333–1346. https://doi.org/10.1002/jmri.26319

56. Does MD (2018) Inferring brain tissue composition and microstructure via MR relaxometry. Neuroimage 182:136–148. https://doi.org/10.1016/j.neuroimage.2017.12.087
57. Nilsson M, Englund E, Szczepankiewicz F, van Westen D, Sundgren PC (2018) Imaging brain tumour microstructure. NeuroImage 182:232–250. https://doi.org/10.1016/j.neuroimage.2018.04.075
58. Fujita S, Buonincontri G, Cencini M, Fukunaga I, Takei N, Schulte RF, Hagiwara A, Uchida W, Hori M, Kamagata K, Abe O, Aoki S (2020) Repeatability and reproducibility of human brain morphometry using three-dimensional magnetic resonance fingerprinting. Hum Brain Mapp 42:275–285. https://doi.org/10.1002/hbm.25232
59. Buonincontri G, Biagi L, Retico A, Cecchi P, Cosottini M, Gallagher FA, Gómez PA, Graves MJ, McLean MA, Riemer F, Schulte RF, Tosetti M, Zaccagna F, Kaggie JD (2019) Multi-site repeatability and reproducibility of MR fingerprinting of the healthy brain at 1.5 and 3.0 T. NeuroImage 195:362–372. https://doi.org/10.1016/j.neuroimage.2019.03.047
60. Menze BH, Jakab A, Bauer S, Kalpathy-Cramer J, Farahani K, Kirby J, Burren Y, Porz N, Slotboom J, Wiest R, Lanczi L, Gerstner E, Weber MA, Arbel T, Avants BB, Ayache N, Buendia P, Collins DL, Cordier N, Corso JJ, Criminisi A, Das T, Delingette H, Demiralp C, Durst CR, Dojat M, Doyle S, Festa J, Forbes F, Geremia E, Glocker B, Golland P, Guo X, Hamamci A, Iftekharuddin KM, Jena R, John NM, Konukoglu E, Lashkari D, Mariz JA, Meier R, Pereira S, Precup D, Price SJ, Raviv TR, Reza SMS, Ryan M, Sarikaya D, Schwartz L, Shin HC, Shotton J, Silva CA, Sousa N, Subbanna NK, Szekely G, Taylor TJ, Thomas OM, Tustison NJ, Unal G, Vasseur F, Wintermark M, Ye DH, Zhao L, Zhao B, Zikic D, Prastawa M, Reyes M, van Leemput K (2015) The multimodal brain tumor image segmentation benchmark (BRATS). IEEE Trans Med Imaging 34:1993–2024. https://doi.org/10.1109/TMI.2014.2377694
61. Kofler F, Berger C, Waldmannstetter D, Lipkova J, Ezhov I, Tetteh G, Kirschke J, Zimmer C, Wiestler B, Menze BH (2020) BraTS Toolkit: translating BraTS brain tumor segmentation algorithms into clinical and scientific practice. Front Neurosci 14. https://doi.org/10.3389/fnins.2020.00125
62. Berglund J, van Niekerk A, Rydén H, Sprenger T, Avventi E, Norbeck O, Glimberg SL, Olesen OV, Skare S (2021) Prospective motion correction for diffusion weighted EPI of the brain using an optical markerless tracker. Magn Reson Med 85:1427–1440. https://doi.org/10.1002/mrm.28524
63. Serrao EM, Kessler DA, Carmo B et al (2020) Magnetic resonance fingerprinting of the pancreas at 1.5 T and 3.0 T. Sci Rep 10:17563. https://doi.org/10.1038/s41598-020-74462-6
64. Sushentsev N, Kaggie JD, Buonincontri G, Schulte RF, Graves MJ, Gnanapragasam VJ, Barrett T (2020) The effect of gadolinium-based contrast agent administration on magnetic resonance fingerprinting-based T 1 relaxometry in patients with prostate cancer. Sci Rep 10:20475. https://doi.org/10.1038/s41598-020-77331-4

5.2 DEEP LEARNING-BASED PARAMETER MAPPING FOR JOINT RELAXATION AND DIFFUSION TENSOR MR FINGERPRINTING

Peer-reviewed conference paper

Authors: CM. Pirkl*, PA. Gómez*, I. Lipp, G. Buonincontri, M. Molina-Romero, A. Sekuboyina, D. Waldmannstetter, J. Dannenberg, S. Endt, A. Merola, JR. Whittaker, V. Tomassini, M. Tosetti, DK. Jones, BH. Menze†, MI. Menzel†

*Contributed equally
†Contributed equally

In: *Proceedings of the Third Conference on Medical Imaging with Deep Learning*. PMLR. Vol. 121, Sept. 2020, pp.638–654. http://proceedings.mlr.press/v121/pirk20a.html. [1]

Abstract: "Magnetic Resonance Fingerprinting (MRF) enables the simultaneous quantification of multiple properties of biological tissues. It relies on a pseudo-random acquisition and the matching of acquired signal evolutions to a precomputed dictionary. However, the dictionary is not scalable to higher-parametric spaces, limiting MRF to the simultaneous mapping of only a small number of parameters (proton density, T_1 and T_2 in general). Inspired by diffusion-weighted SSFP imaging, we present a proof-of-concept of a novel MRF sequence with embedded diffusion-encoding gradients along all three axes to efficiently encode orientational diffusion and T_1 and T_2 relaxation. We take advantage of a convolutional neural network (CNN) to reconstruct multiple quantitative maps from this single, highly under-sampled acquisition. We bypass expensive dictionary matching by learning the implicit physical relationships between the spatiotemporal MRF data and the T_1,T_2 and diffusion tensor parameters. The predicted parameter maps and the derived scalar diffusion metrics agree well with state-of-the-art reference protocols. Orientational diffusion information is captured as seen from the estimated primary diffusion directions. In addition to this, the joint acquisition

and reconstruction framework proves capable of preserving tissue abnormalities in multiple sclerosis lesions."

Contribution of thesis author: Algorithmic development and implementation, experimental design, data analysis, manuscript preparation and editing.

Proceedings of Machine Learning Research 121:638–654, 2020 MIDL 2020 – Full paper track

Deep learning-based parameter mapping for joint relaxation and diffusion tensor MR Fingerprinting

Carolin M. Pirkl[*1,2] CAROLIN.PIRKL@TUM.DE
Pedro A. Gómez[*1] PEDRO.GOMEZ@TUM.DE
Ilona Lipp[3,4,5] LIPPI@CARDIFF.AC.UK
Guido Buonincontri[6,7] GUIDO.BUONINCONTRI@GMAIL.COM
Miguel Molina-Romero[1] MIGUEL.MOLINA@TUM.DE
Anjany Sekuboyina[1,8] ANJANY.SEKUBOYINA@TUM.DE
Diana Waldmannstetter[1] DIANA.WALDMANNSTETTER@TUM.DE
Jonathan Dannenberg[2,9] JONATHAN.DANNENBERG@TU-DORTMUND.DE
Sebastian Endt[1,2] SEBASTIAN.ENDT@TUM.DE
Alberto Merola[3,5] ALBERTO.MEROLA@AICURA-MEDICAL.COM
Joseph R. Whittaker[3,10] WHITTAKERJ3@CARDIFF.AC.UK
Valentina Tomassini[3,4,11] VALENTINA.TOMASSINI@UNICH.IT
Michela Tosetti[6,7] MICHELA.TOSETTI@FSM.UNIPI.IT
Derek K. Jones[3,12] JONESD27@CARDIFF.AC.UK
Bjoern H. Menze[†1,13,14] BJOERN.MENZE@TUM.DE
Marion I. Menzel[†2,9] MENZEL@GE.COM

[1] *Department of Informatics, Technical University of Munich, Garching, Germany*
[2] *GE Healthcare, Munich, Germany*
[3] *Cardiff University Brain Research Imaging Centre (CUBRIC), Cardiff University School of Psychology, Cardiff, United Kingdom*
[4] *Institute of Psychological Medicine and Clinical Neurosciences, Cardiff University School of Medicine, Cardiff, United Kingdom*
[5] *Max Planck Institute for Human Cognitive and Brain Sciences, Leipzig, Germany*
[6] *Fondazione Imago7, Pisa, Italy*
[7] *IRCCS Fondazione Stella Maris, Pisa, Italy*
[8] *Department of Neuroradiology, Klinikum rechts der Isar, Munich, Germany*
[9] *Department of Physics, Technical University of Munich, Garching, Germany*
[10] *Cardiff University School of Physics and Astronomy, Cardiff, United Kingdom*
[11] *Institute for Advanced Biomedical Technologies (ITAB), Department of Neurosciences, Imaging and Clinical Sciences, School of Medicine, University "G. d'Annunzio" of Chieti-Pescara, Chieti, Italy*
[12] *Mary McKillop Institute for Health Research, Faculty of Health Sciences, Australian Catholic University, Melbourne, Australia*
[13] *Center for Translational Cancer Research, Munich, Germany*
[14] *Munich School of BioEngineering, Garching, Germany*

Abstract

[*] Contributed equally
[†] Contributed equally

JOINT RELAXATION AND DIFFUSION TENSOR MR FINGERPRINTING

Magnetic Resonance Fingerprinting (MRF) enables the simultaneous quantification of multiple properties of biological tissues. It relies on a pseudo-random acquisition and the matching of acquired signal evolutions to a precomputed dictionary. However, the dictionary is not scalable to higher-parametric spaces, limiting MRF to the simultaneous mapping of only a small number of parameters (proton density, T1 and T2 in general). Inspired by diffusion-weighted SSFP imaging, we present a proof-of-concept of a novel MRF sequence with embedded diffusion-encoding gradients along all three axes to efficiently encode orientational diffusion and T1 and T2 relaxation. We take advantage of a convolutional neural network (CNN) to reconstruct multiple quantitative maps from this single, highly undersampled acquisition. We bypass expensive dictionary matching by learning the implicit physical relationships between the spatiotemporal MRF data and the T1, T2 and diffusion tensor parameters. The predicted parameter maps and the derived scalar diffusion metrics agree well with state-of-the-art reference protocols. Orientational diffusion information is captured as seen from the estimated primary diffusion directions. In addition to this, the joint acquisition and reconstruction framework proves capable of preserving tissue abnormalities in multiple sclerosis lesions.

Keywords: Magnetic Resonance Fingerprinting, Convolutional Neural Network, Image Reconstruction, Diffusion Tensor, Multiple Sclerosis

1. Introduction

Magnetic Resonance Imaging (MRI) has emerged as a powerful diagnostic imaging technique as it is capable of non-invasively providing a multitude of complementary image contrasts. Commonly used routine MRI protocols however lack standardization and mainly present qualitative information. To infer comprehensive diagnostic information, image analysis therefore requires extensive postprocessing for co-registration, motion-correction etc., a problem that exponentiates in multi-contrast acquisitions. Hence, fully quantitative multi-parametric acquisitions have long been the goal of research in MR to overcome the subjective, qualitative image evaluation (Thust et al., 2018). Progressing from qualitative, contrast-weighted MRI to quantitative mapping, Magnetic Resonance Fingerprinting (MRF) has emerged as a promising framework for the simultaneous quantification of multiple tissue properties (Ma et al., 2013). It aims at inferring multiple quantitative maps – proton density, T1 and T2 relaxation times in general – from a single, highly accelerated acquisition. MRF is based on matching the signal time-courses, acquired with pseudo-random variation of imaging parameters, to a dictionary of precomputed signal evolutions. As the dictionary is typically simulated with fine granularity of all foreseeable parameter combinations, this places a substantial burden on computational resources (Weigel et al., 2010; Ganter, 2018). Due to these memory and processing demands, the use of a dictionary becomes infeasible in higher-parametric spaces like in case of diffusion tensor quantification.

Over the last years, first diffusion-weighted MRF techniques have been proposed (Jiang et al., 2016, 2017; Rieger et al., 2018). However, the transient nature of MRF signals makes them highly vulnerable to motion artifacts, especially when aiming at encoding the full diffusion tensor – a drawback long-known from diffusion-weighted SSFP (DW-SSFP) techniques (McNab and Miller, 2010; Bieri and Scheffler, 2013). Susceptibility to motion together with the exponential scaling of the dictionary size with the dimensionality of the parameter space pose a significant challenge for the computation of the diffusion tensor,

limiting diffusion-weighted MRF applications to the estimation of the mean diffusivity, captured by the apparent diffusion coefficient, so far.

Also, recent work on combining MRF acquisition schemes with deep learning-based approaches for parameter inference has demonstrated to outperform conventional template matching algorithms in terms reconstruction quality and computation time (Cohen et al., 2018; Golbabaee et al., 2019; Fang et al., 2019).

In this proof-of-concept-study, we combine a novel MRF-type sequence and a deep learning-based multi-parametric mapping to simultaneously quantify T1 and T2 relaxation, and orientational diffusion. This work presets three main contributions:

1. We first present an MRF scheme with embedded diffusion-encoding gradients along all three axes to encode orientational diffusion information, whilst simultaneously maintaining differential weightings to T1 and T2.

2. Inspired by the promising results of image quality transfer ideas (Tanno et al., 2017; Alexander et al., 2017), we take advantage of a convolutional neural network (CNN) to reliably reconstruct paramatric maps of T1, T2 and the full diffusion tensor from the acquired MRF image time-series. With standard diffusion tensor imaging (DTI) analysis, it is then possible to derive scalar diffusion measures, and to estimate the principal diffusion direction.

3. We evaluate our approach on healthy subjects and on a clinical cohort of multiple sclerosis (MS) patients with substantial modifications of the brain micro-structure.

2. Material and methods

2.1. Relaxation and diffusion-sensitized MRF sequence

Inspired by DW-SSFP-based techniques, we propose an MRF acquisition scheme (Figure 1) that is sensitized to relaxation and orientational diffusion: We extend the steady state precession MRF methodology (Jiang et al., 2015) and insert mono-polar diffusion-encoding gradients before each readout. To encode the full diffusion tensor, we sensitize the MRF signal to 30 diffusion directions as it evolves in the transient state. Along the acquisition train ($t = 1224$ repetitions, 32 s/slice), we repeat each diffusion-encoding direction 34 times before applying the next diffusion gradient direction. Directions of the diffusion-encoding gradients are chosen based on the electrostatic repulsion algorithm (Jones et al., 1999) and have amplitudes $g_{x,y,z}$ with $-40\,\mathrm{mT/m} \leq g_{x,y,z} \leq 40\,\mathrm{mT/m}$ and a duration $\delta = 3\,\mathrm{ms}$. Every 6 directions, we incorporate non-diffusion weighted, unbalanced gradients ($g_{x,y,z} = 1\,\mathrm{mT/m}$). In each repetition, we acquire an undersampled image with one arm of a variable density spiral. To sample the entire k-space, 34 spiral interleaves are required. The spiral arms are rotated with the golden angle from one repetition to the next. To increase sensitivity to diffusion, the spiral readout ($TE = 6\,\mathrm{ms}$) happens after the diffusion gradient, similar to DW-SSFP imaging (Buxton, 1993). We rely on an initial inversion pulse ($TI = 18\,\mathrm{ms}$) that is followed by a train of constant flip angles with $\alpha = 37°$. In the latter part of the sequence, repeating variable flip angle ramps ($0° \leq \alpha \leq 49°$) are applied. TR is set constant during diffusion-encoding ($TR = 22\,\mathrm{ms}$) with longer waiting periods ($TR = 50\,\mathrm{ms}$) when changing diffusion-encoding directions. As the diffusion-sensitization accumulates over multiple

repetitions, each timepoint of the acquired image time-series has a unique combination of diffusion-weighting and T1 and T2 contrast.

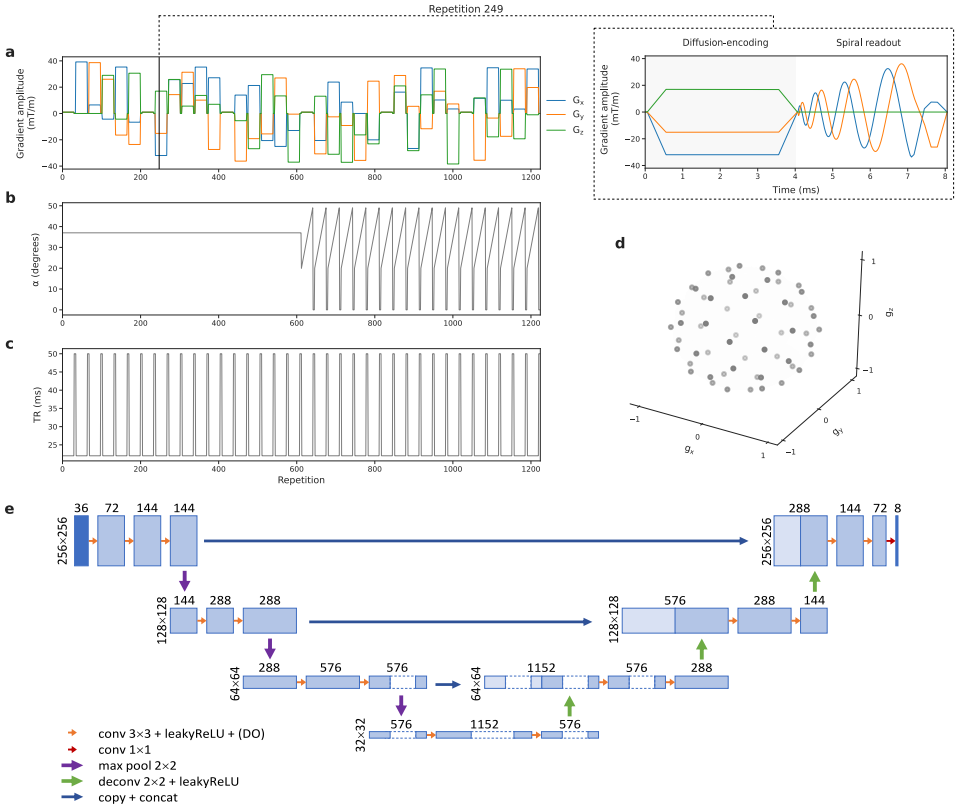

Figure 1: MRF acquisition and reconstruction framework. a) Pseudo-random variation of diffusion-encoding gradients. The diffusion-encoding direction is changed every 34 repetitions. In each repetition (here repetition 249), diffusion-encoding is followed by a spiral readout. b) Constant flip angles followed by variable flip angle ramps. c) TR pattern with longer waiting periods when changing diffusion-encoding directions. d) Spherical representation of the encoded diffusion directions. e) CNN architecture with the spatiotemporal magnitude MRF image series ($T = 36$ temporal channels) as input and quantitative maps of T1 and T2 relaxation times and the diffusion tensor elements ($Q = 8$ quantitative channels) as output.

2.2. Data acquisition and processing

As part of an IRB-approved study (Lipp et al., 2019), data from 11 MS patients and 9 healthy controls were acquired on a 3T HDx MRI system (GE Medical Systems, Milwaukee, WI) using an 8-channel receive-only head RF coil (GE Medical Devices), after ob-

taining written informed consent . The protocol included a single-shot EPI-DTI sequence, DESPOT1 (Deoni, 2007) and DESPOT2 (Deoni et al., 2003) sequences, high-resolution T2 and PD-weighted sequences, a FLAIR sequence for MS lesion segmentation, and a T1-weighted FSPGR sequence. In addition to these clinical sequences, 8-12 subsequent, axial slices, covering the middle portion of the brain, were acquired with the proposed MRF sequence. The main scan parameters of all acquisitions are shown in Table 2 in Appendix A.

MRF image time-series We applied a sliding-window scheme (Cao et al., 2017) to reconstruct mixed-contrast images from consecutive spiral interleaves of the MRF acquisition. With a window size of 34, which corresponds to the spiral undersampling factor, we retrospectively fill up the undersampled k-space and reduce aliasing artifacts. We use a sliding-window stride of 34 to jointly reconstruct the consecutive images that were acquired with the same diffusion-encoding. By doing so, we reduce the dimensionality of the spatiotemporal MRF image data to $T = 36$ images along the temporal axis.

Reference parameter maps Following the DESPOT1/2 approaches, we derived T1 maps from the SPGR and IR-SPGR images, and T2 maps from the phase-cycled bSSFP data. The EPI-DTI data were corrected for head motion, distortions induced by the diffusion-weighted gradients, and EPI-induced geometrical distortions by registering each diffusion image to the T1-weighted anatomical image using elastix (Klein et al., 2010). We then estimated the diffusion tensor with its diagonal (D_{xx}, D_{yy}, D_{zz}) and off-diagonal (D_{xy}, D_{xz}, D_{yz}) elements using ExploreDTI (Leemans et al., 2009). MS lesions were semi-manually segmented on the T2-weighted image, also consulting the FLAIR and the PD-weighted images using the Jim software package (Xinapse Systems). We obtained white matter (WM), gray matter (GM), and cerebrospinal fluid (CSF) masks from the lesion filled and brain-extracted T1-weighted images with FAST (Zhang et al., 2001). We then transformed the relaxation and diffusion tensor maps and the tissue segmentations to the MRF image space using ANTs (Avants et al., 2011), which incorporated a reorientation of the diffusion tensor images.

Database With the processing pipeline described above, we created a database of 216 datasets in total, comprising both data from MS patients and healthy subjects. Each of the 216 datasets is a pair of the magnitude MRF image series $\mathbf{x} \in \mathbb{R}^{N \times N \times T}$ and the $Q = 8$ reference maps of T1, T2 and the 6 diffusion tensor elements $\mathbf{y} \in \mathbb{R}^{N \times N \times Q}$ with $N \times N = 256 \times 256$ being the spatial dimension.

2.3. CNN-based parameter mapping

We propose a CNN architecture to learn a non-linear relationship between the spatiotemporal MRF image data and multiple quantitative maps as an output. As such, the model presented in this work allows us to directly infer quantitative relaxation and diffusion information by capturing the temporal and neighborhood context features (Balsiger et al., 2019).

CNN architecture For this multivariate regression, we propose a U-Net architecture (Ronneberger et al., 2015) which was previously shown to offer high quality parameter maps in MRF reconstruction (Fang et al., 2020) tasks. We implemented the convolutional-deconvolutional architecture as depicted in Figure 1 using TensorFlow. Our model receives

the spatiotemporal MRF magnitude image data $\mathbf{x}$ with its $T = 36$ temporal channels as input. In the contracting path, feature extraction is alternated by max-pooling to create a low-dimensional latent representation from the MRF image input. In the expansive path, the low-dimensional feature space is gradually decoded and upsampled to output quantitative maps $\mathbf{y}$ with $Q = 8$ parametric channels for T1, T2, and the 6 unique elements of the diffusion tensor. Using skip connections, the feature maps in the expansive path are concatenated with high-resolution feature maps from the contracting path, merging global context from the latent space with preserved spatial details from the input space.

Data pre-processing To foster effective network training, we normalized the magnitude MRF image series between $[0, 1]$ using its minimum and maximum intensities, $\mathbf{x}' = \frac{\mathbf{x}-\min(\mathbf{x})}{\max(\mathbf{x})-\min(\mathbf{x})}$. To account for the widely varying scales for relaxation and diffusion tensor parameters, we transformed each quantitative map $\mathbf{y}_q$ to a fixed range of $\mathbf{y}'_q \in [0, 1]$ for T1, T2 and diagonal diffusion tensor maps, and $\mathbf{y}'_q \in [-1, 1]$ for off-diagonal diffusion tensor maps $\mathbf{y}'_q = \frac{\mathbf{y}_q}{\max(|q_{min}|, |q_{max}|)}$, using the global minimum and maximum parameter values q_{min} and q_{max}. By doing so, we allowed directionality in the off-diagonal elements, captured as negative and positive value ranges, to equally impact the loss function. We also ensure that the loss function is implicitly balanced over all parameters and is not governed by the parameter with the highest magnitude, i.e. T1.

Experimental setup We trained the CNN for 400 epochs with a batch size of 5, using Adam optimization to minimize the L1 loss function with a learning rate of 0.0001, and a dropout rate of 0.25. For performance evaluation, we performed a 10-fold cross-validation on the 20 subjects, whereby each experimental instance consisted of 2 test subjects and 18 remaining subjects for training. Aiming at an efficient and robust reconstruction method, we increased the heterogeneity of the dataset as we ensured that training and testing datasets comprised both healthy subjects and MS patients. Network training for one instance of the cross-validation took 3.5 h on a Nvidia GeForce TITAN Xp GPU. The CNN training progress is illustrated in Figure 4 in Appendix B.

We applied standard DTI analysis to derive scalar diffusion metrics, i.e. mean diffusivity (MD), axial diffusivity (AD), radial diffusivity (RD), and fractional anisotropy (FA) from both the predicted and the reference diffusion tensors. To reflect the characteristic fiber orientation in WM, we obtained a colored FA map based on the primary diffusion eigenvector. We evaluated the reconstruction quality of our framework based on the structural similarity index measure (SSIM) and the root mean squared error (RMSE) between the CNN prediction and the DESPOT1/2 and EPI-DTI reference methods. To ensure comparability in terms of physical value ranges of the parameters, RMSE was derived from the normalized parameter maps $\mathbf{y}'$.

3. Results

It can be visually observed from Figure 2 that predicted relaxation and diffusion tensor maps are largely consistent with state-of-the-art methods, which is confirmed by the voxel-wise comparison in the difference maps. This is the case even though the input image series as obtained by the sliding-window reconstruction are impacted by artifacts due to

motion, undersampling and destructive interference between readout and diffusion-encoding gradients. Quantitatively, we achieved a comparable reconstruction performance for T1 and T2 with respect to DESPOT1/2 methods, while diagonal diffusion tensor elements show better agreement with the DTI reference than off-diagonal elements (Table 1). Specifically, it is more difficult for the CNN to reconstruct off-diagonal diffusion tensor information in WM and MS lesions than in GM and CSF. Overall, we reliably recovered diffusion and relaxation information, also in regions of diagnostic importance such as MS lesions, indicating generalization capability of our method. Figure 3 suggests that our framework is capable of reliably reconstructing diffusion information as the image quality of the scalar MD, AD, RD and FA maps is comparable to the EPI-DTI reference. The colored FA maps and the overlay of the primary eigenvectors of the predicted and reference diffusion tensors show that the principal diffusion direction and thus the characteristic fiber structure in WM is captured as illustrated by the enlarged portions of the derived maps. In both healthy WM tissue and MS lesions, RMSE suggests higher agreement with the reference maps for MD, AD and RD than FA (Table 1). This is in line with the overall SSIM which is higher for MD, AD and RD than for FA. Figure 5 in Appendix C depicts an exemplary dataset with significant artifacts due to patient motion. Here, the CNN is not able to successfully disentangle T1, T2 and diffusion information in severely corrupted regions.

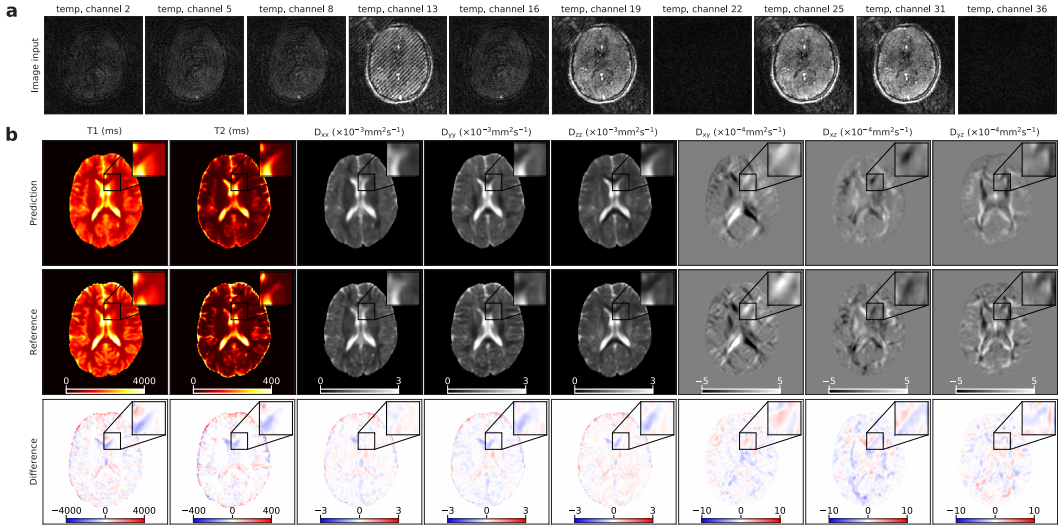

Figure 2: CNN reconstruction for a representative test dataset. a) Spatiotemporal MRF data show artifacts due to spatial undersampling, gradient interferences and motion. b) Predicted maps of T1, T2 and diffusion tensor elements do not show visual artifacts, providing satisfying image quality as demonstrated by the enlarged image sections. Voxel-wise difference maps do not reveal substantial differences between the proposed MRF framework and conventional reference methods.

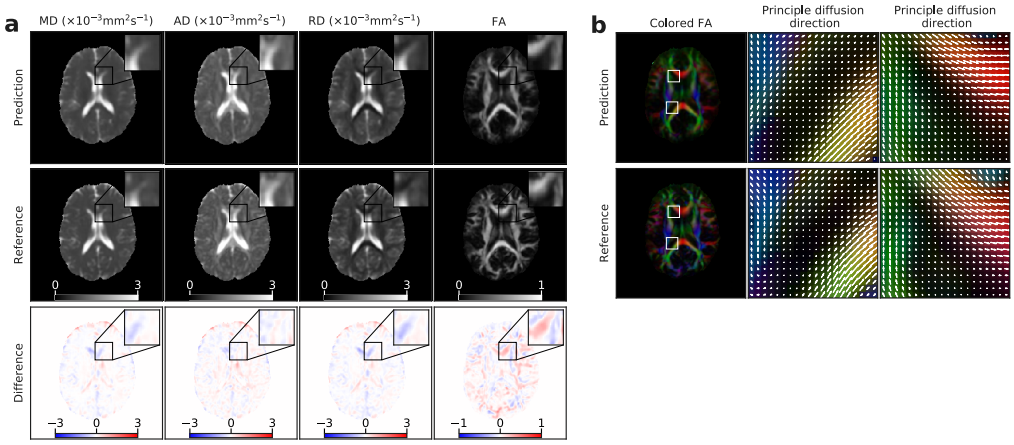

Figure 3: Diffusion tensor analysis for a representative test dataset. a) Scalar diffusion metrics, i.e. MD, AD, RD and FA, derived from predicted and reference diffusion tensors show good visual agreement. Voxel-wise difference maps and the enlarged views confirm that the reconstruction quality is largely consistent with the reference methods. b) Colored FA maps and the primary diffusion direction indicate the predominant diffusion direction in main WM-tracts.

Table 1: Quantitative comparison of our MRF framework with DESPOT1/2 and EPI-DTI reference methods.

		Relaxation and diffusion tensor maps							
Metric	**Region**	**T1**	**T2**	**D_{xx}**	**D_{yy}**	**D_{zz}**	**D_{xy}**	**D_{xz}**	**D_{yz}**
SSIM	—	0.91 ± 0.04	0.9 ± 0.04	0.94 ± 0.03	0.94 ± 0.03	0.94 ± 0.03	0.83 ± 0.05	0.81 ± 0.05	0.82 ± 0.05
RMSE	Whole brain	0.15 ± 0.06	0.18 ± 0.06	0.07 ± 0.03	0.08 ± 0.03	0.07 ± 0.03	0.1 ± 0.03	0.11 ± 0.02	0.1 ± 0.02
	CSF	0.19 ± 0.04	0.25 ± 0.06	0.1 ± 0.03	0.1 ± 0.03	0.09 ± 0.03	0.07 ± 0.02	0.07 ± 0.03	0.07 ± 0.02
	GM	0.14 ± 0.06	0.16 ± 0.07	0.07 ± 0.03	0.07 ± 0.03	0.07 ± 0.03	0.08 ± 0.02	0.08 ± 0.02	0.08 ± 0.02
	WM	0.09 ± 0.05	0.09 ± 0.07	0.05 ± 0.03	0.05 ± 0.03	0.05 ± 0.03	0.12 ± 0.04	0.14 ± 0.04	0.13 ± 0.04
	MS lesion	0.11 ± 0.07	0.1 ± 0.08	0.06 ± 0.04	0.06 ± 0.04	0.06 ± 0.04	0.15 ± 0.07	0.17 ± 0.06	0.16 ± 0.06

		Diffusion metric maps			
Metric	**Region**	**MD**	**AD**	**RD**	**FA**
SSIM	—	0.94 ± 0.03	0.93 ± 0.03	0.94 ± 0.03	0.91 ± 0.03
RMSE	Whole brain	0.11 ± 0.05	0.12 ± 0.05	0.11 ± 0.05	0.11 ± 0.03
	CSF	0.13 ± 0.06	0.14 ± 0.06	0.13 ± 0.05	0.08 ± 0.06
	GM	0.11 ± 0.05	0.11 ± 0.06	0.11 ± 0.05	0.09 ± 0.03
	WM	0.07 ± 0.05	0.08 ± 0.04	0.07 ± 0.05	0.13 ± 0.03
	MS lesion	0.09 ± 0.07	0.11 ± 0.06	0.1 ± 0.07	0.14 ± 0.06

4. Discussion and conclusion

In this work, we propose a relaxation and diffusion-sensitized MRF sequence combined with a CNN-based multivariate regression. We approach the underlying MRF sequence design and the deep-learning based parameter inference as a joint task. In this way, we can relax

the MR acquisition requirements and efficiently encode T1 and T2 relaxation times together with orientational diffusion information. With our joint MRF acquisition and reconstruction framework, we present a proof-of-concept of fast multi-parameter quantification. We simultaneously measure and reconstruct quantitative relaxation and diffusion tensor maps, significantly reduce the scan time (32 s/slice), and make extensive post-processing pipelines of conventional multi-contrast imaging redundant.

Following the concept of DW-SSFP imaging, the accumulation of T1 and T2-weighting and diffusion-sensitization along multiple repetitions and echo-pathways is what makes our signal encoding and hence the MRF acquisition so efficient. However, this is also what challenges the reconstruction the most: First, the signal dependence on T1, T2 and flip angles is relatively complicated. This impedes diffusion quantification in DW-SSFP approaches as all other signal contributions need to be known to isolate the diffusion effect. Second, the high scan efficiency comes at the cost of image quality, while the transient nature of the diffusion-sensitized signal makes the acquisition highly vulnerable to brain pulsation and patient motion. Also, in the actual measurement the primary signal evolution, governed by relaxation and diffusion effects, is contaminated by secondary terms from various experimental sources, such as non-Gaussian noise, coherent and incoherent motion, stimulated or spurious echoes due to the interplay of diffusion-encoding and readout gradients – and most of the time a combination of them. These secondary signal contributions are known to cause image artifacts that are spatially correlated. Also, as we use multi-coil imaging and have aliasing due to spiral undersampling, spatial mixing of tissue components is an inevitable consequence of the acquisition scheme. We thus approach the multi-parameter inference task with a CNN architecture to take advantage of all information available, i.e. the temporal and spatial relationships, to characterize the individual signal contributions. Moreover, the deep learning approach benefits from the implicit physical relationships between the scalar and tensorial parameters (Tax et al., 2018; Bernin and Topgaard, 2013) to recover the underlying relaxation and orientational diffusion information.

We have demonstrated that our CNN-based reconstruction framework resolved image corruptions and reliably mitigated pulsation artifacts. Severe head motion however turned out to be the major challenge. As only data from MS patients were affected by severe motion artifacts, we hypothesize that this is because the diffusion-sensitized MRF data from MS patients were acquired at the end of a 1.5 hours scanning session so that patients tended to get restless. The session for healthy controls was comparatively shorter (˜40 minutes). Compared to steady-state MRI sequences, MRF relies on transient MR signals. As such, diffusion-weighted MRF schemes are by design more sensitive to motion artifacts than steady-state diffusion-weighted EPI. However, EPI-based DTI suffers from EPI-induced distortions that must be corrected retrospectively. This does not apply to our case: First, we use spiral readouts instead of EPI in the MRF acquisition. Second, due to the significantly shorter timing with monopolar diffusion-encoding gradients, eddy-current induced blurring is reduced compared to approaches based on bipolar gradients. As this is the first study to explore the simultaneous quantification of relaxation and orientational diffusion in an MRF setting, we are confident that we will benefit from the recent advances on how to cope with motion in DW-SSFP – either prospectively or retrospectively.

The proposed MRF framework is based on the diffusion tensor model. Although it is robust and widely accepted, it has the inherent limitation that it fails for crossing fibers.

This shortcoming equally holds for conventional, state-of-the-art DTI methods. Overall, our framework has nevertheless proven to provide relaxation and diffusion tensor maps which agree well with the clinical reference. This might be attributed to the computationally efficient U-Net architecture that has particularly shown convincing performance on small biomedical image datasets. That is, the predictive performance of our model and its ability to resolve even severe motion artifacts could certainly benefit from more training data.

We also anticipate that image artifacts, which mask the fine anisotropic structures, are the main reason why the off-diagonal diffusion tensor elements are not captured as well as diagonal elements. We also believe that a thorough assessment of the individual diffusion encoding directions and their effect on the final diffusion tensor quantification is as important as ameliorating motion artifacts. However, in the proposed MRF scheme diffusion-weightings propagate over multiple repetitions, similar to diffusion SSFP techniques. This results in a mixing of signal pathways which have experienced different histories of diffusion-encoding gradients (strength and direction). With the current dataset, it is thus not possible to retrospectively investigate the effectiveness of the individual diffusion encoding directions that have been applied in full detail. It is thus subject to our current and follow-up work to investigate this in dedicated experiments. We expect that resultant adjustments in the sequence design, specifically in the way we incorporate diffusion-encoding, and techniques such as adaptive spoiling will increase the robustness of the acquisition in first place. Reduced image artifacts, in turn, will enhance the predictive quality of our CNN and allow us to fully regain the characteristic fiber structure in high anisotropy WM regions. We also believe, that proceeding to more advanced deep learning approaches now have a chance to improve on our baseline.

In conclusion, we present a novel MRF-type sequence which simultaneously encodes T1, T2 and orientational diffusion information. We rely on a deep learning-based approach to reconstruct multi-parametric outputs from spatiotemporal MRF data corrupted by artifacts due to spiral undersampling, motion, and the interference of diffusion-encoding and readout gradients. We bypass conventional dictionary matching by learning the intrinsic physical connections between the scalar and tensorial tissue parameters, and thereby propose a scalable MRF application which can be extended to further quantitative contrasts.

Acknowledgments

Data were acquired as part of a project funded by the MS Society UK. Carolin M. Pirkl is supported by Deutsche Forschungsgemeinschaft (DFG) through TUM International Graduate School of Science and Engineering (IGSSE), GSC 81. Derek K. Jones is supported by a Wellcome Trust Investigator Award (096646/Z/11/Z) and a Wellcome Trust Strategic Award (104943/Z/14/Z). The TITAN Xp GPU used for this research was donated by the NVIDIA Corporation.

References

Daniel C. Alexander, Darko Zikic, Aurobrata Ghosh, Ryutaro Tanno, Viktor Wottschel, Jiaying Zhang, Enrico Kaden, Tim B. Dyrby, Stamatios N. Sotiropoulos, Hui Zhang, and

Antonio Criminisi. Image quality transfer and applications in diffusion MRI. *NeuroImage*, 152:283–298, May 2017. ISSN 1053-8119. doi: 10.1016/j.neuroimage.2017.02.089.

Brian B. Avants, Nicholas J. Tustison, Gang Song, Philip A. Cook, Arno Klein, and James C. Gee. A Reproducible Evaluation of ANTs Similarity Metric Performance in Brain Image Registration. *NeuroImage*, 54(3):2033–2044, February 2011. ISSN 1053-8119. doi: 10.1016/j.neuroimage.2010.09.025.

Fabian Balsiger, Olivier Scheidegger, Pierre G. Carlier, Benjamin Marty, and Mauricio Reyes. On the Spatial and Temporal Influence for the Reconstruction of Magnetic Resonance Fingerprinting. In M. Jorge Cardoso, Aasa Feragen, Ben Glocker, Ender Konukoglu, Ipek Oguz, Gozde Unal, and Tom Vercauteren, editors, *Proceedings of The 2nd International Conference on Medical Imaging with Deep Learning*, volume 102 of *Proceedings of Machine Learning Research*, pages 27–38, London, United Kingdom, July 2019. PMLR.

Diana Bernin and Daniel Topgaard. NMR diffusion and relaxation correlation methods: New insights in heterogeneous materials. *Current Opinion in Colloid & Interface Science*, 18(3):166–172, 2013. ISSN 1359-0294. doi: 10.1016/j.cocis.2013.03.007.

Oliver Bieri and Klaus Scheffler. Fundamentals of balanced steady state free precession MRI. *Journal of magnetic resonance imaging: JMRI*, 38(1):2–11, July 2013. ISSN 1522-2586. doi: 10.1002/jmri.24163.

Richard B. Buxton. The diffusion sensitivity of fast steady-state free precession imaging. *Magnetic Resonance in Medicine*, 29(2):235–243, February 1993. ISSN 0740-3194. doi: 10.1002/mrm.1910290212.

Xiaozhi Cao, Congyu Liao, Zhixing Wang, Ying Chen, Huihui Ye, Hongjian He, and Jianhui Zhong. Robust sliding-window reconstruction for Accelerating the acquisition of MR fingerprinting. *Magnetic Resonance in Medicine*, 78(4):1579–1588, 2017. ISSN 1522-2594. doi: 10.1002/mrm.26521.

Ouri Cohen, Bo Zhu, and Matthew S. Rosen. MR fingerprinting Deep RecOnstruction NEtwork (DRONE). *Magnetic Resonance in Medicine*, 80(3):885–894, 2018. doi: 10.1002/mrm.27198.

Sean C. L. Deoni. High-resolution T1 mapping of the brain at 3T with driven equilibrium single pulse observation of T1 with high-speed incorporation of RF field inhomogeneities (DESPOT1-HIFI). *Journal of magnetic resonance imaging: JMRI*, 26(4):1106–1111, October 2007. ISSN 1053-1807. doi: 10.1002/jmri.21130.

Sean C. L. Deoni, Brian K. Rutt, and Terry M. Peters. Rapid combined T1 and T2 mapping using gradient recalled acquisition in the steady state. *Magnetic Resonance in Medicine*, 49(3):515–526, March 2003. ISSN 0740-3194. doi: 10.1002/mrm.10407.

Zhenghan Fang, Yong Chen, Mingxia Liu, Lei Xiang, Qian Zhang, Qian Wang, Weili Lin, and Dinggang Shen. Deep Learning for Fast and Spatially-Constrained Tissue Quantification from Highly-Accelerated Data in Magnetic Resonance Fingerprinting. *IEEE*

Transactions on Medical Imaging, 38(10):2364–2374, Oct 2019. ISSN 1558-254X. doi: 10.1109/TMI.2019.2899328.

Zhenghan Fang, Yong Chen, Sheng-Che Hung, Xiaoxia Zhang, Weili Lin, and Dinggang Shen. Submillimeter MR fingerprinting using deep learning–based tissue quantification. *Magnetic Resonance in Medicine*, 84:579– 591, 2020. ISSN 1522-2594. doi: 10.1002/mrm.28136.

Carl Ganter. Configuration Model. In *Proceedings of the 26th Annual Meeting of International Society for Magnetic Resonance in Medicine (ISMRM)*, Paris, France, 2018.

Mohammad Golbabaee, Dongdong Chen, Pedro A. Gómez, Marion I. Menzel, and Mike E. Davies. Geometry of Deep Learning for Magnetic Resonance Fingerprinting. In *ICASSP 2019 - 2019 IEEE International Conference on Acoustics, Speech and Signal Processing (ICASSP)*, pages 7825–7829, May 2019. doi: 10.1109/ICASSP.2019.8683549. ISSN: 1520-6149.

Yun Jiang, Dan Ma, Nicole Seiberlich, Vikas Gulani, and Mark A. Griswold. MR fingerprinting using fast imaging with steady state precession (FISP) with spiral readout. *Magnetic Resonance in Medicine*, 74(6):1621–1631, December 2015. ISSN 1522-2594. doi: 10.1002/mrm.25559.

Yun Jiang, Jesse Ian Hamilton, Katharine L. Wright, Dan Ma, Nicole Seiberlich, Vikas Gulani, and Mark A. Griswold. Simultaneous Quantification of T1, T2 and Diffusion with Diffusion-weighted drive-equilibrium prepared Magnetic Resonance Fingerprinting. In *Proceedings of the 24th Annual Meeting of International Society for Magnetic Resonance in Medicine (ISMRM)*, Singapore, 2016.

Yun Jiang, Jesse Ian Hamilton, Wei-Ching Lo, Katharine L. Wright, Dan Ma, Andrew J. Coristine, Nicole Seiberlich, Vikas Gulani, and Mark A. Griswold. Simultaneous T1, T2 and Diffusion Quantification using Multiple Contrast Prepared Magnetic Resonance Fingerprinting. In *Proceedings of the 25th Annual Meeting of International Society for Magnetic Resonance in Medicine (ISMRM)*, Honolulu, HI, USA, 2017.

D. K. Jones, M. A. Horsfield, and A. Simmons. Optimal strategies for measuring diffusion in anisotropic systems by magnetic resonance imaging. *Magnetic Resonance in Medicine*, 42(3):515–525, September 1999. ISSN 0740-3194.

Stefan Klein, Marius Staring, Keelin Murphy, Max A. Viergever, and Josien P. W. Pluim. elastix: a toolbox for intensity-based medical image registration. *IEEE transactions on medical imaging*, 29(1):196–205, January 2010. ISSN 1558-254X. doi: 10.1109/TMI.2009.2035616.

Alexander Leemans, Ben Jeurissen, Jan Sijbers, and Derek K. Jones. ExploreDTI : a graphical toolbox for processing , analyzing , and visualizing diffusion MR data. In *Proceedings of the 17th Annual Meeting of International Society for Magnetic Resonance in Medicine (ISMRM)*, Honolulu, HI, USA, 2009.

Ilona Lipp, Derek K. Jones, Sonya Bells, Eleonora Sgarlata, Catherine Foster, Rachael Stickland, Alison E. Davidson, Emma C. Tallantyre, Neil P. Robertson, Richard G. Wise, and Valentina Tomassini. Comparing MRI metrics to quantify white matter microstructural damage in multiple sclerosis. *Human Brain Mapping*, 40(10):2917–2932, 2019. ISSN 1097-0193. doi: 10.1002/hbm.24568.

Dan Ma, Vikas Gulani, Nicole Seiberlich, Kecheng Liu, Jeffrey L. Sunshine, Jeffrey L. Duerk, and Mark A. Griswold. Magnetic Resonance Fingerprinting. *Nature*, 495(7440): 187–192, March 2013. ISSN 0028-0836. doi: 10.1038/nature11971.

Jennifer A. McNab and Karla L. Miller. Steady-state diffusion-weighted imaging: theory, acquisition and analysis. *NMR in biomedicine*, 23(7):781–793, August 2010. ISSN 1099-1492. doi: 10.1002/nbm.1509.

Benedikt Rieger, Mehmet Akçakaya, Lothar Schad, and Sebastian Weingärtner. Simultaneous quantification of T1, T2 and Apparent Diffusion Coefficient using Magnetic Resonance Fingerprinting based on Echo Planar Imaging. In *Proceedings of the 26th Annual Meeting of International Society for Magnetic Resonance in Medicine (ISMRM)*, Paris, France, 2018.

Olaf Ronneberger, Philipp Fischer, and Thomas Brox. U-Net: Convolutional Networks for Biomedical Image Segmentation. In Nassir Navab, Joachim Hornegger, William M. Wells, and Alejandro F. Frangi, editors, *Medical Image Computing and Computer-Assisted Intervention – MICCAI 2015*, pages 234–241. Springer International Publishing, 2015. ISBN 978-3-319-24574-4.

R. Tanno, D. E. Worrall, A. Gosh, E. Kaden, S. N. Sotiropoulos, Antonio Criminisi, and D.C. Alexander. Bayesian Image Quality Transfer with CNNs: Exploring Uncertainty in dMRI Super-Resolution. In *20th International Conference on Medical Image Computing and Computer Assisted Intervention (MICCAI)*, Quebec City, Quebec, Canada, 2017. MICCAI 2017 - Springer.

Chantal M.W. Tax, João P. de Almeida Martins, Filip Szczepankiewicz, Carl-Fredrik Westin, Maxime Chamberland, Daniel Topgaard, and Derek K. Jones. From physical chemistry to human brain biology: unconstrained inversion of 5-dimensional diffusion-T2 correlation data. In *Proceedings of the 26th Annual Meeting of International Society for Magnetic Resonance in Medicine (ISMRM)*, Paris, France, 2018.

S. C. Thust, S. Heiland, A. Falini, H. R. Jäger, A. D. Waldman, P. C. Sundgren, C. Godi, V. K. Katsaros, A. Ramos, N. Bargallo, M. W. Vernooij, T. Yousry, M. Bendszus, and M. Smits. Glioma imaging in Europe: A survey of 220 centres and recommendations for best clinical practice. *European Radiology*, 28(8):3306–3317, August 2018. ISSN 1432-1084. doi: 10.1007/s00330-018-5314-5.

M. Weigel, S. Schwenk, V. G. Kiselev, K. Scheffler, and J. Hennig. Extended phase graphs with anisotropic diffusion. *Journal of Magnetic Resonance (San Diego, Calif.: 1997)*, 205 (2):276–285, August 2010. ISSN 1096-0856. doi: 10.1016/j.jmr.2010.05.011.

Y. Zhang, M. Brady, and S. Smith. Segmentation of brain MR images through a hidden Markov random field model and the expectation-maximization algorithm. *IEEE transactions on medical imaging*, 20(1):45–57, January 2001. ISSN 0278-0062. doi: 10.1109/42.906424.

Appendix A. Scan parameters

Table 2: Scan parameters. For each of the sequences, the main acquisition parameters are provided.

	Relaxation and diffusion-sensitized MRF scheme	**Clinical reference sequences**				
		DTI	**DESPOT1/2**	**T1-weighted**	**PD/T2-weighted**	**FLAIR (T2-weighted)**
		Single-shot diffusion-weighted EPI	SPGR / IR-SPGR / bSSFP	FSPGR	SE	SE / IR
Native resolution (mm^3)	$1.2 \times 1.2 \times 5.0$	$1.8 \times 1.8 \times 2.4$	$1.7 \times 1.7 \times 1.7$	$1.0 \times 1.0 \times 1.0$	$0.94 \times 0.94 \times 4.5$	$0.86 \times 0.86 \times 4.5$
Matrix size	256×256	$96 \times 96 \times 36$	$128 \times 128 \times 88$	$256 \times 256 \times 172$	256×256	256×256
Field of view (mm)	225	230	220	256	240	220
Slices	8-12	57	None - 3D	None - 3D	36 (3mm + 1.5mm gap)	36 (3mm + 1.5mm gap)
TE (ms)	6	94.5	2.1 / 2.1 / 1.6	3.0	9.0 / 80.6	122.3
TR (ms)	22, 50	16000	4.7 / 4.7 / 3.2	7.8	3000	9502
TI (ms)	18	-	- / 450 / -	450	-	2250
Flip angle α (°)	37, $0 \leq \alpha \leq 49$ ramps	90	[3, 4, 5, 6, 7, 8, 9, 13, 18] / [5] / [10.6, 14.1, 18.5, 23.8, 29.1, 35.3, 45, 60]	20	90	90
b-values (s/mm^2)	-	1200	-	-	-	-
Gradient amplitude $g_{x,y,z}$ (mT/m)	$-40 \leq g_{x,y,z} \leq 40$	-	-	-	-	-
Gradient duration δ (ms)	3	-	-	-	-	-
Spiral interleaves (number)	34	-	-	-	-	-
Total acquisition time (min)	4.2-6.4	12.5	10	7.5	2	3

Appendix B. CNN training progress

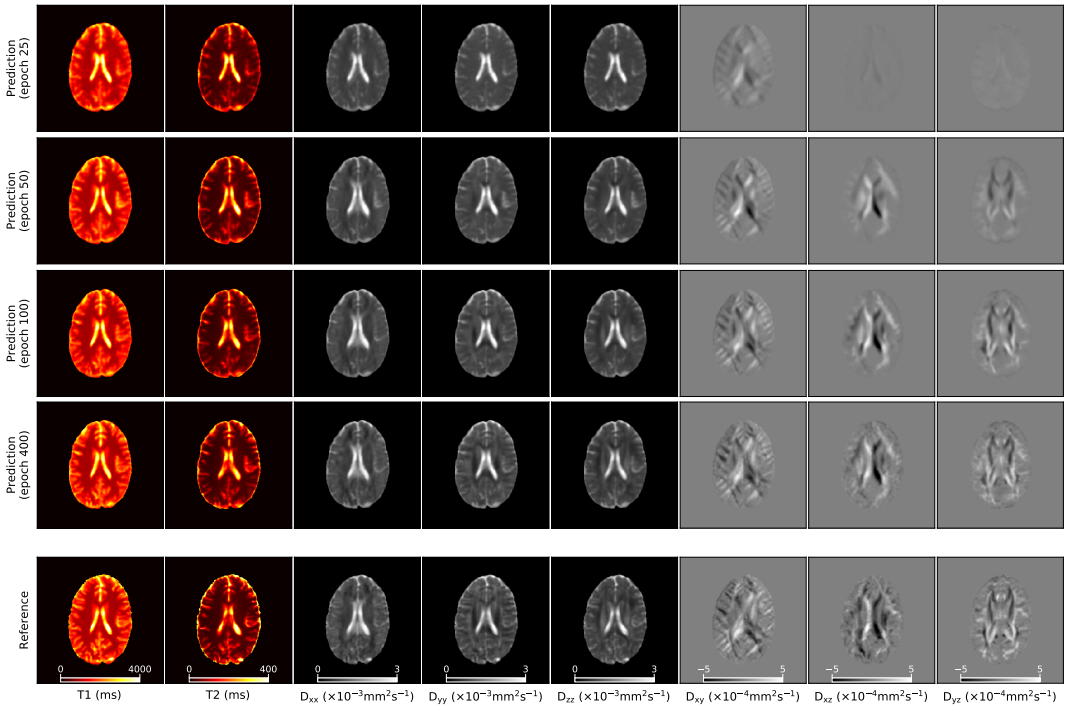

Figure 4: CNN training progress. Predicted relaxation and diffusion tensor maps are shown for increasing number of training epochs (top rows) together with the clinical reference (bottom row). The CNN reconstructs main anatomical structures after a few training epochs while finer structural details of the parameter maps become more pronounced at later stages. With increasing number of epochs, the network learns to gradually recover directional diffusion information in the diffusion tensor maps, eventually revealing the characteristic fiber structures in WM.

Appendix C. CNN reconstruction in case of severe motion artifacts

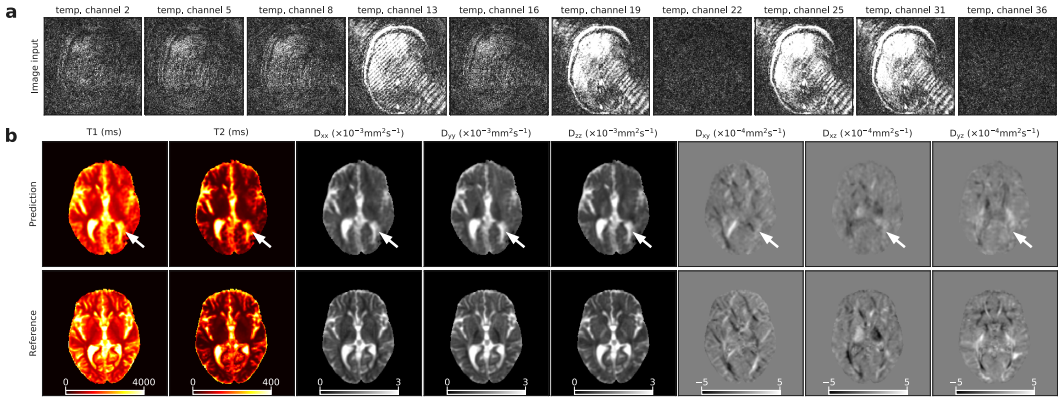

Figure 5: CNN reconstruction for a representative test dataset with severe artifacts. a) MRF images have significant artifacts due to head motion. b) Predicted maps indicate that the CNN was not able to recover relaxation and diffusion information in regions which are severely corrupted (arrow).

5.3 RESIDUAL LEARNING FOR 3D MOTION CORRECTED QUANTITATIVE MRI: ROBUST CLINICAL T1, T2 AND PROTON DENSITY MAPPING

Peer-reviewed conference paper

Authors: CM. Pirkl, M. Cencini, JW. Kurzawski, D. Waldmannstetter, H. Li, A. Sekuboyina, S. Endt, L. Peretti, G. Donatelli, R. Pasquariello, M. Costagli, G. Buonincontri, M. Tosetti, MI. Menzel†, BH. Menze†

†Contributed equally

In press: *Proceedings of the Forth Conference on Medical Imaging with Deep Learning*. PMLR. [3]

Abstract: "Subject motion is one of the major challenges in clinical routine MR imaging. Despite ongoing research, motion correction has remained a complex problem without a universal solution. In advanced quantitative MR techniques, such as MR Fingerprinting, motion does not only affect a single image, like in single-contrast MRI, but disrupts the entire temporal evolution of the magnetization and causes parameter quantification errors due to a mismatch between the acquired and simulated signals. In this work, we present a deep learning-empowered retrospective motion correction for rapid 3D whole-brain multiparametric MRI based on Quantitative Transient-state Imaging (QTI). We propose a patch-based 3D multiscale convolutional neural network (CNN) that learns the residual error, i.e. after initial navigator-based correction, between motion-affected quantitative T_1, T_2 and proton density maps and their motion-free counterparts. For efficient model training despite limited data availability, we propose a physics-informed simulation to apply continuous motion-patterns to motion-free data. We evaluate the performance of the residual CNN on 1.5 T and 3 T MRI data of ten healthy volunteers. We analyze the generalizability of the model when applied to real clinical cases, including pediatric and adult patients with large brain lesions. Our study demonstrates that image quality can be significantly improved after correcting for subject motion. This has im-

portant implications in clinical setups where large amounts of motion affected data must be discarded."

Contribution of thesis author: Algorithmic development and implementation, experimental design, data analysis, manuscript preparation and editing.

Proceedings of Machine Learning Research 1–15, 2021 Full Paper – MIDL 2021

Residual learning for 3D motion corrected quantitative MRI: Robust clinical T1, T2 and proton density mapping

Carolin M. Pirkl[1,2] CAROLIN.PIRKL@TUM.DE
Matteo Cencini[3,4] MATTEO.CENCINI@GMAIL.COM
Jan W. Kurzawski[5] JAN.KURZAWSKI@GMAIL.COM
Diana Waldmannstetter[1] DIANA.WALDMANNSTETTER@TUM.DE
Hongwei Li[1,6] HONGWEI.LI@TUM.DE
Anjany Sekuboyina[1,7] ANJANY.SEKUBOYINA@TUM.DE
Sebastian Endt[1,2] SEBASTIAN.ENDT@TUM.DE
Luca Peretti[8,3,4] LUCAPERETTI.LP@GMAIL.COM
Graziella Donatelli[9,4] GRAZIELLA_DONATELLI@HOTMAIL.COM
Rosa Pasquariello[3] ROSA.PASQUARIELLO@FSM.UNIPI.IT
Mauro Costagli[3,10] MAURO.COSTAGLI@FSM.UNIPI.IT
Guido Buonincontri[3,4] GUIDO.BUONINCONTRI@GMAIL.COM
Michela Tosetti[3,4] MICHELA.TOSETTI@FSM.UNIPI.IT
Marion I. Menzel[*2,11] MENZEL@GE.COM
Bjoern H. Menze[*1,6] BJOERN.MENZE@UZH.CH

[1] *Department of Computer Science, Technical University of Munich, Garching, Germany*
[2] *GE Healthcare, Munich, Germany*
[3] *IRCCS Fondazione Stella Maris, Pisa, Italy*
[4] *Fondazione Imago7, Pisa, Italy*
[5] *Pisa Division, National Institute for Nuclear Physics (INFN), Pisa, Italy*
[6] *Department of Quantitative Biomedicine, University of Zurich, Zurich, Switzerland*
[7] *Department of Neuroradiology, Klinikum rechts der Isar, Munich, Germany*
[8] *Department of Computer Science, University of Pisa, Pisa, Italy*
[9] *Azienda Ospedaliero-Universitaria Pisana, Pisa Italy*
[10] *Department of Neuroscience, Rehabilitation, Ophtalmology, Genetics, Maternal and Child Sciences (DINOGMI), University of Genova, Genova, Italy*
[11] *Department of Physics, Technical University of Munich, Garching, Germany*

Abstract

Subject motion is one of the major challenges in clinical routine MR imaging. Despite ongoing research, motion correction has remained a complex problem without a universal solution. In advanced quantitative MR techniques, such as MR Fingerprinting, motion does not only affect a single image, like in single-contrast MRI, but disrupts the entire temporal evolution of the magnetization and causes parameter quantification errors due to a mismatch between the acquired and simulated signals. In this work, we present a deep learning-empowered retrospective motion correction for rapid 3D whole-brain multiparametric MRI based on Quantitative Transient-state Imaging (QTI). We propose a patch-based 3D multiscale convolutional neural network (CNN) that learns the residual error, i.e. after initial navigator-based correction, between motion-affected quantitative

[*] Contributed equally

T1, T2 and proton density maps and their motion-free counterparts. For efficient model training despite limited data availability, we propose a physics-informed simulation to apply continuous motion-patterns to motion-free data. We evaluate the performance of the residual CNN on 1.5T and 3T MRI data of ten healthy volunteers. We analyze the generalizability of the model when applied to real clinical cases, including pediatric and adult patients with large brain lesions. Our study demonstrates that image quality can be significantly improved after correcting for subject motion. This has important implications in clinical setups where large amounts of motion affected data must be discarded.

Keywords: 3D multiparametric MRI, motion correction, deep learning, residual learning, multiscale CNN

1. Introduction

Motion robustness is a key feature for routine imaging in general. It is especially crucial for pediatric or elderly patients and for patients affected by diseases that prevent them from maintaining a still position throughout the acquisition. It is therefore a clinical priority to develop techniques that effectively resolve motion artifacts. As their appearance highly depends on the individual acquisition, e.g. the used readout schemes, the targeted clinical question, the condition of the patient and the body region to be imaged, there is no universal solution. Consequently, a number of conceptionally different correction methods have been presented, ranging from prospective to retrospective, image-based methods (Zaitsev et al., 2015; Godenschweger et al., 2016).

Fast 3D multiparametric MRI techniques based on transient-state MRI (Ma et al., 2018; Gómez et al., 2020) are excellent candidates for the clinical practice, as they offer high quantification accuracy together with high repeatability and reproducibility (Buonincontri et al., 2021). Their reduced scan times enable improved motion robustness compared to conventional quantitative MRI with lengthy scanning protocols. While motion artifacts are generally reduced in these fast acquisition schemes, they are not entirely immune to motion. In fact, subject movements do not only affect a single time point of the acquisition, but corrupt the entire temporal magnetization evolution, captured by the acquired k-t space, and therewith subsequent parameter estimation. While previous work on motion correction for transient-state imaging has mainly concentrated on 2D acquisition schemes (Mehta et al., 2018; Cruz et al., 2019; Xu et al., 2019), there is only little work on motion correction for 3D multiparametric MRI.

Kurzawski et al. (2020) presented a navigator-based retrospective rigid motion correction for a 3D Quantitative Transient-state Imaging (QTI) technique based on a segmented readout scheme to acquire the k-t-space. Their proposed motion correction strategy relied upon self-navigators embedded within each acquisition segment, which enabled the recovery of a critical amount of the underlying parameter information degraded due to subject motion occurring between consecutive segments. Despite significant improvement of the image quality, resulting quantitative T1, T2 and proton density (PD) maps showed remaining artifacts originating from subject movements on a time-scale below the temporal resolution of the self-navigators of 7 s.

Here, we propose a deep learning (DL) method to resolve artifacts due to continuous motion that are not captured by the navigator-based approach. Our work is motivated by recent advances of DL at the interface between MR physics and medical computer vision

that have been demonstrated to make MR imaging more robust to subject motion (Usman et al., 2020; Oksuz, 2021; Gong et al., 2021; Pawar et al., 2018; Miao et al., 2016; Hou et al., 2018a,b), e.g. by directly removing motion-induced artifacts or by estimating the underlying motion parameters for subsequent realignment. We adopt the concept of residual learning (Zhang et al., 2017; Jin et al., 2017; Liu et al., 2020) and propose a 3D multiscale residual convolutional neural network (CNN) to improve on the previously presented navigator-based motion correction, presetting the following contributions: (1) We propose a 3D multiscale residual CNN to learn the non-linear relationship between the motion-corrupted T1, T2 and PD maps and the residual error maps, i.e. the deviation from the motion-free counterpart that remained after navigator-based correction (Kurzawski et al., 2020). (2) We rely on a 3D CNN architecture that captures the intrinsically 3D nature of the subject movements together with the 3D MR acquisition scheme to efficiently resolve motion artifacts and infer high-quality T1, T2 and PD maps. (3) We present a physics-informed simulation framework to retrospectively apply realistic continuous motion patterns to motion-free datasets, enabling a supervised training setup without the necessity for large amounts of paired acquisitions or fully sampled data. (4) We evaluate the performance of the proposed method on 1.5T and 3T MRI data of ten healthy volunteers who underwent QTI imaging twice: the first time they kept their head as still as possible, and the second time they voluntarily moved their heads during acquisition. We also apply our method to clinical cases, including pediatric and adult patients with large brain lesions, to demonstrate its generalizability and capability to improve motion-affected datasets in cases with pathological findings.

2. Material and methods

2.1. Residual learning for retrospective 3D motion correction

We propose a residual learning technique to resolve artifacts that could not be corrected by the navigator-based method of Kurzawski et al. (2020), which is recapped below to present a more complete picture. We demonstrate our method with its key components, the residual CNN model and the physics-informed motion simulation, on data acquired with 3D QTI.

Navigator-based rigid motion correction The navigator-based correction identifies motion-induced misalignment in the acquired image-time series. To do so, the full k-t-space data is subdivided into subsequently acquired segments, from which we reconstruct equal-contrast navigator images. These navigators are then aligned to the first baseline navigator to estimate the spatial mismatch and to subsequently correct the k-t-space data accordingly. The corrected k-t-space data is then fed into the reconstruction pipeline as described in 2.2 to yield the motion-corrected parametric maps. The massive spatial undersampling of the fast 3D acquisition scheme limits the resolvable motion time-scale to 7 s as the lower SNR in temporally higher resolved self-navigators hampers a correct realignment.

Residual learning CNN architecture and training We propose a 3D patch-based multiscale residual CNN to learn the deviation of the motion-corrupted parameter maps from the high-quality, motion-free reference. Learning a residual mapping has been shown to be more effective than a direct mapping (Zhang et al., 2017; Tamada et al., 2019; Ulas et al., 2018) as the residual maps capture a more sparse representations of the artifacts.

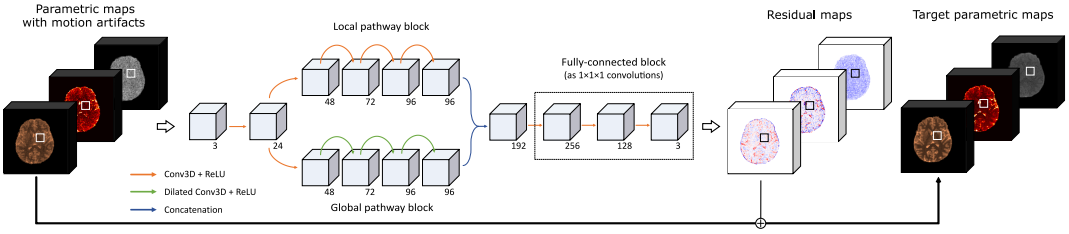

Figure 1: The multiscale CNN receives the parametric maps after navigator-based correction as input and outputs the residual maps.

The proposed CNN architecture[1] (Figure 1) receives a 3D input patch ($24 \times 24 \times 24$ voxels) of the quantitative maps degraded by motion artifacts that remained after navigator-based correction. The quantitative T1, T2 and PD parameters are reflected by three input channels. The model then spans out in a local and a global pathway. This dual pathway structure was shown to efficiently account for spatial image information on multiple scales (Kamnitsas et al., 2017; Kim et al., 2017; Ulas et al., 2018): The local path (with 3D convolutions and ReLU activations) processes more localized, spatially adjacent features. The dilated 3D convolutional layers in the global path allow to gather more global, contextual information due to an increased receptive field (Table A.2). Local and global features are concatenated and fed into a block of fully-connected layers, efficiently processing the decoded spatial relationships. To maintain the spatial dimensions throughout the network, the fully-connected layers are implemented as convolutional layers with $1 \times 1 \times 1$ kernels, to eventually output the residual maps, i.e. the difference of the navigator-corrected and the motion-free maps. We trained the residual CNN based on in-vivo 3D QTI data from ten healthy volunteers. For each subject, two datasets were acquired with the instruction to hold still for the first scan and to rapidly move the head during the second session as detailed by Kurzawski et al. (2020). All subjects were scanned on a 1.5T and a 3T scanner (HDxt and MR750 scanners, GE Healthcare, Milwaukee, WI) with the sequence parameters described in 2.2. For a supervised training setup, we only considered the motion-free data and created a database of artificially motion-corrupted 3D QTI data as described below. The in-vivo data with real motion was only used for testing. The DL-model was then trained to learn the residual maps between the parametric maps with simulated motion artifacts and the motion-free counterpart. The retrospectively corrupted data of seven subjects were used for model training and two subjects' data for validation, with $10,000/3,000$ randomly sampled 3D patches, respectively. The remaining subject data was held back for testing. We trained the residual CNN for a maximum of 100 epochs with a batch size of 20, using Adam optimization to minimize the L1 loss function with a learning rate of $1e^{-4}$, keeping the model state with the best validation loss.

Physics-informed simulation of motion-corrupted data To allow the proposed DL-model to learn how diverse motion patterns propagate to the inferred multiparametric

1. Code available on https://github.com/CarolinMA/MRP_MoCo

maps, we simulated motion-corrupted data from the motion-free 3D QTI acquisitions. To do so, we applied continuous rigid motion patterns, i.e. translation and rotation, to the individual time frames of the acquired k-t-space. To imitate continuous head movements, we continuously varied the misalignment of consecutive k-t-space time points. We achieved a realistic artifact appearance as we applied ranges of the artificial translation and rotation patterns as experimentally observed by Kurzawski et al. (2020), i.e. translations $-20\,\text{mm} \leq \Delta x, \Delta y, \Delta z \leq 20\,\text{mm}$ and rotations $-20° \leq \Delta roll, \Delta pitch, \Delta yaw \leq 20°$. We then performed a navigator-based correction to mitigate artifacts due to inter-segment movements in the first place. The thereby obtained parametric maps with remaining artifacts due to intra-segment movements, illustrated in Figure A.1, were the input to the CNN.

2.2. Data acquisition and processing

In-vivo data All in-vivo data presented in this study were acquired in accordance with the 1964 Helsinki declaration and its later amendments or comparable ethical standards. Approval was granted by the local ethics boards.

MR acquisition and reconstruction In-vivo data from ten healthy volunteers, a pediatric and an adult patient were scanned with an inversion-prepared 3D SSFP QTI implementation (Gómez et al., 2020) with variable flip angle ramps, TI=18 ms, TE=0.5 ms and TR=8.5 ms. The acquisition of transient state image series relies on in-plane spirals with spherical rotations to sample the k-t-space (=3D+time, i.e. $225 \times 225 \times 225\text{mm}^3$ field of view with $1.125 \times 1.125 \times 1.125\text{mm}^3$ isotropic voxel size and 880 time points). By design, the acquisition is built by consecutive segments (n=56) of the same excitation scheme, each with a duration of 7 s, and iteratively fills the k-t-space by randomly permuting in-plane and spherical rotation angles of the readouts. The k-t-space data are then reconstructed using zero-filling, followed by projection onto a low rank subspace, gridding onto a Cartesian grid, 3D inverse fast Fourier transform and subsequent coil sensitivity estimation and combination. Quantitative maps of T1, T2 and PD are estimated by matching the reconstructed subspace images to a pre-computed dictionary with granularity and parameter ranges as specified in Kurzawski et al. (2020).

2.3. Experimental setup

Cross-validation experiment on healthy volunteer data We evaluated the performance of the residual CNN, trained on solely simulated motion, in a ten-fold cross-validation experiment by repeating the training setup, as described in 2.1, ten times. Following this leave-one-out scheme, the data of the held-back volunteer with real motion after initial navigator-based correction was used for model testing in each instance. At test time, we divided the parametric maps into 3D patches of $24 \times 24 \times 24$ voxels, shifted along all three dimensions with a step size of 4 voxels, for patch-wise CNN processing. Predicted residual error patches are added to the motion-corrupted input and averaged to eventually yield the full 3D motion-corrected T1, T2 and PD maps. We ran the cross-validation experiment for 1.5T and 3T data individually. The obtained quantitative maps were compared to the co-registered motion-free reference using the voxel-wise concordance correlation coefficient (CCC) and coefficient of determination (R^2) as performance metrics.

Generalization analysis on clinical quantitative MRI For further performance analysis, we applied the best-performing model in the cross-validation experiment to clinical 3D QTI scans of a pediatric (8-year old) patient with subtotal agenesis of the corpus callosum, scanned at 1.5T, and an adult patient with glioblastoma, scanned at 3T.

3. Results and discussion

Cross-validation experiment on healthy volunteer data The proposed 3D residual CNN, trained on purely artificially corrupted data, provided T1, T2 and PD maps with an image quality comparable to the motion-free reference maps. This is observed when visually comparing the quantitative maps of a representative test case of the cross-validation experiment for both the 1.5T (Figure 2(*a*), Figure A.2) and 3T data (Figure 2(*b*), Figure A.3).

Quantitative evaluation of the cross-validation experiment by means of the CCC and R^2 (Table A.1) substantiates the qualitative finding and reflects the improvement achieved by the navigator-based realignment and the subsequent residual CNN. For both 1.5T and 3T data, quantitative measures indicate that the residual CNN further improved the outcome of the navigator-based correction for all parametric maps. As already visually observed, mean CCC and R^2 values reflect the higher impact of the DL-model on T2 and PD than T1 maps. Furthermore, Table A.1 shows that after CNN-based motion-correction, we achieved better correspondence with the motion-free reference for the 3T data than for the 1.5T scans. However, from Figure 2(*a*) and Figure A.2 we observe that the residual CNN does not only remove motion-induced artifacts, but additionally suppresses noise-like aliasing. This effect is more pronounced for the 1.5T data with intrinsically lower SNR and image quality than for a 3T field-strength with higher SNR. The additional denoising results in parametric maps with image qualities that go beyond the motion-free reference, which in turn explains the lower overall agreement observed with the motion-free reference acquisitions.

The cross-validation experiment shows that the combination of the residual CNN with the navigator-based correction efficiently resolves head movements on two time-scales: 1) The self-navigator-based estimation and subsequent realignment of motion-induced displacements in the k-t-space has proven to recover a significant amount of the parameter information corrupted by abrupt inter-segment movements. 2) With the 3D residual multi-scale CNN, we reliably resolve residual artifacts and phase inconsistencies due to continuous intra-segment movements that are unresolved by the limited temporal resolution of the self-navigators, providing high-quality and artifact-free parameter maps.

The proposed physics-informed motion simulation allows us to retrospectively apply continuous motion directly to the k-t-space and propagate it through the reconstruction pipeline. We make implicit use of the forward encoding operator from k-space to parameter-space to generate self-contained, paired training data for supervised model training. Thus, we present an efficient training scheme that does not require large amounts of motion and motion-free data pairs to be acquired. Also, in contrast to other physics-guided methods, we do not rely on fully sampled data to be used as reference for supervised network training. This is from particular practical relevance as the acquisition of fully-sampled 3D+time QTI data is infeasible due to prohibitively long scan times (Yaman et al., 2020).

The 3D patch-based CNN implementation allowed us to fully capture the spatial correlations that inevitably arise from 1) the subject movements in the 3D space, which cause

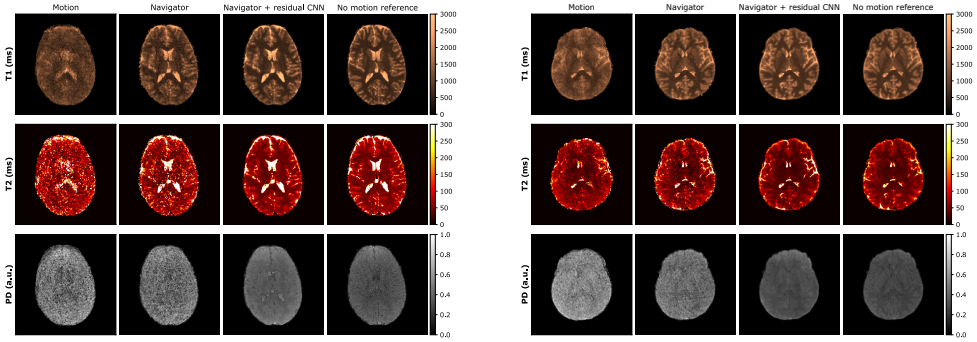

(*a*) 1.5T (*b*) 3T

Figure 2: Proposed motion correction for representative volunteer scans at 1.5T (a) and 3T (b) (axial views). T1, T2 and PD maps show pronounced motion-induced artifacts (*Motion*) compared to the *No motion reference*. Remaining artifacts after *Navigator*-based correction are resolved by the residual CNN (*Navigator + residual CNN*), providing high-quality parameter maps.

spatially correlated image artifacts, and 2) the 3D design of the MR acquisition with spatial undersampling and multicoil imaging that provoke a mixing of signal components. With the adaption of the residual learning concept, we transferred the non-linear disentangling of the primary parameter information and the secondary image artifacts into the sparse representation of the residual maps.

Generalization analysis on clinical quantitative MRI For the clinical test cases at 1.5T and 3T, Figure 3, Figure A.4 and Figure A.5 indicate that the residual CNN yields high-quality, artifact-free parametric maps. In both cases, the navigator-based approach did not improve image quality of the parametric maps as much as seen for the volunteer data (Figure 2, Figure A.2, Figure A.3). This is attributed to the fact that there were no pronounced abrupt movements but the patients moved their heads continuously, i.e. on a faster scale of what can be resolved by the self-navigators. The patient datasets also showcase the generalization capabilities of the residual CNN. We observed reliable motion-correction results in the presence of pathological findings in both adult and pediatric patients whose brain anatomy differs from that of healthy adults in the training data.

Limitations and outlook Although the proposed multiscale CNN has shown convincing efficiency and functionality in this proof of concept, more advanced DL architectures might have the potential to improve on our baseline. We also plan to further investigate on the intrinsic denoising capacities of our method as revealed by the 1.5T experiments. As suggested from the clinical evaluation, patient data seemed to be affected by continuous head movements without any abrupt position changes. It is hence subject to our current and follow-up work to investigate what motion scales can be resolved by the residual CNN when applied as a stand-alone tool. We also plan to explore potential application scenarios of the presented DL-empowered motion correction in other body regions and motion patterns.

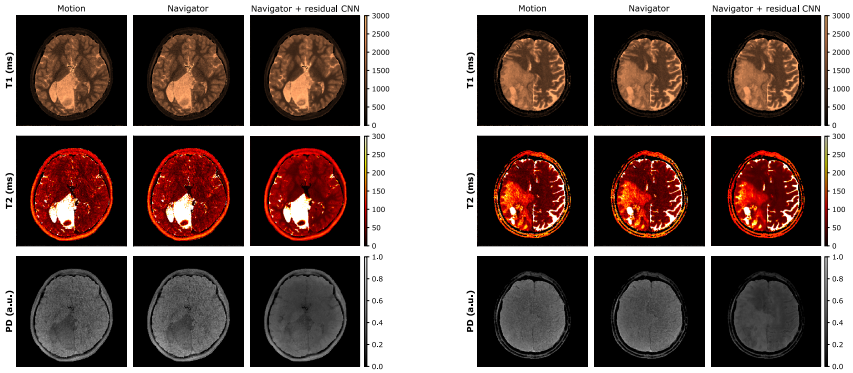

(*a*) Pediatric patient (1.5T) (*b*) Adult patient (3T)

Figure 3: Proposed motion correction for representative clinical test cases (axial views). (a) Pediatric patient with subtotal agenesis of the corpus callosum and interhemispheric cyst, scanned at 1.5T. (b) Adult patient with glioblastoma in the temporo-parietal region with cystic-necrotic and hemorrhagic components, and marked perilesional edema, scanned at 3T. For both patients, the residual CNN improved image quality of all parametric maps (*Navigator + residual CNN*), mitigating image artifacts attributed to head movements during scan sessions.

4. Conclusion

In this work, we propose a 3D multiscale residual CNN for retrospective motion correction in fast 3D whole-brain multiparametric MRI. We present a physics-informed motion simulation, allowing for efficient model training without the requirement of large amounts of paired data. The 3D CNN architecture captures the intrinsically 3D relationships of the motion-induced corruptions to reliably recover high-quality T1, T2 and PD maps. Taking advantage of the sparsity in the residual maps, we can substantially improve the quality of quantitative maps suffering from subject movement - in case of healthy volunteers but also for pediatric and adult patients with pathological findings. This is particularly important in clinical setups where scans frequently have to be repeated, possibly under sedation, because of motion artifacts. With fast scanning time and higher motion-immunity, quantitative MRI may become a standard for clinical practices.

Acknowledgments

This project receives financial support from the Italian Ministry of Health and the Tuscany Region under the project Ricerca Finalizzata, grant No. GR-2016-02361693, Deutsche Forschungsgemeinschaft (DFG) through Research Training Group GRK 2274, TUM International Graduate School of Science and Engineering (IGSSE), GSC 81, and the European Union's Horizon 2020 research and innovation programme, grant agreement No. 952172.

References

Guido Buonincontri, Jan W. Kurzawski, Joshua D Kaggie, Tomasz Matys, Ferdia A Gallagher, Matteo Cencini, Graziella Donatelli, Paolo Cecchi, Mirco Cosottini, Nicola Martini, Francesca Frijia, Domenico Montanaro, Pedro A. Gómez, Rolf F Schulte, Alessandra Retico, and Michela Tosetti. Three dimensional MRF obtains highly repeatable and reproducible multi-parametric estimations in the healthy human brain at 1.5T and 3T. *NeuroImage*, 226:117573, February 2021. ISSN 1053-8119. doi: 10.1016/j.neuroimage.2020.117573.

Gastão Cruz, Olivier Jaubert, Torben Schneider, Rene M. Botnar, and Claudia Prieto. Rigid motion-corrected magnetic resonance fingerprinting. *Magnetic Resonance in Medicine*, 81(2):947–961, 2019. ISSN 1522-2594. doi: https://doi.org/10.1002/mrm.27448.

F. Godenschweger, U. Kägebein, D. Stucht, U. Yarach, A. Sciarra, R. Yakupov, F. Lüsebrink, P. Schulze, and O. Speck. Motion correction in MRI of the brain. *Physics in Medicine and Biology*, 61(5):R32–56, March 2016. ISSN 1361-6560. doi: 10.1088/0031-9155/61/5/R32.

Ting Gong, Qiqi Tong, Zhiwei Li, Hongjian He, Hui Zhang, and Jianhui Zhong. Deep learning-based method for reducing residual motion effects in diffusion parameter estimation. *Magnetic Resonance in Medicine*, 85(4):2278–2293, 2021. ISSN 1522-2594. doi: https://doi.org/10.1002/mrm.28544.

Pedro A. Gómez, Matteo Cencini, Mohammad Golbabaee, Rolf F. Schulte, Carolin Pirkl, Izabela Horvath, Giada Fallo, Luca Peretti, Michela Tosetti, Bjoern H. Menze, and Guido Buonincontri. Rapid three-dimensional multiparametric MRI with quantitative transient-state imaging. *Scientific Reports*, 10(1):13769, August 2020. ISSN 2045-2322. doi: 10.1038/s41598-020-70789-2.

B. Hou, B. Khanal, A. Alansary, S. McDonagh, A. Davidson, M. Rutherford, J. V. Hajnal, D. Rueckert, B. Glocker, and B. Kainz. 3-D Reconstruction in Canonical Co-Ordinate Space From Arbitrarily Oriented 2-D Images. *IEEE Transactions on Medical Imaging*, 37(8):1737–1750, August 2018a. ISSN 1558-254X. doi: 10.1109/TMI.2018.2798801.

Benjamin Hou, Nina Miolane, Bishesh Khanal, Matthew C. H. Lee, Amir Alansary, Steven McDonagh, Jo V. Hajnal, Daniel Rueckert, Ben Glocker, and Bernhard Kainz. Computing CNN Loss and Gradients for Pose Estimation with Riemannian Geometry. In Alejandro F. Frangi, Julia A. Schnabel, Christos Davatzikos, Carlos Alberola-López, and Gabor Fichtinger, editors, *Medical Image Computing and Computer Assisted Intervention – MICCAI 2018*, Lecture Notes in Computer Science, pages 756–764, Cham, 2018b. Springer International Publishing. ISBN 978-3-030-00928-1. doi: 10.1007/978-3-030-00928-1_85.

K. H. Jin, M. T. McCann, E. Froustey, and M. Unser. Deep Convolutional Neural Network for Inverse Problems in Imaging. *IEEE Transactions on Image Processing*, 26(9):4509–4522, September 2017. ISSN 1941-0042. doi: 10.1109/TIP.2017.2713099.

Konstantinos Kamnitsas, Christian Ledig, Virginia F. J. Newcombe, Joanna P. Simpson, Andrew D. Kane, David K. Menon, Daniel Rueckert, and Ben Glocker. Efficient multi-scale 3D CNN with fully connected CRF for accurate brain lesion segmentation. *Medical Image Analysis*, 36:61–78, February 2017. ISSN 1361-8415. doi: 10.1016/j.media.2016.10.004.

Ki Hwan Kim, Seung Hong Choi, and Sung-Hong Park. Improving Arterial Spin Labeling by Using Deep Learning. *Radiology*, 287(2):658–666, December 2017. ISSN 0033-8419. doi: 10.1148/radiol.2017171154.

Jan W. Kurzawski, Matteo Cencini, Luca Peretti, Pedro A. Gómez, Rolf F. Schulte, Graziella Donatelli, Mirco Cosottini, Paolo Cecchi, Mauro Costagli, Alessandra Retico, Michela Tosetti, and Guido Buonincontri. Retrospective rigid motion correction of three-dimensional magnetic resonance fingerprinting of the human brain. *Magnetic Resonance in Medicine*, 84(5):2606–2615, 2020. ISSN 1522-2594. doi: https://doi.org/10.1002/mrm.28301.

Junchi Liu, Mehmet Kocak, Mark Supanich, and Jie Deng. Motion artifacts reduction in brain MRI by means of a deep residual network with densely connected multi-resolution blocks (DRN-DCMB). *Magnetic Resonance Imaging*, 71:69–79, September 2020. ISSN 0730-725X. doi: 10.1016/j.mri.2020.05.002.

Dan Ma, Yun Jiang, Yong Chen, Debra McGivney, Bhairav Mehta, Vikas Gulani, and Mark Griswold. Fast 3D magnetic resonance fingerprinting for a whole-brain coverage. *Magnetic Resonance in Medicine*, 79(4):2190–2197, 2018. ISSN 1522-2594. doi: 10.1002/mrm.26886.

Bhairav Bipin Mehta, Dan Ma, Eric Yann Pierre, Yun Jiang, Simone Coppo, and Mark Alan Griswold. Image reconstruction algorithm for motion insensitive MR Fingerprinting (MRF): MORF. *Magnetic Resonance in Medicine*, 80(6):2485–2500, 2018. ISSN 1522-2594. doi: https://doi.org/10.1002/mrm.27227.

S. Miao, Z. J. Wang, and R. Liao. A CNN Regression Approach for Real-Time 2D/3D Registration. *IEEE Transactions on Medical Imaging*, 35(5):1352–1363, May 2016. ISSN 1558-254X. doi: 10.1109/TMI.2016.2521800.

Ilkay Oksuz. Brain MRI artefact detection and correction using convolutional neural networks. *Computer Methods and Programs in Biomedicine*, 199:105909, February 2021. ISSN 1872-7565. doi: 10.1016/j.cmpb.2020.105909.

Kamlesh Pawar, Zhaolin Chen, N Jon Shah, and Gary F Egan. Motion Correction in MRI using Deep Convolutional Neural Network. In *Proceedings of the 26th Annual Meeting of International Society for Magnetic Resonance in Medicine (ISMRM)*, page 3, Paris, France, 2018.

Daiki Tamada, Marie-Luise Kromrey, Shintaro Ichikawa, Hiroshi Onishi, and Utaroh Motosugi. Motion Artifact Reduction Using a Convolutional Neural Network for Dynamic Contrast Enhanced MR Imaging of the Liver. *Magnetic Resonance in Medical Sciences*, 19(1):64–76, April 2019. ISSN 1347-3182. doi: 10.2463/mrms.mp.2018-0156.

Cagdas Ulas, Giles Tetteh, Michael J. Thrippleton, Paul A. Armitage, Stephen D. Makin, Joanna M. Wardlaw, Mike E. Davies, and Bjoern H. Menze. Direct Estimation of Pharmacokinetic Parameters from DCE-MRI Using Deep CNN with Forward Physical Model Loss. In Alejandro F. Frangi, Julia A. Schnabel, Christos Davatzikos, Carlos Alberola-López, and Gabor Fichtinger, editors, *Medical Image Computing and Computer Assisted Intervention – MICCAI 2018*, Lecture Notes in Computer Science, pages 39–47, Cham, 2018. Springer International Publishing. ISBN 978-3-030-00928-1. doi: 10.1007/978-3-030-00928-1_5.

Muhammad Usman, Siddique Latif, Muhammad Asim, Byoung-Dai Lee, and Junaid Qadir. Retrospective Motion Correction in Multishot MRI using Generative Adversarial Network. *Scientific Reports*, 10(1):4786, March 2020. ISSN 2045-2322. doi: 10.1038/s41598-020-61705-9.

Zhongbiao Xu, Huihui Ye, Mengye Lyu, Hongjian He, Jianhui Zhong, Yingjie Mei, Zhifeng Chen, Ed X. Wu, Wufan Chen, Qianjin Feng, and Yanqiu Feng. Rigid motion correction for magnetic resonance fingerprinting with sliding-window reconstruction and image registration. *Magnetic Resonance Imaging*, 57:303–312, April 2019. ISSN 0730-725X. doi: 10.1016/j.mri.2018.11.001.

Burhaneddin Yaman, Seyed Amir Hossein Hosseini, Steen Moeller, Jutta Ellermann, Kâmil Uğurbil, and Mehmet Akçakaya. Self-supervised learning of physics-guided reconstruction neural networks without fully sampled reference data. *Magnetic Resonance in Medicine*, 84(6):3172–3191, 2020. ISSN 1522-2594. doi: https://doi.org/10.1002/mrm.28378.

Maxim Zaitsev, Julian. Maclaren, and Michael Herbst. Motion Artefacts in MRI: a Complex Problem with Many Partial Solutions. *Journal of magnetic resonance imaging : JMRI*, 42(4):887–901, October 2015. ISSN 1053-1807. doi: 10.1002/jmri.24850.

K. Zhang, W. Zuo, Y. Chen, D. Meng, and L. Zhang. Beyond a Gaussian Denoiser: Residual Learning of Deep CNN for Image Denoising. *IEEE Transactions on Image Processing*, 26(7):3142–3155, July 2017. ISSN 1941-0042. doi: 10.1109/TIP.2017.2662206.

Appendix A. Supplementary figures and tables

A.1. Physics-informed simulation of motion-corrupted data

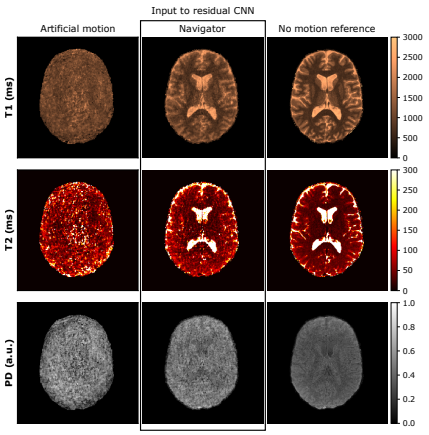

(*a*) Axial views

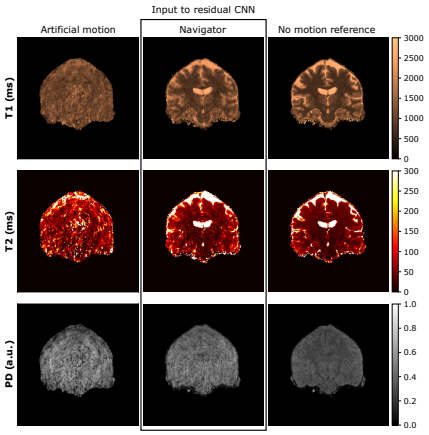

(*b*) Coronal views

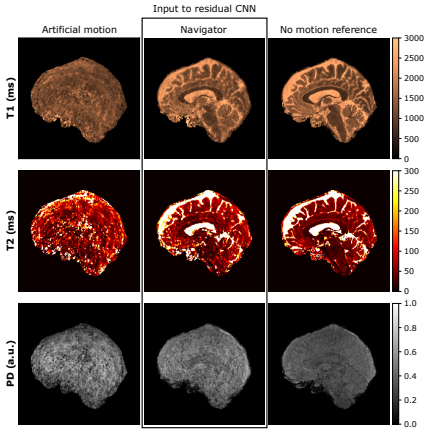

(*c*) Sagittal views

Figure A.1: Physics-informed motion simulation illustrated for a representative volunteer dataset acquired at 3T. Continuous rigid, i.e. translation and rotation, motion patterns are applied to the individual time frames of the acquired motion-free k-t-space data (*No motion reference*), imitating continuous head movements (*Artificial motion*). Navigator-based motion correction is then applied to mitigate artifacts due to inter-segment movements in the first place (*Navigator*). The obtained parametric maps with remaining artifacts due to continuous intra-segment movements are the input to the residual CNN.

A.2. Cross-validation experiment on healthy volunteer data

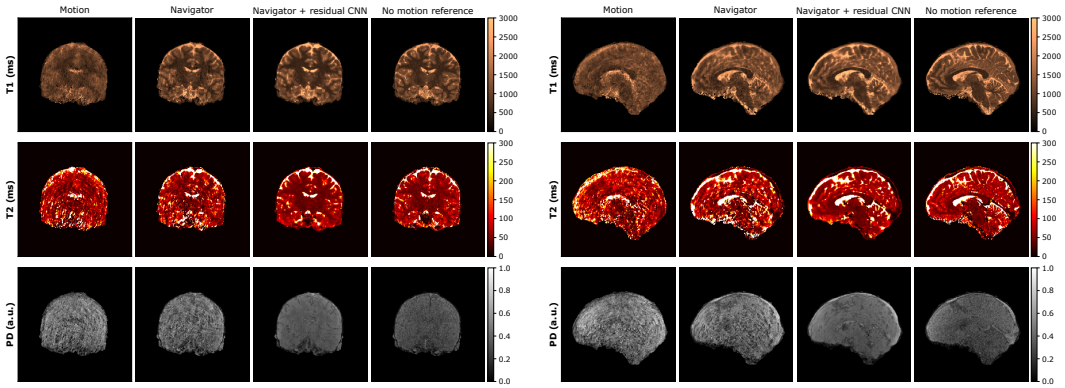

(*a*) Coronal views (*b*) Sagittal views

Figure A.2: Proposed motion correction for a representative volunteer test dataset acquired at 1.5T (coronal and sagittal views).

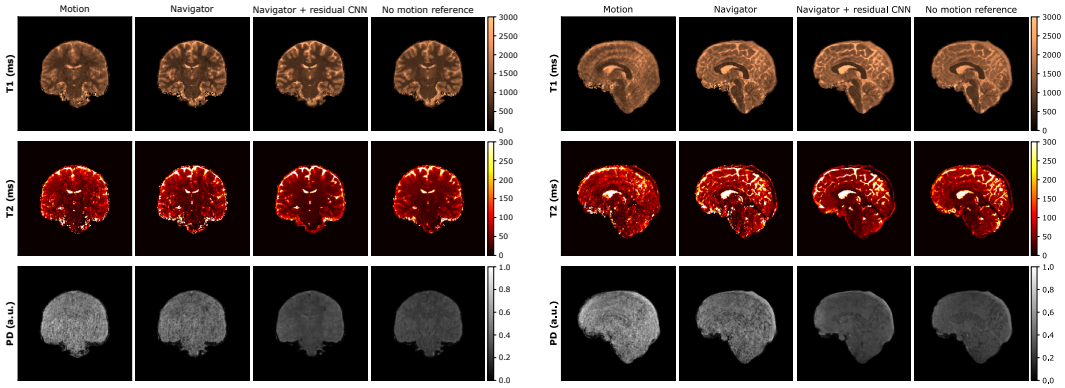

(*a*) Coronal views (*b*) Sagittal views

Figure A.3: Proposed motion correction for a representative volunteer test dataset acquired at 3T (coronal and sagittal views).

Table A.1: Quantitative evaluation of the cross-validation experiment for motion-corrupted, measured volunteer data summarized by concordance correlation coefficient (CCC) and coefficient of determination (R^2) metrics between the result of the respective correction method, i.e. only navigator-based correction (*Navigator*) and navigator-based correction with subsequent residual CNN-based correction (*Navigator + residual CNN*), and the motion-free parameter maps as reference.

		1.5T			**3T**		
Correction	**Metrics**	T1	T2	PD	T1	T2	PD
No correction	CCC	0.48	0.38	0.48	0.68	0.55	0.44
Navigator		0.72	0.61	0.61	0.82	0.75	0.60
Navigator + residual CNN		**0.78**	**0.71**	**0.71**	**0.87**	**0.83**	**0.83**
No correction	R^2	0.51	0.38	0.5	0.68	0.56	0.78
Navigator		0.72	0.61	0.63	0.81	0.76	0.87
Navigator + residual CNN		**0.79**	**0.72**	**0.76**	**0.87**	**0.84**	**0.91**

A.3. Generalization analysis on clinical quantitative MRI

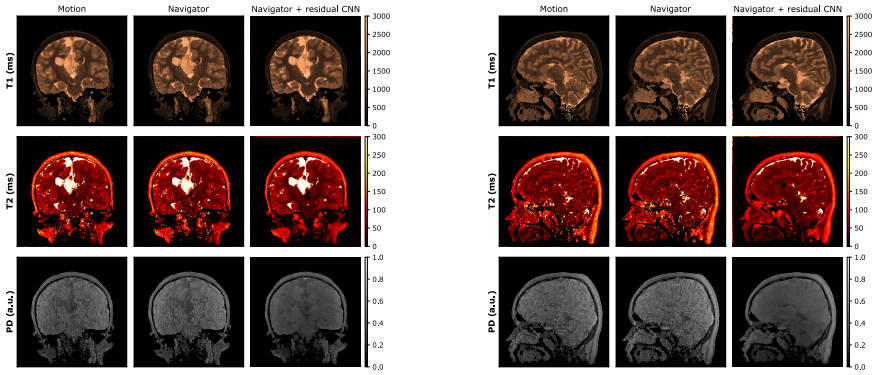

(*a*) Coronal views (*b*) Sagittal views

Figure A.4: Proposed motion correction for the pediatric case acquired at 1.5T (coronal and sagittal views).

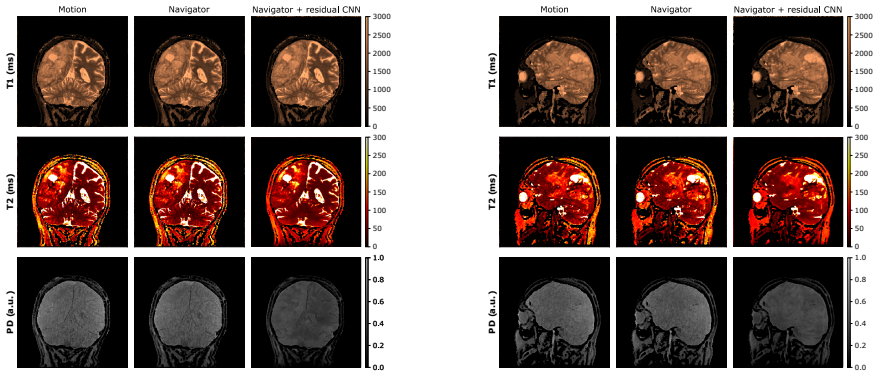

(*a*) Coronal views (*b*) Sagittal views

Figure A.5: Proposed motion correction for the adult patient's dataset acquired at 3T (coronal and sagittal views).

A.4. Ablation study

Table A.2: Cross-validation experiment for quantitative comparison of the proposed *multiscale CNN* with global and local paths and a *singlescale CNN* comprising only two local paths, both applied after initial *Navigator*-based correction. Motion-correction performance is again summarized by concordance correlation coefficient (CCC) and coefficient of determination (R^2) between the motion-corrected and the motion-free parameter maps.

		1.5T			**3T**		
CNN implementation	**Metrics**	**T1**	**T2**	**PD**	**T1**	**T2**	**PD**
Navigator + multiscale CNN (global + local path)	CCC	**0.78**	**0.71**	**0.71**	**0.87**	**0.83**	**0.83**
Navigator + singlescale CNN (2 local paths)	CCC	0.75	0.65	0.63	0.85	0.78	0.77
Navigator + multiscale CNN (global + local pathway)	R^2	**0.79**	**0.72**	**0.76**	**0.87**	**0.84**	**0.91**
Navigator + singlescale CNN (2 local paths)	R^2	0.75	0.66	0.68	0.86	0.8	0.87

Part III

DISCUSSION AND CONCLUSION

6 DISCUSSION

The core of this dissertation is to present methodological advances towards fast and robust multiparametric MRI empowered by DL concepts. To this end, contributing to the translation of applied research on quantitative MRI methods into clinical practice was the main research motive of this work.

Inspired by the seminal work on MRF [62], multiparametric MRI based on transient-state imaging constitutes the core methodological framework of this work. This publication-based dissertation is comprised of three first-author journal and conference publications in Chapter 5, which are supplemented by three first-author conference abstracts that are strongly related to these works in Appendix A.

The following practical challenges of quantitative MRI that arise from the interests and needs for broad clinical application were addressed from three different perspectives:

EFFICIENT QUANTIFICATION OF T_1, T_2 AND PD With a particular focus on fast multiparametric MRI for neuroradiology application, 3D whole-brain T_1, T_2, and PD mapping with QTI was optimized for clinical deployment in routine glioma imaging protocols. Initial clinical experience showed that the highly accelerated acquisition meets the tight time constraints in clinical practice and the CS reconstruction combined with a NN-based parameter inference produced parametric maps with relevant image quality and resolution. Synthesizing qualitative MRI contrasts can make conventional T_1-weighted, T_2-weighted and FLAIR sequences obsolete and paves the way to considerably shortened routine brain imaging protocols. With regard to a potential suitability as a MRI biomarker, 3D QTI demonstrated comprehensive information about tumor (sub-) structures captured in T_1 and T_2 parameters and quantifiable differentiation of healthy and diseased tissue that goes beyond the solely qualitative analysis of contrast-weighted MRI. (Section 5.1 [2], Section A.2 [5] and [7])

JOINT RELAXATION TIMES AND DIFFUSION TENSOR QUANTIFICATION Although advanced quantitative MRI techniques have proven to provide important insights for comprehensive tissue characterization, the extensive post-processing for data harmonization that is necessary for inferring diagnostically useful information, is still a major barrier. For this reason, the rich patho-physiological information that could in theory be retrieved from state-of-the-art MRI protocols with multiple but individual quantitative and qualitative

sequences, is commonly underutilized in clinical practice. To tackle this problem, another motive of this work was to expand MRF-based multiparameter quantification beyond joint T_1 and T_2 mapping only to also include anisotropic diffusion effects. The motivation for this project was twofold: With regard to the clinical practice, multiparametric information that is readily available in the same, natural image space significantly simplifies clinical data analysis workflows and eventually makes parameter-driven tissue characterization more user-friendly. From a technical perspective, jointly encoding for relaxation and diffusion information has great potential for increasing scan efficiency by exploiting the inherent relationships between the respective biophysical processes. The great efficiency gain, which simultaneous relaxation and diffusion encoding might promise, however, comes at the expense of various sources of artifacts that overlay with the primarily encoded parameter information. This poses a major challenge for reconstructing parameter maps from the transient signal responses. Only a spatially-constraint CNN architecture proved capable of solving this multivariate regression problem. Capturing both temporal and spatial correlation, high-quality maps of T_1, T_2 and the diffusion tensor elements were reliably reconstructed. This would have been infeasible with established parameter fitting algorithms. The proposed DL model was able to disentangle primary signal components from secondary effects due to spiral undersampling, the interference of diffusion-encoding and readout gradients or subject movements propagating through the signal evolution. This was the case for healthy volunteers and multiple sclerosis patients. The demonstrated generalization to regions of diagnostic importance such as white matter lesions is a crucial requirement for clinical deployment. (Section 5.2 [1], Section A.1 [4] and referenced in [91, 113, 114])

RETROSPECTIVE 3D MOTION CORRECTION FOR FAST MULTIPARAMETRIC MRI While fast multiparametric mapping via transient-state encoding has shown promising results in the aforementioned studies, a major barrier for clinical translation nevertheless arises in case of patient motion - a complex problem that has existed since the inception of MRI as a medical imaging modality [115]. And despite significant technological advances, motion artifacts have remained an enormous issue for clinical practice as they frequently render MRI scans diagnostically useless. Although susceptibility to motion is not a problem unique to quantitative MRI, it is amplified due to the prolonged scanning or the transient nature of temporal signal encoding. Therefore, the third project within this work aimed at increasing motion robustness of fast multiparametric MRI with 3D QTI by taking advantage of the previously demonstrated capabilities of DL for (motion) artifact reduction. The proposed two-stage correction with its

key building blocks - a realignment based on self-navigators and a subsequent CNN-based residual learning - reliably mitigated motion-induced artifacts and inferred high-quality T_1, T_2 and PD maps. This was demonstrated for healthy volunteer data and importantly also for real clinical cases, including pediatric and adult patients with large brain lesions. As such, this constitutes another technical improvement on the way to fast and robust multiparametric MRI that is critical for its integration into clinical routine protocols (Section 5.3 [3]).

The adoption of DL methods for accelerating multiparametric MRI and for increasing its robustness, e.g. to spatial undersampling or subject motion, is at the core of this dissertation. The unparalleled success of DL has taken the entire field of medical imaging a major step forward and has triggered significant advances with regard to the fundamental challenges of MRI. Thus, DL has emerged extremely powerful also in bridging the gap towards a wider clinical deployment of quantitative MRI with the potential to further increase the capabilities and the diagnostic outcome of MRI.

However, to actually have a positive impact on clinical practice, recently proposed DL-enabled technical improvements, which also include the work presented in this dissertation, require extensive clinical validation. This requirement goes beyond the initial feasibility or generalizability analyses performed in the works relevant to this thesis. Although the proposed methodological advances proved successful in a bandwidth of mixed study cohorts of both healthy volunteers and patients with different clinical pictures, stages of disease and treatment histories, these test scenarios were still highly defined and only partially covered the actual clinical radiology practice. Therefore, dedicated reproducibility studies need to follow up on these initial proof of concepts, including, for example, longitudinal evaluation to reveal potential benefits for monitoring treatment responses along the course of disease.

For a clinically impactful improvement of the current state of the art in radiology workflows, another major bottleneck of DL methods is the general requirement of large amounts of training data, which has remained an open or only partly solved challenge in particular for supervised learning approaches [116]. Despite the successful proof of concept, the rather small dataset was a clear limitation for the proposed CNN-based joint T_1, T_2 and diffusion tensor mapping [1]. It is strongly believed that more available training data could further increase the reconstruction performance of the DL model, e.g. in cases of severe motion corruption.

Unlike other application fields of DL, the entire MRI signal and hence image formation process - from (undersampled) acquisition to reconstruction - follows the laws of MR physics. Therefore, the possibility to cast the underlying physical laws into mathematical mod-

els, gives rise to physics-informed surrogate NNs [98]. In particular, physics-driven forward simulations have proven to be efficient and versatile means to circumvent the need for paired training data in the course of this dissertation [3] and other works [94, 117, 118].

7

CONCLUSIONS AND OUTLOOK

With the goal of pushing the state of the art in quantitative MRI forward, the methodological improvements proposed in this dissertation are primarily driven by linking novel concepts at the interface of MR physics and computer science. To this end, the key aspects of this thesis are a highly accelerated, spatially undersampled acquisition of transient-state signals combined with DL methods for reconstruction and parameter inference.

On the methodological side, these key building blocks leave room for further improvement in several aspects. Combining massive undersampling in both the spatial and the parameter domain with high performance reconstruction algorithms, and DL methods in particular, significantly increased parameter mapping efficiency. As such, continuing to explore the optimization potential in transient-state imaging schemes can further enhance its clinical potential and is hence subject to future work. In the spirit of end-to-end learning [87], DL-driven MRI sequence optimization could be a potentially promising research direction on the way to faster scanning, higher robustness, better SNR or increased quantification capabilities [68, 70, 119]. Likewise, DL approaches that build directly on the raw k-space domain [82, 86] or that account for the complex nature of MRI data [83, 120] could further increase reconstruction performance, whilst ensuring consistency with the actually acquired data. The contribution of this thesis is primarily focused on supervised learning paradigms, which are considered the most effective training strategy so far. However, research on semi-supervised or unsupervised training setups is actively evolving with the goal to achieve robust training of deep NNs despite the lack of paired MRI training data [121]. As such, it is subject of future work to explore suitable training strategies beyond supervised learning with regard to MRI in general and quantitative MRI in specific. The current high pace of DL advances will certainly trigger further progress towards higher acceleration, sparser sampling schemes or faster reconstruction runtimes.

From a clinical perspective, extensive evaluation, sensitivity analysis and stress testing of the proposed methodological and algorithmic advances for large, diverse patient cohorts, including adults and pediatrics, and multiple diagnostic issues is crucial for establishing multiparametric MRI as a quantitative image-based biomarker. Aiming for a precise and sensitive tissue characterization in general and pathology assessment in particular, the ability to reveal multicomponent parameter estimates on a subvoxel level would certainly further

increase the diagnostic value of quantitative MRI and constitutes another promising step towards personalized medicine [122–124]. Also, transferring the presented acquisition and reconstruction framework to body regions outside the brain, e.g. with more diffuse, non-rigid motion patterns such as abdominal imaging, would be an interesting direction for future work [125, 126].

Part IV

APPENDIX

A

PEER-REVIEWED CONFERENCE ABSTRACTS

This chapter summarizes peer-reviewed conference abstracts that complement the main contributions of the author to improve fast and robust multiparametric MRI in Chapter 5. Deep learning-enabled diffusion tensor MR Fingerprinting introduces the concept of joint relaxation and diffusion tensor MRF and is considered prior work to the publication [1] in Section 5.2. Accelerated 3D multiparametric MRI in glioma patients - Initial clinical experience summarizes early clinical experience with 3D QTI when integrated into routine glioma imaging with a primary focus on technical viability aspects. It lays the foundation for the extended feasibility study [2] in Section 5.1. Synchronizing dimension reduction and parameter inference in 3D multiparametric MRI: A hybrid neural network approach demonstrates a NN framework that combines a learnt latent-space compression of the acquired transient-state signal with a subsequent inference of T_1, T_2 and PD estimates. The layout of the conference abstracts was harmonized.

A.1 DEEP LEARNING-ENABLED DIFFUSION TENSOR MR FINGERPRINTING

Peer-reviewed conference abstract

Authors: CM. Pirkl, I. Lipp, G. Buonincontri, M. Molina-Romero, A. Sekuboyina, D. Waldmannstetter, J. Dannenberg, V. Tomassini, M. Tosetti, DK. Jones, MI. Menzel, BH. Menze, PA. Gómez

In: *Proceedings of the 27th Annual Meeting of the International Society for Magnetic Resonance in Medicine (ISMRM)*. Montréal, QC, Canada, 2019. [4].

Synopsis: "MR Fingerprinting enables the quantification of multiple tissue properties from a single, time-efficient scan. Here we present a novel Diffusion Tensor MR Fingerprinting acquisition scheme that is simultaneously sensitive to T_1, T_2 and the full diffusion tensor. We circumvent the longstanding issue of phase errors in diffusion encoding and expensive dictionary matching by using a neural network architecture capable of learning the non-linear relation between fingerprints and multiparametric maps, robustly mitigating motion, undersampling and phase artifacts. As such, our framework enables the simultaneous quantification of relaxation parameters together with the diffusion tensor from a single, highly accelerated acquisition."

Contribution of thesis author: Algorithmic development and implementation, experimental design, data analysis, abstract preparation and editing.

DEEP LEARNING-ENABLED DIFFUSION TENSOR MR FINGERPRINTING

Carolin M. Pirkl[1,2], Ilona Lipp[3,4], Guido Buonincontri[5], Miguel Molina-Romero[1,2], Anjany Sekuboyina[1,6], Diana Waldmannstetter[1], Jonathan Dannenberg[2,7], Valentina Tomassini[3,4], Michela Tosetti[5], Derek K. Jones[3], Marion I. Menzel[2], Bjoern H. Menze[1], Pedro A. Gómez[1,2]

[1] Computer Science, Technical University of Munich, Garching, Germany,
[2] GE Healthcare, Munich, Germany,
[3] Cardiff University Brain Research Imaging Centre (CUBRIC), Cardiff University School of Psychology, Cardiff, United Kingdom,
[4] Division of Psychological Medicine and Clinical Neurosciences, Cardiff University School of Medicine, Cardiff, United Kingdom,
[5] Imago7 Foundation, Pisa, Italy,
[6] Department of Neuroradiology, Klinikum rechts der Isar,Munich, Germany,
[7] Department of Physics, Technical University of Munich, Garching, Germany

SYNOPSIS

MR Fingerprinting enables the quantification of multiple tissue properties from a single, time-efficient scan. Here we present a novel Diffusion Tensor MR Fingerprinting acquisition scheme that is simultaneously sensitive to T1, T2 and the full diffusion tensor. We circumvent the longstanding issue of phase errors in diffusion encoding and expensive dictionary matching by using a neural network architecture capable of learning the non-linear relation between fingerprints and multiparametric maps, robustly mitigating motion, undersampling and phase artifacts. As such, our framework enables the simultaneous quantification of relaxation parameters together with the diffusion tensor from a single, highly accelerated acquisition.

INTRODUCTION

MR Fingerprinting (MRF) provides a framework for simultaneous quantification of multiple tissue parameters from a single, time-efficient acquisition [1]. Recently, attempts have been made to develop diffusion-weighted MRF techniques. However, the transient nature of MRF

signals makes them highly susceptible to severe motion artifacts, especially when considering the full diffusion tensor (DT). Susceptibility to motion, together with the exponential scaling of the dictionary with the dimensionality of the parameter space, pose a significant challenge and limit existing diffusion-weighted MRF applications to the estimation of the apparent diffusion coefficient [2–5]. Here we present a novel Diffusion Tensor MRF (DT-MRF) acquisition, where diffusion-encoding gradients in all three spatial dimensions encode the full DT. Inspired by image quality transfer ideas [6, 7], we take advantage of neural networks to recover information from images corrupted from phase errors due to motion and spatial undersampling artefacts to reliably reconstruct T1 and T2 maps together with the DT maps from a single acquisition.

METHODS

Building on diffusion-weighted steady-state free precession literature [8], we propose a diffusion-sensitive MRF-type acquisition as follows (Figure 1a-e). Diffusion-encoding directions are varied randomly every 34 repetitions, with non-diffusion-weighted unbalanced gradients added every six directions. In total, 30 diffusion directions, chosen based on the electrostatic repulsion algorithm [9], are acquired. An initial inversion pulse is followed by a train of constant flip angles with repeating variable flip angle ramps in the latter part of the sequence to increase T1 and T2 sensitivity. Repetition times are set constant during diffusion-encoding with longer waiting periods in-between directions. During each repetition, one arm of an undersampled spiral interleave is acquired. Image time-series are obtained using sliding-window reconstruction.

In an IRB-approved study, data from eleven patients with Multiple Sclerosis (MS) and nine healthy subjects were acquired on a 3 T HDx MRI system (GE Healthcare, Milwaukee, WI) using an eight channel receive-only head RF coil, after obtaining written informed consent. The protocol (see Table 1) included diffusion tensor imaging (DTI), DESPOT1/2 sequences and a high resolution T1w acquisition for co-registering all modalities. In addition to these clinical sequences, 8-12 axial slices, covering the middle portion of the brain were acquired with our DT-MRF sequence. We obtained T1 and T2 maps from DESPOT1/2 and calculated the DT from the DTI dataset. These clinical gold-standard maps constitute the ground-truth for the deep learning approach.

Bypassing conventional dictionary matching [10, 11], we propose a modified UNET architecture to learn a non-linear function between the temporal evolution of the DT-MRF magnitude images, and the quantitative relaxation and DT maps, scaled from 0 to 1, as output (Figure 1f). The model was implemented using TensorFlow and

Table 1: Acquisition parameters. For each of the sequences, main parameters are provided.

	DT-MRF sequence	**Clinical gold-standard sequences**		
		DTI	**DESPOT1/2**	**T1w**
Sequence(s)	DT-MRF	Single-shot DW-EPI	SPGR, IR-SPGR, bSSFP	FSPGR
Native resolution (mm^2)	1.2×1.2	1.8×1.8	1.7×1.7	1.0×1.0
Field of view (mm^2)	225×225	230×230	220×220	256×256
Number of slices	$10-12$	57	3D	3D
Native slice thickness (mm)*	5	2.4	1.7	1
TE (ms)	6	94.5	SPGR: 2.1 bSSFP: 1.6 IR-SPGR: 2.1	3
TR (ms)	22, 50	16000	SPGR: 4.7 bSSFP: 3.2 IR-SPGR: 4.7	7.8
TI (ms)	18	-	IR-SPGR: 450	-
FA (°)	37, $0-49$ ramps	90	SPGR: 3, 4, 5, 6, 7, 8, 9, 13, 18 bSSFP: 0.6, 14.1, 18.5, 23.8, 29.1, 35.3, 45, 60 IR-SPGR: 5	20
b-value (s/mm^2)	-	1200	-	-
Spiral interleaves (number)	34	-	-	-
Total acquisition time (min)	2.5	12.5	10	7.5

* Clinical gold-standard maps where resampled to a slice thickness of 5 mm

trained for 650 epochs using L2 loss with ADAM optimizer, batch size of 5, learning rate of 1e-4 and dropout rate of 0.5. Aiming at an efficient and robust reconstruction method, we trained our model on healthy subjects and MS patients. We calculated mean diffusivity (MD), axial diffusivity (AD), radial diffusivity (RD) and fractional anisotropy (FA) metrics from the predicted and gold standard DT [12].

RESULTS

Predicted maps correlate highly with the DESPOT1/2 and DTI gold-standard, respectively (Figure 2). The quantification errors for the diffusion metrics also indicate good agreement with the gold-standard. Figure 3 shows estimated maps for T1, T2 and the DT elements together with the reference for two representative test datasets. High consistency between the predicted maps and traditional, gold-standard methods can be visually observed. The corresponding diffusion metrics confirm this good correspondence and demonstrate that directional information in the predicted DT is preserved (Figure 4).

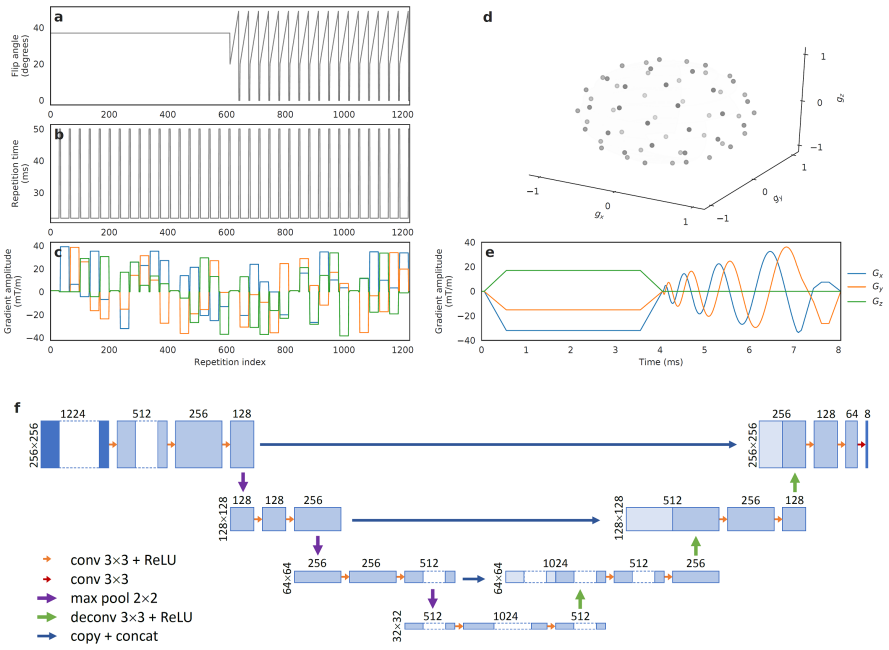

Figure 1: DT-MRF acquisition and deep learning reconstruction framework. a, Constant flip angles followed by variable flip angle ramps. b, Repetition time pattern with longer waiting periods when changing diffusion-encoding directions. c, Random variation of diffusion-encoding gradients. d, Spherical representation of the acquired diffusion directions. e, Diffusion-encoding and spiral readout gradients. f, The UNET architecture receives the spatiotemporal magnitude image data (256×256, 1224 channels) as input and outputs quantitative maps of T1, T2 and the DT (256×256, 8 channels). The database was partitioned into disjunct sets (including MS patients and healthy subjects) for training (13 subjects), validation (2 subjects) and testing (5 subjects).

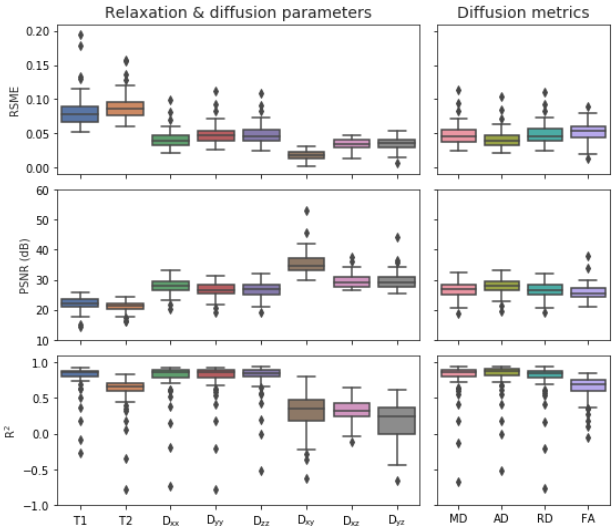

Figure 2: Prediction quality for the test dataset with root-mean-square error (RMSE), peak signal-to-noise ratio (PSNR) and R^2-score between prediction and reference (calculated for individual slices) as primary performance metrics. To ensure comparability, RMSE was derived from the scaled maps. T1 and T2 estimates indicate good consistency with the gold-standard. Estimated DT elements agree well with the gold-standard in terms of RMSE and PSNR; R^2 indicates higher correlation for diagonal than off-diagonal elements. The DT-MRF framework allowed for reliable quantification of directional information as demonstrated by the high correlation of predicted and reference diffusion metrics MD, AD, RF and FA.

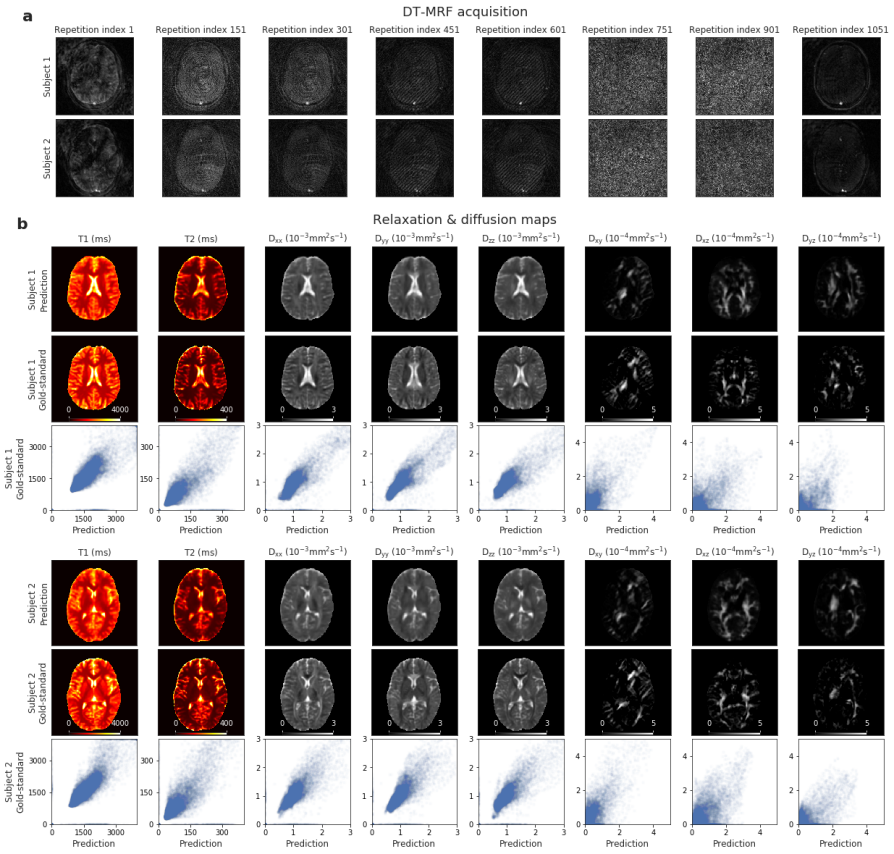

Figure 3: Image input time-series, predicted and gold-standard T1 and T2 maps together with the DT elements for two representative test volumes. a, Exemplary samples from the magnitude image time-series show motion and spatial undersampling artefacts. b, Predicted maps do not show visual artifacts, offering satisfying image quality. Quantitative relaxation as well as DT maps and indicate good consistency with gold-standard methods as seen from the scatter plots.

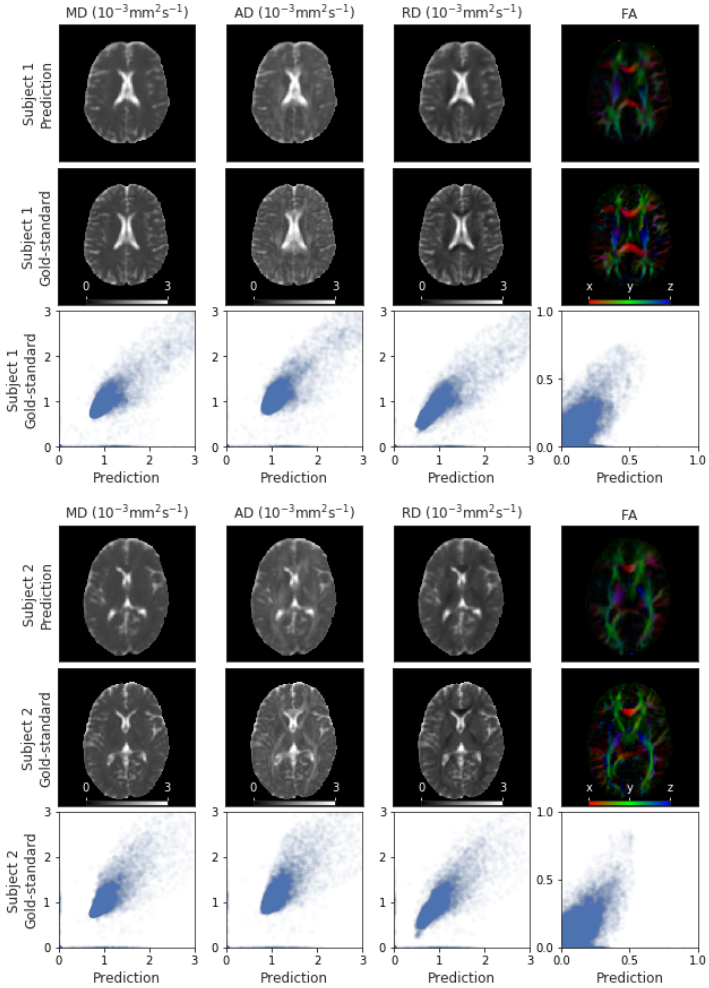

Figure 4: Diffusion metrics MD, AD, RD and FA calculated from predicted and gold-standard DT maps for two representative test volumes. Predicted and reference MD, AD and RD show good visual agreement. Our method is able to reliably recover the predominant diffusion direction in white matter even though FA is slightly underestimated in high anisotropy areas.

DISCUSSION

The proposed DT-MRF scheme simultaneously encodes T1, T2 and the DT with a highly accelerated acquisition (12 s/slice). In combination with the deep learning-based reconstruction, this enables fast parameter inference, providing artifact-free quantitative relaxation and DT maps whilst making expensive postprocessing pipelines of conventional multi-modality imaging redundant. Despite achieving high correlation with respect to gold-standard DTI, the network does not fully recover the characteristic fiber structure of high anisotropy areas but still captures directional information. We expect that further improvements in the diffusion-encoding and neural network reconstruction will be able to even further improve its predictive quality and is hence subject of future work.

CONCLUSION

We propose a novel DT-MRF acquisition and reconstruction framework. Taking advantage of deep learning architectures, we reconstruct multiparametric outputs from spatiotemporal MRF data corrupted by motion, phase errors and undersamp-ling artifacts. We provide a proof-of-concept for simultaneous quantification of T1 and T2 relaxation maps and DT maps with a MRF-type acquisition scheme that goes beyond ADC mapping alone. Additionally, we show that circumventing conventional dictionary matching paves the way to innovative higher-dimensional MRF applications.

BIBLIOGRAPHY

[1] Dan Ma, Vikas Gulani, Nicole Seiberlich, et al. "Magnetic Resonance Fingerprinting." In: *Nature* 495.7440 (Mar. 2013), pp. 187–192.

[2] Ouri Cohen and Matthew R. Rosen. "Simultaneous Diffusion, PD, T1, and T2 Mapping with Optimized MR Fingerprinting EPI." In: *Proceedings of the 26th Annual Meeting of the International Society for Magnetic Resonance in Medicine (ISMRM)*. Paris, France, 2018.

[3] Benedikt Rieger, Mehmet Akçakaya, Lothar Schad, et al. "Simultaneous quantification of T1, T2 and Apparent Diffusion Coefficient using Magnetic Resonance Fingerprinting based on Echo Planar Imaging." In: *Proceedings of the 26th Annual Meeting of International Society for Magnetic Resonance in Medicine (ISMRM)*. Paris, France, 2018.

[4] Yun Jiang, Jesse Ian Hamilton, Wei-Ching Lo, et al. "Simultaneous T1, T2 and Diffusion Quantification using Multiple Contrast Prepared Magnetic Resonance Fingerprinting." In: *Proceedings of the 25th Annual Meeting of International Society for Magnetic Resonance in Medicine (ISMRM)*. Honolulu, HI, USA, 2017.

[5] Yun Jiang, Jesse Ian Hamilton, Katharine L. Wright, et al. "Simultaneous Quantification of T1, T2 and Diffusion with Diffusion-weighted drive-equilibrium prepared Magnetic Resonance Fingerprinting." In: *Proceedings of the 24th Annual Meeting of International Society for Magnetic Resonance in Medicine (ISMRM)*. Singapore, 2016.

[6] Daniel C Alexander, Darko Zikic, Aurobrata Ghosh, et al. "Image quality transfer and applications in diffusion MRI." In: *NeuroImage* 152.2017 (2017), pp. 283–298.

[7] Ryutaro Tanno, Daniel E. Worrall, Aurobrata Ghosh, et al. "Bayesian Image Quality Transfer with CNNs: Exploring Uncertainty in dMRI Super-Resolution." In: *MICCAI*. 2017.

[8] Jennifer A. McNab and Karla L. Miller. "Steady-state diffusion-weighted imaging: theory, acquisition and analysis." In: *NMR in biomedicine* 23.7 (Aug. 2010), pp. 781–793.

[9] D. K. Jones, M. A. Horsfield, and A. Simmons. "Optimal strategies for measuring diffusion in anisotropic systems by magnetic resonance imaging." In: *Magnetic Resonance in Medicine* 42.3 (Sept. 1999), pp. 515–525.

[10] Pedro A. Gómez, Miguel Molina-Romero, Cagdas Ulas, et al. "Simultaneous Parameter Mapping, Modality Synthesis, and Anatomical Labeling of the Brain with MR Fingerprinting." In: *Medical Image Computing and Computer-Assisted Intervention – MICCAI 2016*. Ed. by Sebastien Ourselin, Leo Joskowicz, Mert R. Sabuncu, et al. Cham: Springer International Publishing, 2016, pp. 579–586. ISBN: 978-3-319-46726-9.

[11] Pedro A. Gómez, Guido Buonincontri, Miguel Molina-Romero, et al. "Accelerated parameter mapping with compressed sensing: an alternative to MR Fingerprinting." In: *Proceedings of the 25th Annual Meeting of International Society for Magnetic Resonance in Medicine (ISMRM)*. Honolulu, HI, USA, 2017.

[12] P. J. Basser, J. Mattiello, and D. Lebihan. "Estimation of the Effective Self-Diffusion Tensor from the NMR Spin Echo." In: *Journal of Magnetic Resonance, Series B* 103.3 (Mar. 1994), pp. 247–254.

A.2 ACCELERATED 3D MULTIPARAMETRIC MRI IN GLIOMA PATIENTS - INITIAL CLINICAL EXPERIENCE

Peer-reviewed conference abstract

Authors: CM. Pirkl, L. Nuñez-Gonzalez, S. Endt, G. Buonincontri, RF. Schulte, PA. Gómez, M. Smits, BH.Menze, MI. Menzel, JA. Hernandez-Tamames

In: *Proceedings of the 28th Annual Meeting of the International Society for Magnetic Resonance in Medicine (ISMRM)*. 2020. [5]

Synopsis: "In brain tumor diagnosis, fully quantitative, multiparametric MRI offers great opportunities as it allows for comprehensive tissue and hence tumor characterization which is essential for treatment planning and monitoring the treatment response. With its highly accelerated acquisition, advanced rapid MR mapping techniques facilitate multiparametric imaging in clinically acceptable scan times, providing quantitative, reproducible and accurate diagnostic information that is less affected by system and interpretation biases. In this work, we present initial clinical results and demonstrate the feasibility of a novel 3D multiparametric quantitative transient-state imaging (QTI) acquisition scheme in glioma patients."

Contribution of thesis author: Conceptualization, algorithmic development and implementation, experimental design, data analysis, abstract preparation and editing.

ACCELERATED 3D MULTIPARAMETRIC MRI IN GLIOMA PATIENTS - INITIAL CLINICAL EXPERIENCE

Carolin M. Pirkl[1,2], Laura Nuñez-Gonzalez[3], Sebastian Endt[1,2], Guido Buonincontri[4,5], Rolf F. Schulte[2], Pedro A. Gómez[1], Marion Smits[3], Bjoern H. Menze[1], Marion I. Menzel[2,6], Juan A. Hernandez-Tamames[3]

[1] Department of Informatics, Technical University of Munich, Munich, Germany,

[2] GE Healthcare, Munich, Germany,

[3] Radiology & Nuclear Medicine, Erasmus University Medical Center, Rotterdam, Netherlands,

[4] Fondazione Imago7, Pisa, Italy,

[5] IRCCS Fondazione Stella Maris, Pisa, Italy,

[6] Department of Physics, Technical University of Munich, Germany

SYNOPSIS

In brain tumor diagnosis, fully quantitative, multiparametric MRI offers great opportunities as it allows for comprehensive tissue and hence tumor characterization which is essential for treatment planning and monitoring the treatment response. With its highly accelerated acquisition, advanced rapid MR mapping techniques facilitate multiparametric imaging in clinically acceptable scan times, providing quantitative, reproducible and accurate diagnostic information that is less affected by system and interpretation biases. In this work, we present initial clinical results and demonstrate the feasibility of a novel 3D multiparametric quantitative transient-state imaging (QTI) acquisition scheme in glioma patients.

INTRODUCTION

Due to its superior soft-tissue contrast, MRI is the method of choice for tissue characterization in brain tumor diagnosis. It also guides treatment planning and is required to monitor treatment response. Here quantitative MRI offers great opportunities as it provides comprehensive diagnostic information. Owing to long acquisition times of conventional quantitative MR techniques, routine imaging protocols for brain tumors mainly present qualitative information [1]. The limitations arising from qualitative imaging and interpretation

also apply to the process of identifying and describing tumor substructures of interest. That is, the rich patho-physiological information of advanced clinical imaging sequences is underutilized as analyzing the complex multi-parametric, multimodal and even multi-temporal image data sets remains a major challenge. Aiming for quantitative imaging biomarkers, advanced rapid multiparametric mapping techniques [2–5] have recently been demonstrated to facilitate multiparametric imaging in clinical acceptable scan times, providing quantitative, reproducible and accurate diagnostic information which is less affected by system and interpretation biases. In this work, we present initial clinical results of a novel 3D multiparametric quantitative transient-state imaging (QTI) acquisition scheme in glioma patients (grade II-IV).

METHODS

As part of an IRB-approved study, data from three glioma patients were acquired on a 3 T MR750 system (GE Healthcare, Milwaukee, WI) after obtaining written informed consent. The MR protocol included conventional, qualitative and quantitative sequences.

In addition to the clinical sequences, the patients were scanned with the proposed 3D QTI acquisition which is based on the following schedule: after an initial adiabatic inversion (TI=18 ms), flip angles ($0.8° \leqslant \text{FA} \leqslant 70°$) are applied in a ramp-up/down pattern with TR/TE=7.8 ms/1.8 ms and 880 repetitions using a varying-density spiral readout ($22.5 \times 22.5 \times 22.5$ cm^3 FOV, $1.25 \times 1.25 \times 1.25$ mm^3 isotropic resolution) with in-plane and spherical rotations [6]. In-plane rotations were incremented with the golden angle from one repetition to the next. Spherical rotations were applied to acquire data in all three spatial dimensions with fully sampled in-plane discs. 3D QTI data was reconstructed using k-space weighted view-sharing [7] and zero-filling, respectively, followed by dimensionality reduction via SVD subspace projection, gridding onto a Cartesian grid using the gpuNUFFT [8], 3D FFT and subsequent coil sensitivity correction. We obtained quantitative maps of T1, T2 and PD by matching the reconstructed subspace images to a dictionary which was computed for T1=[100:20:4000] ms and T2=[20:4:600] ms using the Extended Phase Graphs formalism [9]. As an alternative to exhaustive dictionary matching, we trained a neural network to infer T1, T2 and PD estimates. As illustrated in Figure 1, the proposed model receives the first 10 singular components of the SVD compressed QTI signal $\mathbf{x}$ as input and outputs the underlying tissue parameters q, i.e. T1, T2 and a PD-related scaling factor, with the final PD estimate $\text{PD} = \frac{\|\mathbf{x}\|_2}{q_3}$. We trained the model on 70 % of the samples in the simulated dataset with added Gaussian noise, using ReLU activation, L1

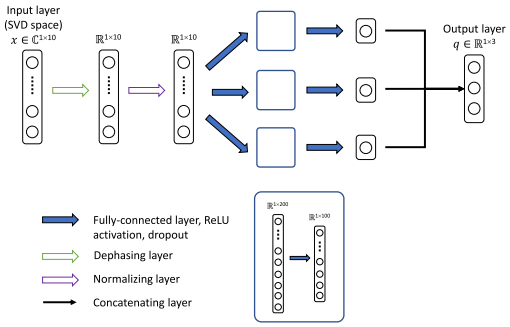

Figure 1: Neural network architecture. The model receives the first 10 singular components of the SVD compressed QTI signal $\mathbf{x}$ as input and outputs the underlying tissue parameters q, i.e. T1, T2 and a PD-related scaling factor, with $\text{PD} = \frac{\|\mathbf{x}\|_2}{q_3}$.

loss and ADAM optimization (learning rate=1e-4, dropout rate=0.8, 1200 epochs).

RESULTS

Isotropic 3D maps of T1, T2 and PD obtained with view-sharing and zero-filling reconstruction, respectively, and subsequent dictionary matching are shown in Figure 2. Figure 3 shows that parametric maps obtained via fast neural network inference (computation time of less than 1 min) are largely consistent with the dictionary matching results (computation time of 16 min). That is, combining GPU gridding, zero-filling and neural network inference in the reconstruction pipeline, we achieved computation times of less than 7 min. As seen from Figure 4, patient movement can affect the estimation of tissue parameters. In case of head motion, 3D QTI achieves an image quality comparable to state-of-the-art FSPGR and CUBE FLAIR sequences.

DISCUSSION

Initial experience with 3D QTI in glioma patients demonstrated fully quantitative, multiparametric MR mapping with high isotropic resolution and acquisition time that make it feasible for use under tight clinical time-constraints. Combining the 3D QTI framework with a neural network for T1, T2 and PD inference proves to be a fast and memory-efficient alternative to a conventional dictionary matching approach. Once trained, the neural network offers fast parameter quantification that is not restricted by the size or the granularity of the dictionary. 3D QTI demonstrated to reliably identify tissue and hence tumor heterogeneity that is captured in T1, T2 and PD parameters. As such, it offers comprehensive tissue assessment of tumor

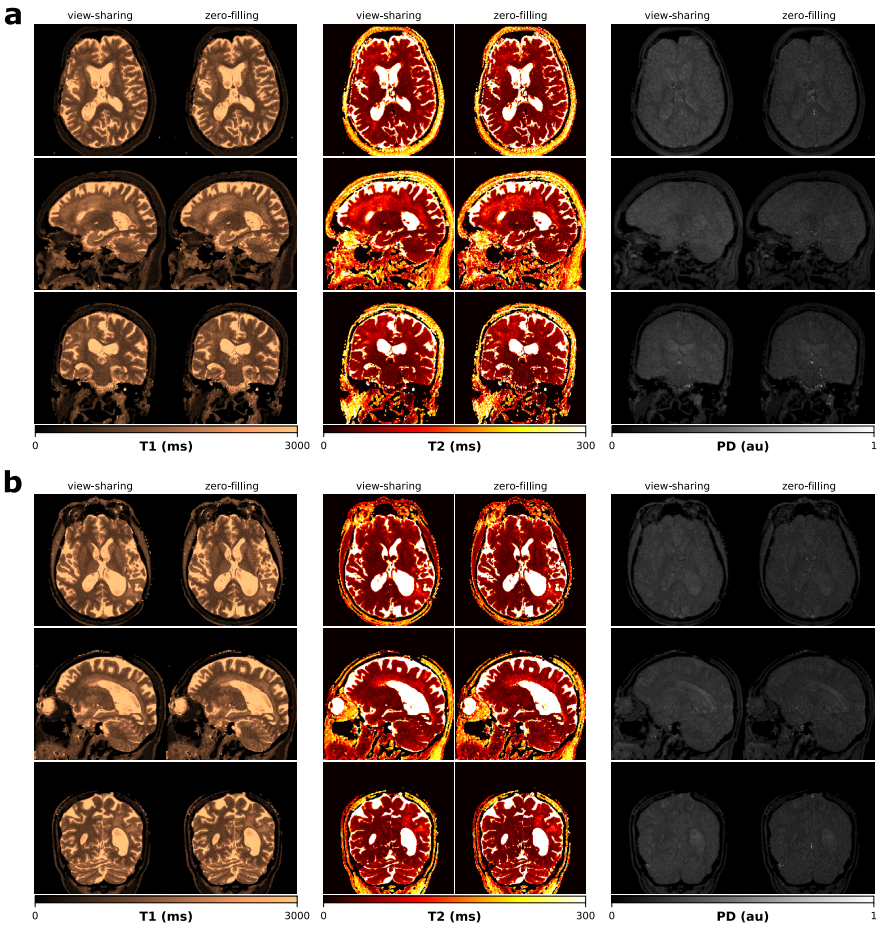

Figure 2: Parametric maps for patient 1 (a) and patient 2 (b). 3D QTI provides quantitative maps of T1, T2 and PD with high image quality. The view-sharing approach can improve spatial consistency compared to naive but fast zero-filling.

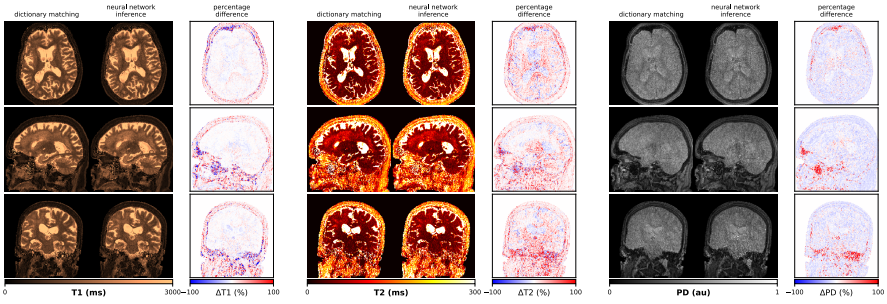

Figure 3: Neural network parameter inference and dictionary matching results when combined with the zero-filling image reconstruction. The trained neural network provides T1, T2 and PD maps with good correspondence with the state-of-the-art dictionary matching results, offering time and memory-efficient parameter inference that is not restricted by the size or the granularity of the dictionary.

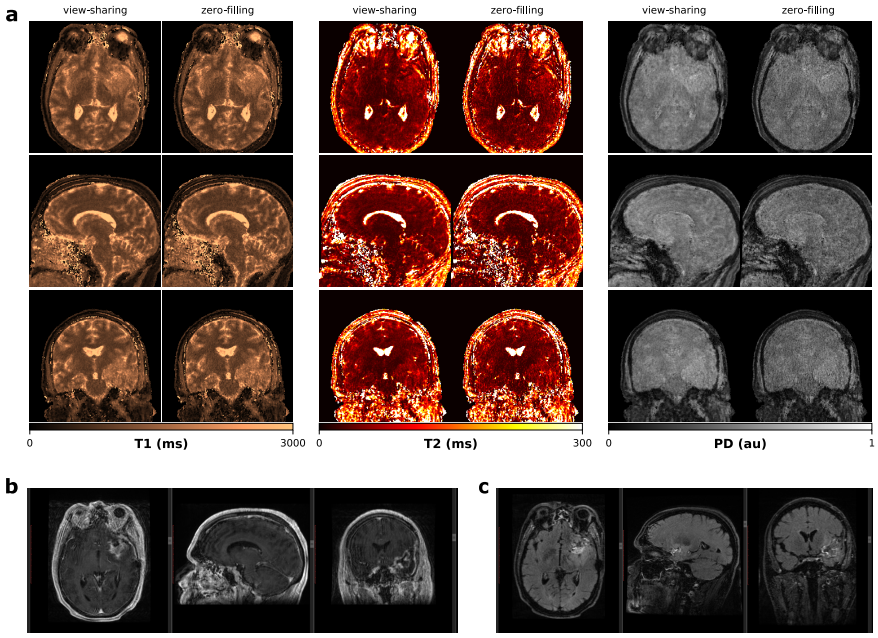

Figure 4: Parameter maps in case of patient motion. Patient movement affect the estimation of tissue parameters (a). With the view-sharing reconstruction pipeline, 3D QTI achieves an image quality which is comparable to state-of-the-art FSPGR (b) and CUBE FLAIR (c) sequences.

sub-structures with the potential to improve disease characterization in brain tumor patients. This is essential to find the optimal treatment strategy and to monitor treatment response along the course of disease.

With the fast acquisition, 3D QTI achieves a motion robustness comparable to qualitative, state-of-the-art protocols which is particularly advantageous for severely diseased patients, and therewith difficulties to lie still during lengthy scanning sessions. Initial experience also showed that patient motion degrades the image quality of estimated parameter maps. However, we are optimistic that combining the 3D QTI framework with a motion correction algorithm [10] can further improve its robustness and is hence subject of future work.

CONCLUSION

This work demonstrates 3D multiparametric quantitative transient-state imaging (QTI) in glioma patients. The 3D QTI framework offers quantitative MRI with acquisition and reconstruction times that make it suitable for application in clinical practice. Its potential to provide fast and quantitative tissue characterization with high isotropic resolution may be particularly beneficial for monitoring treatment response in brain tumor patients.

ACKNOWLEDGEMENTS

Carolin M Pirkl is supported by Deutsche Forschungsgemeinschaft (DFG) through TUM International Graduate School of Science and Engineering (IGSSE), GSC 81.

BIBLIOGRAPHY

[1] S. C. Thust, S. Heiland, A. Falini, et al. "Glioma imaging in Europe: A survey of 220 centres and recommendations for best clinical practice." In: *European Radiology* 28.8 (Aug. 2018), pp. 3306–3317.

[2] Pedro A. Gómez, Miguel Molina-Romero, Guido Buonincontri, et al. "Designing contrasts for rapid, simultaneous parameter quantification and flow visualization with quantitative transient-state imaging." In: *Scientific Reports* 9.1 (June 2019), p. 8468.

[3] Xiaozhi Cao, Huihui Ye, Congyu Liao, et al. "Fast 3D brain MR fingerprinting based on multi-axis spiral projection trajectory." In: *Magnetic Resonance in Medicine* 82.1 (2019), pp. 289–301.

[4] Alessandro Sbrizzi, Oscar van der Heide, Martijn Cloos, et al. "Fast quantitative MRI as a nonlinear tomography problem." In: *Magnetic resonance imaging* 46 (Feb. 2018), pp. 56–63.

[5] J. B. M. Warntjes, O. Dahlqvist Leinhard, J. West, et al. "Rapid magnetic resonance quantification on the brain: Optimization for clinical usage." In: *Magnetic Resonance in Medicine* 60.2 (Aug. 2008), pp. 320–329.

[6] Xiaozhi Cao, Huihui Ye, Congyu Liao, et al. "Fast 3D brain MR fingerprinting based on multi-axis spiral projection trajectory." In: *Magnetic Resonance in Medicine* 82.1 (2019), pp. 289–301.

[7] Guido Buonincontri, Laura Biagi, Pedro A Gómez, et al. "Spiral keyhole imaging for MR fingerprinting." In: *Proceedings of the 25th Annual Meeting of the International Society for Magnetic Resonance in Medicine (ISMRM)*. Honolulu, HI, USA, 2017.

[8] Florian Knoll, Andreas Schwarzl, Clemens Diwoky, et al. "gpuNUFFT – An Open-Source GPU Library for 3D Gridding with Direct Matlab Interface." In: *Proceedings of the 22th Annual Meeting of International Society for Magnetic Resonance in Medicine (ISMRM)*. Milan, Italy, 2014.

[9] M. Weigel, S. Schwenk, V. G. Kiselev, et al. "Extended phase graphs with anisotropic diffusion." In: *Journal of Magnetic Resonance (San Diego, Calif.: 1997)* 205.2 (Aug. 2010), pp. 276–285.

[10] Jan W. Kurzawski, Matteo Cencini, Pedro A. Gómez, et al. "Three-dimensional motion correction in Magnetic Resonance Fingerprinting (MRF)." In: *Proceedings of the 27th Annual Meeting of the International Society for Magnetic Resonance in Medicine (ISMRM)*. Montréal, QC, Canada, 2019.

A.3 SYNCHRONIZING DIMENSION REDUCTION AND PARAMETER INFERENCE IN 3D MULTIPARAMETRIC MRI: A HYBRID NEURAL NETWORK APPROACH

Peer-reviewed conference abstract

Authors: CM. Pirkl, I. Horvath, S. Endt, G. Buonincontri, MI. Menzel, PA. Gómez, BH. Menze

In: *Proceedings of the 28th Annual Meeting of the International Society for Magnetic Resonance in Medicine (ISMRM)*. 2020. [6]

Synopsis: "We synchronize dimension reduction and parameter inference and propose a hybrid neural network with a signal-encoding layer followed by a dual-pathway structure, for parameter prediction and recovery of the artifact-free signal evolution. Complementing the fast acquisition of coupled multiparametric MR signals, multiple studies have dealt with improving and accelerating parameter quantification using machine learning techniques. Here we demonstrate our model with a 3D multiparametric MRI framework and show that it is capable of reliably inferring T_1, T_2 and PD estimates, while its trained latent-space projection facilitates efficient data compression already in k-space and thereby significantly accelerates image reconstruction."

Contribution of thesis author: Algorithmic development and implementation, experimental design, data acquisition and analysis, abstract preparation and editing.

SYNCHRONIZING DIMENSION REDUCTION AND PARAMETER INFERENCE IN 3D MULTIPARAMETRIC MRI: A HYBRID NEURAL NETWORK APPROACH

Carolin M. Pirkl[1,2], Izabela Horvath[1,2], Sebastian Endt[1,2], Guido Buonincontri[3,4], Marion I. Menzel[2,5], Pedro A. Gómez[1], Bjoern H. Menze[1]

[1] Department of Informatics, Technical University of Munich, Munich, Germany,
[2] GE Healthcare, Munich, Germany,
[3] Fondazione Imago7, Pisa, Italy,
[4] IRCCS Fondazione Stella Maris, Pisa, Italy,
[5] Department of Physics, Technical University of Munich, Germany

SYNOPSIS

Complementing the fast acquisition of coupled multiparametric MR signals, multiple studies have dealt with improving and accelerating parameter quantification using machine learning techniques. Here we synchronize dimension reduction and parameter inference and propose a hybrid neural network with a signal-encoding layer followed by a dual-pathway structure, for parameter prediction and recovery of the artifact-free signal evolution. We demonstrate our model with a 3D multiparametric MRI framework and show that it is capable of reliably inferring T1, T2 and PD estimates, while its trained latent-space projection facilitates efficient data compression already in k-space and thereby significantly accelerates image reconstruction.

INTRODUCTION

Advanced multiparametric MR techniques [1–4] have proven to offer reliable and accurate quantification of multiple tissue parameters from a single, time-efficient scan. The fast acquisition, however, comes at the cost of an expensive reconstruction to mitigate aliasing artifacts and low SNR due to spatial undersampling [5–7]. Also, the heavy memory and computational requirements for matching the acquired signal evolutions to a precomputed dictionary are very inefficient. Multiple works, including machine learning based approaches, have been presented for accelerating parameter inference [8–10]. So far, these works are generally limited to the estimation of T1 and T2

and either take the full signal evolution as input or rely on a predefined signal compression. Here we propose a hybrid neural network architecture that jointly learns to

1. efficiently compress the acquired, complex signal evolutions in the time domain,
2. reliably infer T1, T2 and PD estimates,
3. recover artifact-free image time-series.

METHODS

We present a proof-of-concept of our hybrid neural network approach for a novel 3D multiparametric quantitative transient-state imaging (QTI) acquisition [5] which is based on the following schedule: after an initial inversion (TI=18 ms), flip angles ($0.8° \leqslant \text{FA} \leqslant 70°$) are applied in a ramp-up/down pattern, inspired by the scheme of Gómez et al. [5], with $\text{TR/TE} = 10.5\,\text{ms}/1.8\,\text{ms}$ and 880 repetitions.

With its dual pathway design Figure 1, the model learns the nonlinear relationship between the complex signal $\mathbf{x}$ input, and the underlying tissue parameters $\mathbf{q}$, i.e. T1, T2 and a proxy for PD, together with the artifact-free signals $\tilde{\mathbf{x}}$ as outputs. To synchronize dimension reduction and parameter inference, the network's first hidden layer is a linear projection, compressing the complex signal evolution to a lower-dimensional, complex latent-space. This is followed by a phase alignment and a signal normalization layer before the network splits into its two pathways (Figure 1a): The 'signal-recovery' pathway specializes into a denoising encoder-decoder setup, receiving the phase-aligned latent-space representation of the signal. The 'parametric' pathway specializes in parameter prediction from the normalized latent-space signal. As the signal-encoding layer of our network is a linear transform, it permutes with the linear FFT and can be directly applied to the k-space data (Figure 1b), enabling fast image reconstruction in the learned lower-dimensional space. The reconstructed QTI latent-space images are then fed to the neural network for parameter inference. From the network prediction, we calculate $\text{PD} = \dfrac{\|\tilde{\mathbf{x}}\|_2}{q_3}$ from the norm of the predicted signal $\|\tilde{\mathbf{x}}\|_2$.

Based on the extended phase graph formulism [11], we created a dataset of synthetic signals for the 3D QTI scheme for $\text{T1} = [100:20:4000]\,\text{ms}$ and $\text{T2} = [20:4:600]\,\text{ms}$ to train our neural network and to obtain a dictionary matching reference. To train the model, we used 50 % of the generated samples and added random Gaussian noise to the synthetic signals for robust training. Using ReLU activation and a parametric combination between L1 loss for parameter estimation, and L2 loss for the denoising autoencoder, we trained the model with ADAM optimization (learning rate = 1e-4, dropout rate= 0.8, 500 epochs).

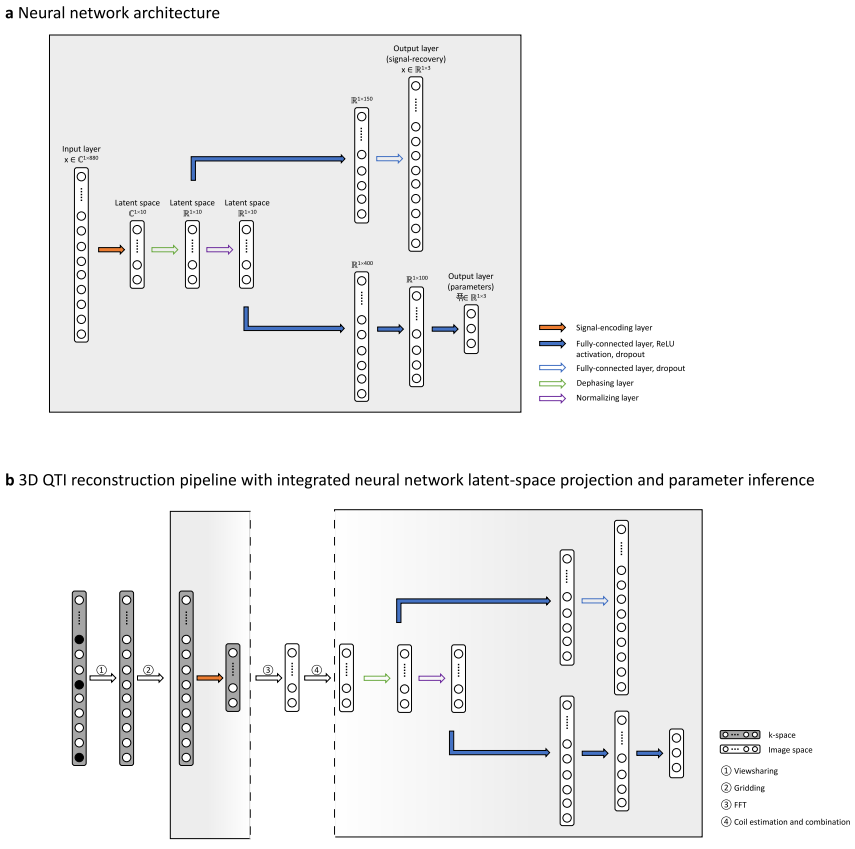

Figure 1: Neural network architecture (a) and its integration into the 3D QTI reconstruction pipeline (b). The proposed model receives the complex QTI signal $\mathbf{x}$ as input and outputs tissue parameter estimates $\mathbf{q}$ together with the artifact-free signal curve $\tilde{\mathbf{x}}$. Being trained on synthetic signal evolutions (image space), the trained, linear signal-encoding layer can be applied on the k-space data prior to the (linear) FFT, facilitating time-efficient image reconstruction in the learned lower-dimensional latent-space.

We validated our method on an in-vivo scan of a healthy volunteer (m, 33 y), after obtaining informed consent in compliance with the German Act on Medical Devices. Data was acquired on a 3 T MR750w system (GE Healthcare, Waukesha, WI) using multi-plane spiral sampling [12] (55 spherical, 880 in-plane rotations) with $22.5 \times 22.5 \times 22.5\,\mathrm{cm}^3$ FOV and $1.25 \times 1.25 \times 1.25\,\mathrm{mm}^3$ isotropic resolution. QTI data was reconstructed using k-space weighted view-sharing [13] and zero-filling, respectively. We compared our deep learning-based approach with conventional dictionary matching. For the latter, we reconstructed the QTI data using the first 10 singular images of a SVD projection [14].

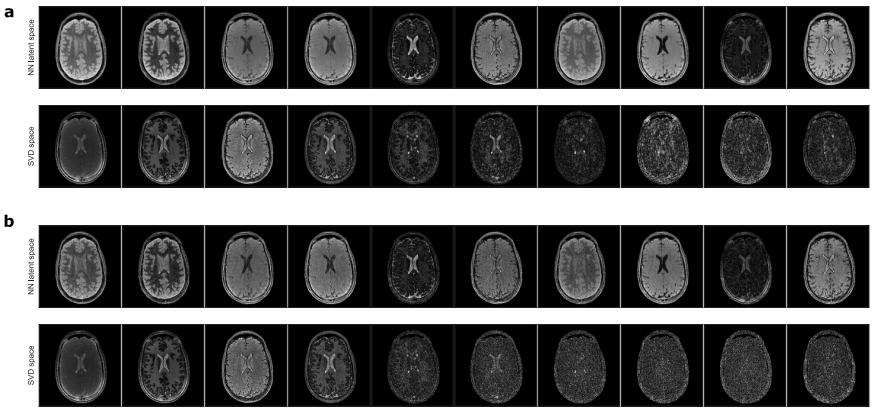

Figure 2: Neural network latent-space representation in comparison with an SVD projection for zero-filling (a) and view-sharing (b) k-space processing. With the signal-encoding layer, we jointly train dimension reduction and parameter inference so that the neural network can find a low-dimensional latent-space representation of the QTI signals tailored for subsequent T1, T2 and PD prediction that is hence not a replicate of the SVD transform.

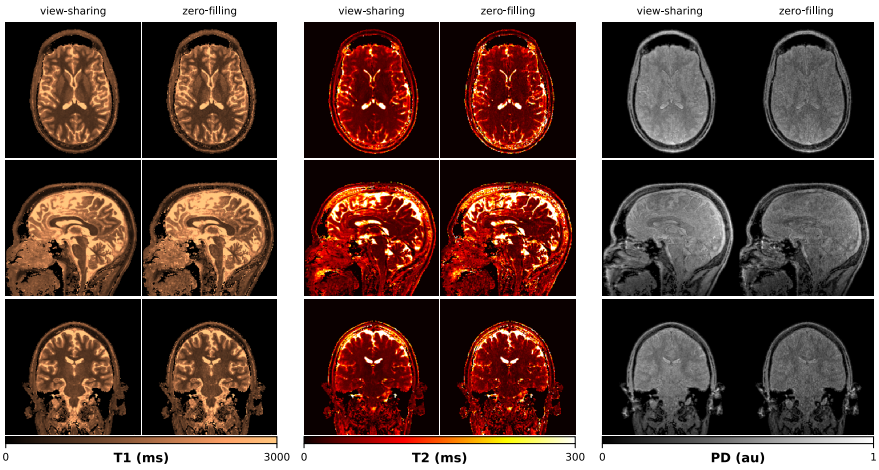

Figure 3: Neural network parameter inference. The proposed framework provides high quality and consistent T1, T2 and PD estimates for both the view-sharing and naive zero-filling QTI image reconstruction scenario.

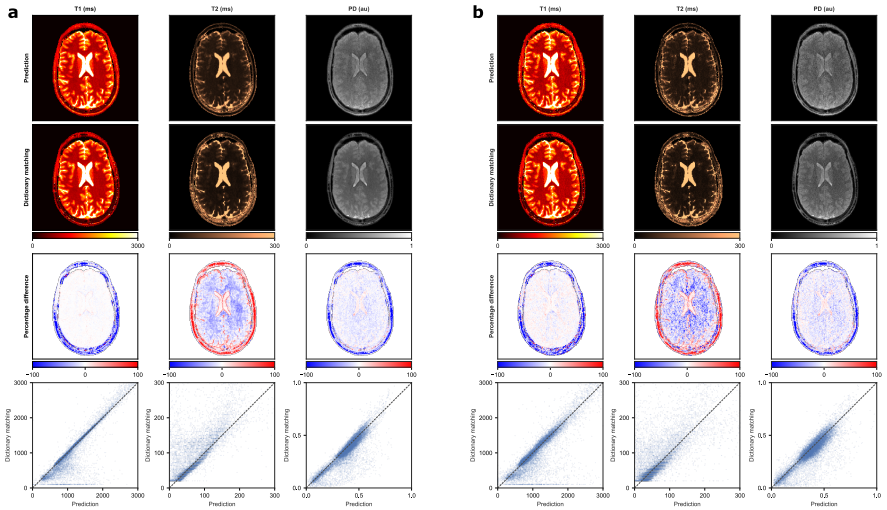

Figure 4: Neural network and dictionary matching parameter inference. The proposed neural network achieves a prediction quality comparable to state-of-the-art dictionary matching for both view-sharing (a) and zero-filling (b) k-space reconstruction. In white matter regions, i.e. in low T1 and T2 ranges, predicted T2 values are higher than the dictionary matching estimates. The neural network inference provides more consistent parameter estimates in the skull.

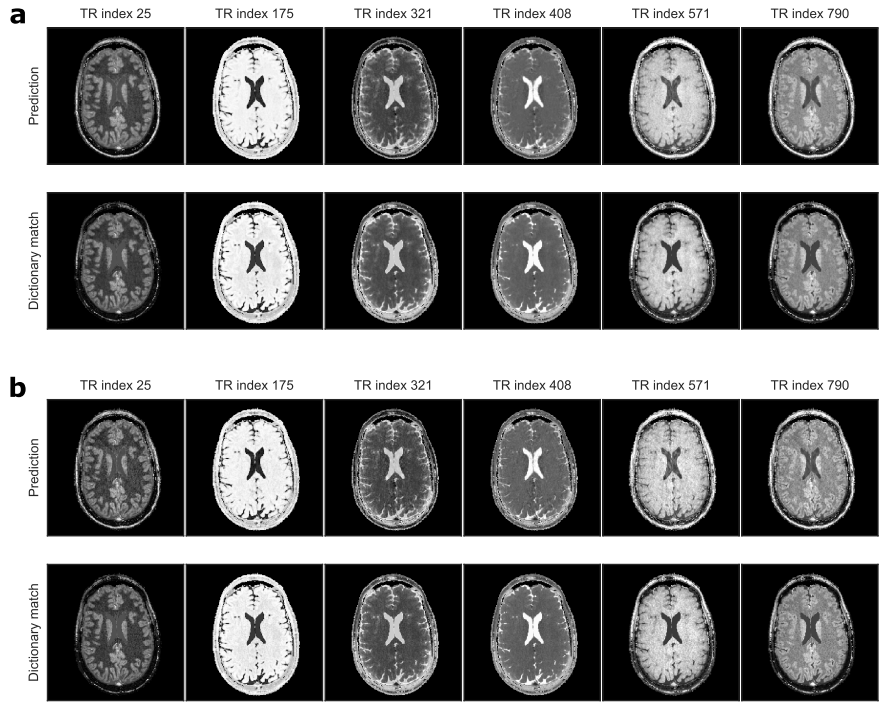

Figure 5: Representative QTI images along the acquisition train. For view-sharing (a) and zero-filling (b) reconstruction, predicted signal curves are consistent with the matched dictionary entries and do not show visual artifacts, providing high image quality.

RESULTS

Figure 2 depicts the learned latent-space representation and the first 10 singular images of the SVD projection for comparison. As seen from Figure 3 and Figure 4, parameter maps which we obtained from the trained neural network ('parametric' pathway) demonstrate high image quality and are largely consistent with the dictionary matching results in the brain region. In white matter, predicted T2 values are higher than the dictionary matching result. The signal curves obtained from the 'signal-recovery' pathway do not show visual artifacts, providing good image quality and agree well with the matched dictionary entries (Figure 5).

DISCUSSION

We demonstrated a dual-pathway model that learns to infer T1, T2 and PD, while simultaneously recovering the artifact-free signal evolution to circumvent time- and memory-expensive dictionary matching – without being bound by dictionary size or granularity.

With the signal-encoding layer, we incorporate dimension reduction into the network architecture. As such, the model can find a low-dimensional latent-space representation of the signals tailored for subsequent parameter inference. When used prior to the FFT in the reconstruction pipeline, this learned transformation allows for efficient compression already in k-space and thereby significantly reduces reconstruction time. Although the network predictions overall agree well with the dictionary matching results, it will be subject of future work to further investigate the discrepancy in low T2 values between both methods with ground truth phantom data.

CONCLUSION

We present a deep learning framework that synchronizes dimension reduction and parameter estimation and addresses the reconstruction pipeline of multiparametric MRI in two ways:

1. With the learned latent-space projection we speed up image reconstruction and
2. efficiently infer T1, T2 and PD parameters with significantly reduced computation times and resources compared to state-of-the-art dictionary matching.

ACKNOWLEDGEMENTS

Carolin M Pirkl is supported by Deutsche Forschungsgemeinschaft (DFG) through TUM International Graduate School of Science and Engineering (IGSSE), GSC 81.

BIBLIOGRAPHY

[1] Dan Ma, Vikas Gulani, Nicole Seiberlich, et al. "Magnetic Resonance Fingerprinting." In: *Nature* 495.7440 (Mar. 2013), pp. 187–192.

[2] J. B. M. Warntjes, O. Dahlqvist Leinhard, J. West, et al. "Rapid magnetic resonance quantification on the brain: Optimization for clinical usage." In: *Magnetic Resonance in Medicine* 60.2 (Aug. 2008), pp. 320–329.

[3] Xiaozhi Cao, Huihui Ye, Congyu Liao, et al. "Fast 3D brain MR fingerprinting based on multi-axis spiral projection trajectory." In: *Magnetic Resonance in Medicine* 82.1 (2019), pp. 289–301.

[4] Alessandro Sbrizzi, Oscar van der Heide, Martijn Cloos, et al. "Fast quantitative MRI as a nonlinear tomography problem." In: *Magnetic resonance imaging* 46 (Feb. 2018), pp. 56–63.

[5] Pedro A. Gómez, Miguel Molina-Romero, Guido Buonincontri, et al. "Designing contrasts for rapid, simultaneous parameter quantification and flow visualization with quantitative transient-state imaging." In: *Scientific Reports* 9.1 (June 2019), p. 8468.

[6] Xiaozhi Cao, Congyu Liao, Zhixing Wang, et al. "Robust sliding-window reconstruction for Accelerating the acquisition of MR fingerprinting." In: *Magnetic Resonance in Medicine* 78.4 (2017), pp. 1579–1588.

[7] Gastao Cruz, Torben Schneider, Tom Bruijnen, et al. "Accelerated magnetic resonance fingerprinting using soft-weighted key-hole (MRF-SOHO)." In: *PLOS ONE* 13.8 (Aug. 2018), e0201808.

[8] Ouri Cohen, Bo Zhu, and Matthew S. Rosen. "MR fingerprinting Deep RecOnstruction NEtwork (DRONE)." In: *Magnetic Resonance in Medicine* 80.3 (2018), pp. 885–894.

[9] Pedro A. Gómez, Guido Buonincontri, Miguel Molina-Romero, et al. "Accelerated parameter mapping with compressed sensing: an alternative to MR Fingerprinting." In: *Proceedings of the 25th Annual Meeting of International Society for Magnetic Resonance in Medicine (ISMRM)*. Honolulu, HI, USA, 2017.

[10] Fabian Balsiger, Amaresha Shridhar Konar, Shivaprasad Chikop, et al. "Magnetic Resonance Fingerprinting Reconstruction via Spatiotemporal Convolutional Neural Networks." In: *Machine Learning for Medical Image Reconstruction*. Ed. by Florian Knoll, Andreas Maier, and Daniel Rueckert. Lecture Notes in Computer Science. Springer International Publishing, 2018, pp. 39–46. ISBN: 978-3-030-00129-2.

[11] M. Weigel, S. Schwenk, V. G. Kiselev, et al. "Extended phase graphs with anisotropic diffusion." In: *Journal of Magnetic Resonance (San Diego, Calif.: 1997)* 205.2 (Aug. 2010), pp. 276–285.

[12] Xiaozhi Cao, Huihui Ye, Congyu Liao, et al. "Fast 3D brain MR fingerprinting based on multi-axis spiral projection trajectory." In: *Magnetic Resonance in Medicine* 82.1 (2019), pp. 289–301.

[13] Guido Buonincontri, Laura Biagi, Pedro A Gómez, et al. "Spiral keyhole imaging for MR fingerprinting." In: *Proceedings of the 25th Annual Meeting of the International Society for Magnetic Resonance in Medicine (ISMRM)*. Honolulu, HI, USA, 2017.

[14] Debra F. McGivney, Eric Pierre, Dan Ma, et al. "SVD compression for magnetic resonance fingerprinting in the time domain." In: *IEEE TMI* 33 (Dec. 2014), pp. 2311–2322.

BIBLIOGRAPHY

[1] Carolin M. Pirkl, Pedro A. Gómez, Ilona Lipp, Guido Buonincontri, Miguel Molina-Romero, Anjany Sekuboyina, Diana Waldmannstetter, Jonathan Dannenberg, Sebastian Endt, Alberto Merola, et al. "Deep learning-based parameter mapping for joint relaxation and diffusion tensor MR Fingerprinting." In: *Proceedings of the Third Conference on Medical Imaging with Deep Learning*. Vol. 121. PMLR, Sept. 2020, pp. 638–654.

[2] Carolin M. Pirkl, Laura Nunez-Gonzalez, Florian Kofler, Sebastian Endt, Lioba Grundl, Mohammad Golbabaee, Pedro A. Gómez, Matteo Cencini, Guido Buonincontri, Rolf F. Schulte, et al. "Accelerated 3D whole-brain T1, T2, and proton density mapping: feasibility for clinical glioma MR imaging." In: *Neuroradiology* (Apr. 2021). ISSN: 1432-1920. DOI: 10.1007/s00234-021-02703-0.

[3] Carolin M Pirkl, Matteo Cencini, Jan W Kurzawski, Diana Waldmannstetter, Hongwei Li, Anjany Sekuboyina, Sebastian Endt, Luca Peretti, Graziella Donatelli, Rosa Pasquariello, et al. "Residual learning for 3D motion corrected quantitative MRI: Robust clinical T1, T2 and proton density mapping." In: *Proceedings of the Forth Conference on Medical Imaging with Deep Learning*. PMLR.

[4] Carolin M. Pirkl, Ilona Lipp, Guido Buonincontri, Miguel Molina-Romero, Anjany Sekuboyina, Diana Waldmannstetter, Jonathan Dannenberg, Valentina Tomassini, Michela Tosetti, Derek K. Jones, et al. "Deep Learning-enabled Diffusion Tensor MR Fingerprinting." In: *Proceedings of the 27th Annual Meeting of International Society for Magnetic Resonance in Medicine (ISMRM)*. Montréal, QC, Canada, 2019.

[5] Carolin M. Pirkl, Laura Nunez-Gonzalez, Sebastian Endt, Guido Buonincontri, Rolf F. Schulte, Pedro A. Gómez, Marion Smits, Bjoern H. Menze, Marion I. Menzel, and Juan A. Hernandez-Tamames. "Accelerated 3D multiparametric MRI in glioma patients - Initial clinical experience." In: *Proceedings of the 28th Annual Meeting of International Society for Magnetic Resonance in Medicine (ISMRM)*. 2020.

[6] Carolin M. Pirkl, Izabela Horvath, Sebastian Endt, Guido Buonincontri, Marion I. Menzel, Pedro A. Gómez, and Bjoern H. Menze. "Synchronizing dimension reduction and parameter inference in 3D multiparametric MRI: A hybrid neural network approach." In: *Proceedings of the 28th Annual Meeting of In-*

ternational Society for Magnetic Resonance in Medicine (ISMRM). 2020.

[7] Pedro A. Gómez, Matteo Cencini, Mohammad Golbabaee, Rolf F. Schulte, Carolin Pirkl, Izabela Horvath, Giada Fallo, Luca Peretti, Michela Tosetti, Bjoern H. Menze, et al. "Rapid three-dimensional multiparametric MRI with quantitative transient-state imaging." In: *Scientific Reports* 10.1 (Aug. 2020), p. 13769. ISSN: 2045-2322. DOI: 10.1038/s41598-020-70789-2.

[8] Mohammad Golbabaee, Guido Buonincontri, Carolin M. Pirkl, Marion I. Menzel, Bjoern H. Menze, Mike Davies, and Pedro A. Gómez. "Compressive MRI quantification using convex spatiotemporal priors and deep encoder-decoder networks." In: *Medical Image Analysis* 69 (Apr. 2021), p. 101945. ISSN: 1361-8415. DOI: 10.1016/j.media.2020.101945.

[9] Mohammad Golbabaee, Carolin Pirkl, Marion I Menzel, Guido Buonincontri, and Pedro A. Gómez. "Deep MR Fingerprinting with total-variation and low-rank subspace priors." In: *Proceedings of the 27th Annual Meeting of International Society for Magnetic Resonance in Medicine (ISMRM)*. Montréal, QC, Canada, 2019.

[10] Carolin Hecking-Veltman, Carolin Pirkl, Jonathan Dannenberg, Rolf F. Schulte, Tim Sprenger, Bjoern H. Menze, and Marion I. Menzel. "Estimation and Correction of Image Phase in diffusion weighted MRI using Deep Learning." In: *Proceedings of the 27th Annual Meeting of International Society for Magnetic Resonance in Medicine (ISMRM)*. Montréal, QC, Canada, 2019.

[11] Niry Andriamanga, Carolin M. Pirkl, Anjany Sekuboyina, Guido Buonincontri, Marion I Menzel, Pedro A. Gómez, Marie Piraud, and Bjoern H. Menze. "Long Short Term Memory Recurrent Neural Network for MR Fingerprinting parameter estimation." In: *Proceedings of the 36th Annual Scientific Meeting of the ESMRMB*. Rotterdam, Netherlands, 2019.

[12] Izabela Horvath, Carolin M. Pirkl, Guido Buonincontri, Marion I. Menzel, Pedro A. Gómez, and Bjoern H. Menze. "Deep learning for 3D MR fingerprinting: a dual pathway parameter mapping and reconstruction approach." In: *Proceedings of the 36th Annual Scientific Meeting of the European Society for Magnetic Resonance in Medicine and Biology (ESMRMB)*. Rotterdam, Netherlands, 2019.

[13] Sebastian Endt, Carolin M. Pirkl, Claudio M. Verdun, Bjoern H. Menze, and Marion I. Menzel. "A deep-learning approach to accelerated T1-T2-relaxation-correlation imaging." In: *Proceedings of the 37th Annual Scientific Meeting of the European Society for Magnetic Resonance in Medicine and Biology (ESMRMB)*. 2020.

[14] Florian Wiesinger, Graeme McKinnon, Sandeep Kaushik, Ana Beatriz Solana, Emil Ljungberg, Mika Vogel, Naoyuki Takei, Rolf Schulte, Carolin Pirkl, Cristina Cozzini, et al. "3D Silent Parameter Mapping: Further refinements & quantitative assessment." In: *Proceedings of the 29th Annual Meeting of International Society for Magnetic Resonance in Medicine (ISMRM)*. 2021.

[15] P. C. Lauterbur. "Image Formation by Induced Local Interactions: Examples Employing Nuclear Magnetic Resonance." In: *Nature* 242.5394 (Mar. 1973), pp. 190–191. ISSN: 1476-4687. DOI: 10.1038/242190a0.

[16] P. Mansfield and A. A. Maudsley. "Medical imaging by NMR." In: *The British Journal of Radiology* 50.591 (Mar. 1977), pp. 188–194. ISSN: 0007-1285, 1748-880X. DOI: 10.1259/0007-1285-50-591-188.

[17] R. Damadian. "Tumor detection by nuclear magnetic resonance." In: *Science (New York, N.Y.)* 171.3976 (Mar. 1971), pp. 1151–1153. ISSN: 0036-8075. DOI: 10.1126/science.171.3976.1151.

[18] Anil Kumar, Dieter Welti, and Richard R Ernst. "NMR Fourier zeugmatography." In: *Journal of Magnetic Resonance (1969)* 18.1 (Apr. 1975), pp. 69–83. ISSN: 0022-2364. DOI: 10.1016/0022-2364(75)90224-3.

[19] Maximilian F. Reiser, Wolfhard Semmler, and Hedvig Hricak, eds. *Magnetic Resonance Tomography*. 1st ed. Springer-Verlag Berlin Heidelberg, 2008. ISBN: 978-3-540-29354-5.

[20] G. N. Hounsfield. "Computerized transverse axial scanning (tomography). 1. Description of system." In: *The British Journal of Radiology* 46.552 (Dec. 1973), pp. 1016–1022. ISSN: 0007-1285. DOI: 10.1259/0007-1285-46-552-1016.

[21] B. J. Perry and C. Bridges. "Computerized transverse axial scanning (tomography). 3. Radiation dose considerations." In: *The British Journal of Radiology* 46.552 (Dec. 1973), pp. 1048–1051. ISSN: 0007-1285. DOI: 10.1259/0007-1285-46-552-1048.

[22] T. F. Budinger, S. E. Derenzo, G. T. Gullberg, W. L. Greenberg, and R. H. Huesman. "Emission computer assisted tomography with single-photon and positron annihilation photon emitters." In: *Journal of Computer Assisted Tomography* 1.1 (Jan. 1977), pp. 131–145. ISSN: 0363-8715. DOI: 10.1097/00004728-197701000-00015.

[23] M. M. Ter-Pogossian, M. E. Phelps, E. J. Hoffman, and N. A. Mullani. "A positron-emission transaxial tomograph for nuclear imaging (PETT)." In: *Radiology* 114.1 (Jan. 1975), pp. 89–98. ISSN: 0033-8419. DOI: 10.1148/114.1.89.

[24] V. R. Fuchs and H. C. Sox. "Physicians' views of the relative importance of thirty medical innovations." In: *Health Affairs (Project Hope)* 20.5 (Oct. 2001), pp. 30–42. ISSN: 0278-2715. DOI: 10.1377/hlthaff.20.5.30.

[25] F. Bloch. "Nuclear Induction." In: *Physical Review* 70.7-8 (Oct. 1946), pp. 460–474. DOI: 10.1103/PhysRev.70.460.

[26] P. A. Bottomley, T. H. Foster, R. E. Argersinger, and L. M. Pfeifer. "A review of normal tissue hydrogen NMR relaxation times and relaxation mechanisms from 1-100 MHz: dependence on tissue type, NMR frequency, temperature, species, excision, and age." In: *Medical Physics* 11.4 (Aug. 1984), pp. 425–448. ISSN: 0094-2405. DOI: 10.1118/1.595535.

[27] Steven Sourbron. "Technical aspects of MR perfusion." In: *European Journal of Radiology* 76.3 (Dec. 2010), pp. 304–313. ISSN: 1872-7727. DOI: 10.1016/j.ejrad.2010.02.017.

[28] H. Y. Carr and E. M. Purcell. "Effects of Diffusion on Free Precession in Nuclear Magnetic Resonance Experiments." In: *Physical Review* 94.3 (May 1954), pp. 630–638. DOI: 10.1103/PhysRev.94.630.

[29] Derek K. Jones. *Diffusion MRI*. Oxford University Press, Nov. 2010. ISBN: 978-0-19-970870-3.

[30] Kyle M. Jones, Alyssa C. Pollard, and Mark D. Pagel. "Clinical applications of chemical exchange saturation transfer (CEST) MRI." In: *Journal of magnetic resonance imaging: JMRI* 47.1 (Jan. 2018), pp. 11–27. ISSN: 1522-2586. DOI: 10.1002/jmri.25838.

[31] Harden M. McConnell. "Reaction Rates by Nuclear Magnetic Resonance." In: *The Journal of Chemical Physics* 28.3 (Mar. 1958), pp. 430–431. ISSN: 0021-9606. DOI: 10.1063/1.1744152.

[32] European Society of Radiology (ESR). "Medical imaging in personalised medicine: a white paper of the research committee of the European Society of Radiology (ESR)." In: *Insights into Imaging* 6.2 (Mar. 2015), pp. 141–155. ISSN: 1869-4101. DOI: 10.1007/s13244-015-0394-0.

[33] National Research Council (US) Committee on A Framework for Developing a New Taxonomy of Disease. *Toward Precision Medicine: Building a Knowledge Network for Biomedical Research and a New Taxonomy of Disease*. The National Academies Collection: Reports funded by National Institutes of Health. Washington (DC): National Academies Press (US), 2011. ISBN: 978-0-309-22222-8.

[34] Paul Tofts. *Quantitative MRI of the brain*. Chichester: Wiley, 2003. ISBN: 978-0-470-84721-3.

[35] Takeshi Yokoo, Won C. Bae, Gavin Hamilton, Afshin Karimi, James P. Borgstede, Brian C. Bowen, Claude B. Sirlin, Christine B. Chung, John V. Crues, William G. Bradley, et al. "A quantitative approach to sequence and image weighting." In: *Journal of Computer Assisted Tomography* 34.3 (June 2010), pp. 317–331. ISSN: 1532-3145. DOI: 10.1097/RCT.0b013e3181d3449a.

[36] Larry G. Kessler, Huiman X. Barnhart, Andrew J. Buckler, Kingshuk Roy Choudhury, Marina V. Kondratovich, Alicia Toledano, Alexander R. Guimaraes, Ross Filice, Zheng Zhang, Daniel C. Sullivan, et al. "The emerging science of quantitative imaging biomarkers terminology and definitions for scientific studies and regulatory submissions." In: *Statistical Methods in Medical Research* 24.1 (Feb. 2015), pp. 9–26. ISSN: 1477-0334. DOI: 10.1177/0962280214537333.

[37] Kathryn E Keenan, Joshua R Biller, Jana G Delfino, Michael A Boss, Mark D Does, Jeffrey L Evelhoch, Mark A Griswold, Jeffrey L Gunter, R Scott Hinks, Stuart W Hoffman, et al. "Recommendations Towards Standards for Quantitative MRI (qMRI) and Outstanding Needs." In: *Journal of magnetic resonance imaging : JMRI* 49.7 (June 2019), e26–e39. ISSN: 1053-1807. DOI: 10.1002/jmri.26598.

[38] Anagha Deshmane, Vikas Gulani, Mark A. Griswold, and Nicole Seiberlich. "Parallel MR imaging." In: *Journal of Magnetic Resonance Imaging* 36.1 (2012), pp. 55–72. ISSN: 1522-2586. DOI: https://doi.org/10.1002/jmri.23639.

[39] Alice Chieh-Yu Yang, Madison Kretzler, Sonja Sudarski, Vikas Gulani, and Nicole Seiberlich. "Sparse Reconstruction Techniques in MRI: Methods, Applications, and Challenges to Clinical Adoption." In: *Investigative radiology* 51.6 (June 2016), pp. 349–364. ISSN: 0020-9996. DOI: 10.1097/RLI.0000000000000274.

[40] Jong Chul Ye. "Compressed sensing MRI: a review from signal processing perspective." In: *BMC Biomedical Engineering* 1.1 (Mar. 2019), p. 8. ISSN: 2524-4426. DOI: 10.1186/s42490-019-0006-z.

[41] Daniele Ravì, Charence Wong, Fani Deligianni, Melissa Berthelot, Javier Andreu-Perez, Benny Lo, and Guang-Zhong Yang. "Deep Learning for Health Informatics." In: *IEEE Journal of Biomedical and Health Informatics* 21.1 (Jan. 2017), pp. 4–21. ISSN: 2168-2208. DOI: 10.1109/JBHI.2016.2636665.

[42] Nicole Seiberlich, Vikas Gulani, Fernando Calamante, Adrienne Campbell-Washburn, Mariya Doneva, Houchun Harry Hu, and Steven Sourbron, eds. *Quantitative Magnetic Resonance Imaging*. Vol. 1. Advances in Magnetic Resonance Technology and Applications. Academic Press, 2020. DOI: 10.1016/B978-0-12-817057-1.00007-X.

[43] Malcolm H. Levitt. *Spin Dynamics: Basics of Nuclear Magnetic Resonance*. 2nd ed. John Wiley & Sons Ltd, 2008. ISBN: 978-0-470-51117-6.

[44] E. Mark Haacke, Robert W Brown, Michael R Thompson, and Ramesh Venkatesan. *Magnetic resonance imaging: physical principles and sequence design*. 2nd ed. John Wiley & Sons Ltd, 1999. ISBN: 978-0-471-35128-3.

[45] Lars G. Hanson. "Is quantum mechanics necessary for understanding magnetic resonance?" In: *Concepts in Magnetic Resonance Part A* 32A.5 (Sept. 2008), pp. 329–340. ISSN: 1552-5023. DOI: 10.1002/cmr.a.20123.

[46] Adolf Fick. "Ueber Diffusion." In: *Annalen der Physik* 170.1 (1855), pp. 59–86. ISSN: 1521-3889. DOI: https://doi.org/10.1002/andp.18551700105.

[47] A. Einstein. "Über die von der molekularkinetischen Theorie der Wärme geforderte Bewegung von in ruhenden Flüssigkeiten suspendierten Teilchen." In: *Annalen der Physik* 322.8 (1905), pp. 549–560. ISSN: 1521-3889. DOI: https://doi.org/10.1002/andp.19053220806.

[48] H. C. Torrey. "Bloch Equations with Diffusion Terms." In: *Physical Review* 104.3 (Nov. 1956), pp. 563–565. DOI: 10.1103/PhysRev.104.563.

[49] P. J. Basser, J. Mattiello, and D. LeBihan. "MR diffusion tensor spectroscopy and imaging." In: *Biophysical Journal* 66.1 (Jan. 1994), pp. 259–267. ISSN: 0006-3495. DOI: 10.1016/S0006-3495(94)80775-1.

[50] Harry Wechsler, ed. *Neural Networks for Perception*. Elsevier, 1992. ISBN: 978-0-12-741252-8. DOI: 10.1016/C2013-0-11676-5.

[51] Bayya Yegnanarayana. *Artificial neural networks*. PHI Learning Pvt. Ltd., 2009.

[52] Yann LeCun, Yoshua Bengio, and Geoffrey Hinton. "Deep learning." In: *Nature* 521.7553 (May 2015), pp. 436–444. ISSN: 1476-4687. DOI: 10.1038/nature14539.

[53] Andreas Maier, Christopher Syben, Tobias Lasser, and Christian Riess. "A gentle introduction to deep learning in medical image processing." In: *Zeitschrift für Medizinische Physik*. Special Issue: Deep Learning in Medical Physics 29.2 (May 2019), pp. 86–101. ISSN: 0939-3889. DOI: 10.1016/j.zemedi.2018.12.003.

[54] Robert Hecht-Nielsen. "Theory of the Backpropagation Neural Network." In: *Neural Networks for Perception*. Ed. by Harry Wechsler. Academic Press, Jan. 1992, pp. 65–93. ISBN: 978-0-12-741252-8. DOI: 10.1016/B978-0-12-741252-8.50010-8.

[55] Jonathan I. Tamir, Martin Uecker, Weitian Chen, Peng Lai, Marcus T. Alley, Shreyas S. Vasanawala, and Michael Lustig. "T2 shuffling: Sharp, multicontrast, volumetric fast spin-echo imaging." In: *Magnetic Resonance in Medicine* 77.1 (2017), pp. 180–195. ISSN: 1522-2594. DOI: https://doi.org/10.1002/mrm.26102.

[56] Sean C.L. Deoni. "Quantitative Relaxometry of the Brain." In: *Topics in magnetic resonance imaging : TMRI* 21.2 (Apr. 2010), pp. 101–113. ISSN: 0899-3459. DOI: 10.1097/RMR.0b013e31821e56d8.

[57] Sean C. L. Deoni, Brian K. Rutt, and Terry M. Peters. "Rapid combined T1 and T2 mapping using gradient recalled acquisition in the steady state." In: *Magnetic Resonance in Medicine* 49.3 (Mar. 2003), pp. 515–526. ISSN: 0740-3194. DOI: 10.1002/mrm.10407.

[58] J. B. M. Warntjes, O. Dahlqvist Leinhard, J. West, and P. Lundberg. "Rapid magnetic resonance quantification on the brain: Optimization for clinical usage." In: *Magnetic Resonance in Medicine* 60.2 (Aug. 2008), pp. 320–329. ISSN: 1522-2594. DOI: 10.1002/mrm.21635.

[59] Philipp Ehses, Nicole Seiberlich, Dan Ma, Felix A. Breuer, Peter M. Jakob, Mark A. Griswold, and Vikas Gulani. "IR TrueFISP with a golden-ratio-based radial readout: Fast quantification of T1, T2, and proton density." In: *Magnetic Resonance in Medicine* 69.1 (2013), pp. 71–81. ISSN: 1522-2594. DOI: 10.1002/mrm.24225.

[60] Shohei Fujita, Akifumi Hagiwara, Masaaki Hori, Marcel Warntjes, Koji Kamagata, Issei Fukunaga, Christina Andica, Tomoko Maekawa, Ryusuke Irie, Mariko Yoshida Takemura, et al. "Three-dimensional high-resolution simultaneous quantitative mapping of the whole brain with 3D-QALAS: An accuracy and repeatability study." In: *Magnetic Resonance Imaging* 63 (Nov. 2019), pp. 235–243. ISSN: 0730-725X. DOI: 10.1016/j.mri.2019.08.031.

[61] Fuyixue Wang, Zijing Dong, Timothy G. Reese, Berkin Bilgic, Mary Katherine Manhard, Jingyuan Chen, Jonathan R. Polimeni, Lawrence L. Wald, and Kawin Setsompop. "Echo planar time-resolved imaging (EPTI)." In: *Magnetic Resonance in Medicine* 81.6 (2019), pp. 3599–3615. ISSN: 1522-2594. DOI: https://doi.org/10.1002/mrm.27673.

[62] Dan Ma, Vikas Gulani, Nicole Seiberlich, Kecheng Liu, Jeffrey L. Sunshine, Jeffrey L. Duerk, and Mark A. Griswold. "Magnetic Resonance Fingerprinting." In: *Nature* 495.7440 (Mar. 2013), pp. 187–192. ISSN: 0028-0836. DOI: 10.1038/nature11971.

[63] Yun Jiang, Dan Ma, Nicole Seiberlich, Vikas Gulani, and Mark A. Griswold. "MR fingerprinting using fast imaging with steady state precession (FISP) with spiral readout." In: *Magnetic Resonance in Medicine* 74.6 (Dec. 2015), pp. 1621–1631. ISSN: 1522-2594. DOI: 10.1002/mrm.25559.

[64] Debra F. McGivney, Rasim Boyacioğlu, Yun Jiang, Megan E. Poorman, Nicole Seiberlich, Vikas Gulani, Kathryn E. Keenan, Mark A. Griswold, and Dan Ma. "Magnetic Resonance Fingerprinting Review Part 2: Technique and Directions." In: *Journal of magnetic resonance imaging : JMRI* 51.4 (Apr. 2020), pp. 993–1007. ISSN: 1053-1807. DOI: 10.1002/jmri.26877.

[65] Pedro A. Gómez, Miguel Molina-Romero, Guido Buonincontri, Marion I. Menzel, and Bjoern H. Menze. "Designing contrasts for rapid, simultaneous parameter quantification and flow visualization with quantitative transient-state imaging." In: *Scientific Reports* 9.1 (June 2019), p. 8468. ISSN: 2045-2322. DOI: 10.1038/s41598-019-44832-w.

[66] Alessandro Sbrizzi, Oscar van der Heide, Martijn Cloos, Annette van der Toorn, Hans Hoogduin, Peter R. Luijten, and Cornelis A.T. van den Berg. "Fast quantitative MRI as a nonlinear tomography problem." In: *Magnetic resonance imaging* 46 (Feb. 2018), pp. 56–63. ISSN: 0730-725X. DOI: 10.1016/j.mri.2017.10.015.

[67] Oscar van der Heide, Alessandro Sbrizzi, Peter R. Luijten, and Cornelis A. T. van den Berg. "High-resolution in vivo MR-STAT using a matrix-free and parallelized reconstruction algorithm." In: *NMR in biomedicine* 33.4 (Apr. 2020), e4251. ISSN: 1099-1492. DOI: 10.1002/nbm.4251.

[68] Bo Zhu, Jeremiah Z. Liu, Neha Koonjoo, Bruce R. Rosen, and Matthew R. Rosen. "AUTOmated pulse SEQuence generation (AUTOSEQ) using Bayesian reinforcement learning in an MRI physics simulation environment." In: *ISMRM Workshop on Machine Learning*. 2017.

[69] Ouri Cohen, Mathieu Sarracanie, Matthew S. Rosen, and Jerome L. Ackerman. "In Vivo Optimized MR Fingerprinting in the Human Brain." In: *Proceedings of the 24th Annual Meeting of International Society for Magnetic Resonance in Medicine (ISMRM)*. Singapore, 2016.

[70] Philip K. Lee, Lauren E. Watkins, Timothy I. Anderson, Guido Buonincontri, and Brian A. Hargreaves. "Flexible and efficient optimization of quantitative sequences using automatic differentiation of Bloch simulations." In: *Magnetic Resonance in Medicine* 82.4 (2019), pp. 1438–1451. ISSN: 1522-2594. DOI: https://doi.org/10.1002/mrm.27832.

[71] M. Weigel, S. Schwenk, V. G. Kiselev, K. Scheffler, and J. Hennig. "Extended phase graphs with anisotropic diffusion." In: *Journal of Magnetic Resonance (San Diego, Calif.: 1997)* 205.2 (Aug. 2010), pp. 276–285. ISSN: 1096-0856. DOI: 10.1016/j.jmr.2010.05.011.

[72] Matthias Weigel. "Extended phase graphs: dephasing, RF pulses, and echoes - pure and simple." In: *Journal of magnetic resonance imaging: JMRI* 41.2 (Feb. 2015), pp. 266–295. ISSN: 1522-2586. DOI: 10.1002/jmri.24619.

[73] Katherine L. Wright, Jesse I. Hamilton, Mark A. Griswold, Vikas Gulani, and Nicole Seiberlich. "Non-Cartesian Parallel Imaging Reconstruction." In: *Journal of magnetic resonance imaging : JMRI* 40.5 (Nov. 2014), pp. 1022–1040. ISSN: 1053-1807. DOI: 10.1002/jmri.24521.

[74] Jesse Hamilton, Dominique Franson, and Nicole Seiberlich. "Recent advances in parallel imaging for MRI." In: *Progress in Nuclear Magnetic Resonance Spectroscopy* 101 (Aug. 2017), pp. 71–95. ISSN: 1873-3301. DOI: 10.1016/j.pnmrs.2017.04.002.

[75] Michael Lustig, David Donoho, and John M. Pauly. "Sparse MRI: The application of compressed sensing for rapid MR imaging." In: *Magnetic Resonance in Medicine* 58.6 (2007), pp. 1182–1195. ISSN: 1522-2594. DOI: https://doi.org/10.1002/mrm.21391.

[76] J.A. Fessler and B.P. Sutton. "Nonuniform fast Fourier transforms using min-max interpolation." In: *IEEE Transactions on Signal Processing* 51.2 (Feb. 2003), pp. 560–574. ISSN: 1941-0476. DOI: 10.1109/TSP.2002.807005.

[77] Florian Knoll, Andreas Schwarzl, Clemens Diwoky, and Daniel K. Sodickson. "gpuNUFFT – An Open-Source GPU Library for 3D Gridding with Direct Matlab Interface." In: *Proceedings of the 22th Annual Meeting of International Society for Magnetic Resonance in Medicine (ISMRM)*. Milan, Italy, 2014.

[78] Martin Blaimer, Felix Breuer, Matthias Mueller, Robin M. Heidemann, Mark A. Griswold, and Peter M. Jakob. "SMASH, SENSE, PILS, GRAPPA: how to choose the optimal method." In: *Topics in magnetic resonance imaging: TMRI* 15.4 (Aug. 2004), pp. 223–236. ISSN: 0899-3459. DOI: 10.1097/01.rmr.0000136558.09801.dd.

[79] Oren N. Jaspan, Roman Fleysher, and Michael L. Lipton. "Compressed sensing MRI: a review of the clinical literature." In: *The British Journal of Radiology* 88.1056 (2015), p. 20150487. ISSN: 1748-880X. DOI: 10.1259/bjr.20150487.

[80] Ge Wang, Jong Chu Ye, Klaus Mueller, and Jeffrey A. Fessler. "Image Reconstruction is a New Frontier of Machine Learning." In: *IEEE Transactions on Medical Imaging* 37.6 (June 2018), pp. 1289–1296. ISSN: 1558-254X. DOI: 10.1109/TMI.2018.2833635.

[81] Javier Montalt-Tordera, Vivek Muthurangu, Andreas Hauptmann, and Jennifer Anne Steeden. "Machine learning in Magnetic Resonance Imaging: Image reconstruction." In: *Physica medica: PM: an international journal devoted to the applications of physics to medicine and biology: official journal of the Italian Association of Biomedical Physics (AIFB)* 83 (Mar. 2021), pp. 79–87. ISSN: 1724-191X. DOI: 10.1016/j.ejmp.2021.02.020.

[82] Y. Han, L. Sunwoo, and J. C. Ye. "k -Space Deep Learning for Accelerated MRI." In: *IEEE Transactions on Medical Imaging* 39.2 (Feb. 2020), pp. 377–386. ISSN: 1558-254X. DOI: 10.1109/TMI.2019.2927101.

[83] D. Lee, J. Yoo, S. Tak, and J. C. Ye. "Deep Residual Learning for Accelerated MRI Using Magnitude and Phase Networks." In: *IEEE Transactions on Biomedical Engineering* 65.9 (Sept. 2018), pp. 1985–1995. ISSN: 1558-2531. DOI: 10.1109/TBME.2018.2821699.

[84] Yoseob Han, Jaejun Yoo, Hak Hee Kim, Hee Jung Shin, Kyunghyun Sung, and Jong Chul Ye. "Deep learning with domain adaptation for accelerated projection-reconstruction MR." In: *Magnetic Resonance in Medicine* 80.3 (2018), pp. 1189–1205. ISSN: 1522-2594. DOI: https://doi.org/10.1002/mrm.27106.

[85] Jo Schlemper, Jose Caballero, Joseph V. Hajnal, Anthony N. Price, and Daniel Rueckert. "A Deep Cascade of Convolutional Neural Networks for Dynamic MR Image Reconstruction." In: *IEEE Transactions on Medical Imaging* 37.2 (Feb. 2018), pp. 491–503. ISSN: 1558-254X. DOI: 10.1109/TMI.2017.2760978.

[86] Kerstin Hammernik, Teresa Klatzer, Erich Kobler, Michael P. Recht, Daniel K. Sodickson, Thomas Pock, and Florian Knoll. "Learning a variational network for reconstruction of accelerated MRI data." In: *Magnetic Resonance in Medicine* 79.6 (2018), pp. 3055–3071. ISSN: 1522-2594. DOI: https://doi.org/10.1002/mrm.26977.

[87] Bo Zhu, Jeremiah Z. Liu, Stephen F. Cauley, Bruce R. Rosen, and Matthew S. Rosen. "Image reconstruction by domain-transform manifold learning." In: *Nature* 555.7697 (Mar. 2018), pp. 487–492. ISSN: 1476-4687. DOI: 10.1038/nature25988.

[88] S.G. Mallat and Zhifeng Zhang. "Matching pursuits with time-frequency dictionaries." In: *IEEE Transactions on Signal Processing* 41.12 (Dec. 1993), pp. 3397–3415. ISSN: 1941-0476. DOI: 10.1109/78.258082.

[89] Debra F. McGivney, Eric Pierre, Dan Ma, and et. al. "SVD compression for magnetic resonance fingerprinting in the time domain." In: *IEEE TMI* 33 (Dec. 2014), pp. 2311–2322. DOI: 10.1109/TMI.2014.2337321.

[90] Mingrui Yang, Dan Ma, Yun Jiang, Jesse Hamilton, Nicole Seiberlich, Mark A. Griswold, and Debra McGivney. "Low rank approximation methods for MR fingerprinting with large scale dictionaries." In: *Magnetic Resonance in Medicine* 79.4 (Apr. 2018), pp. 2392–2400. ISSN: 1522-2594. DOI: 10.1002/mrm.26867.

[91] Jesse I. Hamilton and Nicole Seiberlich. "Machine Learning for Rapid Magnetic Resonance Fingerprinting Tissue Property Quantification." In: *Proceedings of the IEEE* 108.1 (Jan. 2020), pp. 69–85. ISSN: 1558-2256. DOI: 10.1109/JPROC.2019.2936998.

[92] Elisabeth Hoppe, Gregor Körzdörfer, Tobias Würfl, Jens Wetzl, Felix Lugauer, Josef Pfeuffer, and Andreas Maier. "Deep Learning for Magnetic Resonance Fingerprinting: A New Approach for Predicting Quantitative Parameter Values from Time Series." In: *Studies in Health Technology and Informatics* 243 (2017), pp. 202–206. ISSN: 0926-9630.

[93] Patrick Virtue, Stella X. Yu, and Michael Lustig. "Better than real: Complex-valued neural nets for MRI fingerprinting." In: IEEE, Sept. 2017, pp. 3953–3957. ISBN: 978-1-5090-2175-8. DOI: 10.1109/ICIP.2017.8297024.

[94] Ouri Cohen, Bo Zhu, and Matthew S. Rosen. "MR fingerprinting Deep RecOnstruction NEtwork (DRONE)." In: *Magnetic Resonance in Medicine* 80.3 (2018), pp. 885–894. ISSN: 1522-2594. DOI: 10.1002/mrm.27198.

[95] Mohammad Golbabaee, Dongdong Chen, Pedro A. Gómez, Marion I. Menzel, and Mike E. Davies. "Geometry of Deep Learning for Magnetic Resonance Fingerprinting." In: *ICASSP 2019 - 2019 IEEE International Conference on Acoustics, Speech and Signal Processing (ICASSP)*. May 2019, pp. 7825–7829. DOI: 10.1109/ICASSP.2019.8683549.

[96] Fabian Balsiger, Olivier Scheidegger, Pierre G. Carlier, Benjamin Marty, and Mauricio Reyes. "On the Spatial and Temporal Influence for the Reconstruction of Magnetic Resonance Fingerprinting." In: *Proceedings of The 2nd International Conference on Medical Imaging with Deep Learning*. Ed. by M. Jorge Cardoso, Aasa Feragen, Ben Glocker, Ender Konukoglu, Ipek Oguz, Gozde Unal, and Tom Vercauteren. Vol. 102. Proceedings of Machine Learning Research. London, United Kingdom: PMLR, July 2019, pp. 27–38.

[97] Z. Fang, Y. Chen, M. Liu, L. Xiang, Q. Zhang, Q. Wang, W. Lin, and D. Shen. "Deep Learning for Fast and Spatially-Constrained Tissue Quantification from Highly-Accelerated Data in Magnetic Resonance Fingerprinting." In: *IEEE Transactions on Medical Imaging* (2019), pp. 1–1. ISSN: 0278-0062. DOI: 10.1109/TMI.2019.2899328.

[98] M. Raissi, P. Perdikaris, and G. E. Karniadakis. "Physics-informed neural networks: A deep learning framework for solving forward and inverse problems involving nonlinear partial differential equations." In: *Journal of Computational Physics* 378 (Feb. 2019), pp. 686–707. ISSN: 0021-9991. DOI: 10.1016/j.jcp.2018.10.045.

[99] Ida Blystad, J. B. Marcel Warntjes, Örjan Smedby, Peter Lundberg, Elna-Marie Larsson, and Anders Tisell. "Quantitative MRI for analysis of peritumoral edema in malignant gliomas." In: *PLOS ONE* 12.5 (May 2017), e0177135. ISSN: 1932-6203. DOI: 10.1371/journal.pone.0177135.

[100] Akifumi Hagiwara, Marcel Warntjes, Masaaki Hori, Christina Andica, Misaki Nakazawa, Kanako Kunishima Kumamaru, Osamu Abe, and Shigeki Aoki. "SyMRI of the Brain: Rapid Quantification of Relaxation Rates and Proton Density, With Synthetic MRI, Automatic Brain Segmentation, and Myelin Measurement." In: *Investigative Radiology* 52.10 (Oct. 2017), pp. 647–657. ISSN: 1536-0210. DOI: 10.1097/RLI.0000000000000365.

[101] Sooyeon Ji, Dongjin Yang, Jongho Lee, Seung Hong Choi, Hyeonjin Kim, and Koung Mi Kang. "Synthetic MRI: Technologies and Applications in Neuroradiology." In: *Journal of Magnetic Resonance Imaging* n/a.n/a (2021). ISSN: 1522-2586. DOI: https://doi.org/10.1002/jmri.27440.

[102] Bhairav Bipin Mehta, Simone Coppo, Debra Frances McGivney, Jesse Ian Hamilton, Yong Chen, Yun Jiang, Dan Ma, Nicole Seiberlich, Vikas Gulani, and Mark Alan Griswold. "Magnetic resonance fingerprinting: a technical review." In: *Magnetic Resonance in Medicine* 81.1 (2019), pp. 25–46. ISSN: 1522-2594. DOI: https://doi.org/10.1002/mrm.27403.

[103] Yun Jiang, Dan Ma, Katharine L. Wright, Nicole Seiberlich, Vikas Gulani, and Mark A. Griswold. "Simultaneous T1, T2, Diffusion and Proton Density Quantification with MR Fingerprinting." In: *Proceedings of the 22nd Annual Meeting of International Society for Magnetic Resonance in Medicine (ISMRM)*. Milan, Italy, 2014.

[104] Yun Jiang, Jesse Ian Hamilton, Katharine L. Wright, Dan Ma, Nicole Seiberlich, Vikas Gulani, and Mark A. Griswold. "Simultaneous Quantification of T1, T2 and Diffusion with Diffusion-weighted drive-equilibrium prepared Magnetic Resonance Fin-

gerprinting." In: *Proceedings of the 24th Annual Meeting of International Society for Magnetic Resonance in Medicine (ISMRM)*. Singapore, 2016.

[105] Yun Jiang, Jesse Ian Hamilton, Wei-Ching Lo, Katharine L. Wright, Dan Ma, Andrew J. Coristine, Nicole Seiberlich, Vikas Gulani, and Mark A. Griswold. "Simultaneous T1, T2 and Diffusion Quantification using Multiple Contrast Prepared Magnetic Resonance Fingerprinting." In: *Proceedings of the 25th Annual Meeting of International Society for Magnetic Resonance in Medicine (ISMRM)*. Honolulu, HI, USA, 2017.

[106] Benedikt Rieger, Mehmet Akçakaya, Lothar Schad, and Sebastian Weingärtner. "Simultaneous quantification of T1, T2 and Apparent Diffusion Coefficient using Magnetic Resonance Fingerprinting based on Echo Planar Imaging." In: *Proceedings of the 26th Annual Meeting of International Society for Magnetic Resonance in Medicine (ISMRM)*. Paris, France, 2018.

[107] Sen Ma, Christopher T. Nguyen, Fei Han, Nan Wang, Zixin Deng, Nader Binesh, Franklin G. Moser, Anthony G. Christodoulou, and Debiao Li. "Three-dimensional simultaneous brain T1, T2, and ADC mapping with MR Multitasking." In: *Magnetic Resonance in Medicine* 84.1 (2020), pp. 72–88. ISSN: 1522-2594. DOI: https://doi.org/10.1002/mrm.28092.

[108] F. Godenschweger, U. Kägebein, D. Stucht, U. Yarach, A. Sciarra, R. Yakupov, F. Lüsebrink, P. Schulze, and O. Speck. "Motion correction in MRI of the brain." In: *Physics in Medicine and Biology* 61.5 (Mar. 2016), R32–56. ISSN: 1361-6560. DOI: 10.1088/0031-9155/61/5/R32.

[109] Bhairav Bipin Mehta, Dan Ma, Eric Yann Pierre, Yun Jiang, Simone Coppo, and Mark Alan Griswold. "Image reconstruction algorithm for motion insensitive MR Fingerprinting (MRF): MORF." In: *Magnetic Resonance in Medicine* 80.6 (2018), pp. 2485–2500. ISSN: 1522-2594. DOI: https://doi.org/10.1002/mrm.27227.

[110] Gastão Cruz, Olivier Jaubert, Torben Schneider, Rene M. Botnar, and Claudia Prieto. "Rigid motion-corrected magnetic resonance fingerprinting." In: *Magnetic Resonance in Medicine* 81.2 (2019), pp. 947–961. ISSN: 1522-2594. DOI: https://doi.org/10.1002/mrm.27448.

[111] Zhongbiao Xu, Huihui Ye, Mengye Lyu, Hongjian He, Jianhui Zhong, Yingjie Mei, Zhifeng Chen, Ed X. Wu, Wufan Chen, Qianjin Feng, et al. "Rigid motion correction for magnetic resonance fingerprinting with sliding-window reconstruction and image registration." In: *Magnetic Resonance Imaging* 57 (Apr. 2019), pp. 303–312. ISSN: 0730-725X. DOI: 10.1016/j.mri.2018.11.001.

[112] Jan W. Kurzawski, Matteo Cencini, Luca Peretti, Pedro A. Gómez, Rolf F. Schulte, Graziella Donatelli, Mirco Cosottini, Paolo Cecchi, Mauro Costagli, Alessandra Retico, et al. "Retrospective rigid motion correction of three-dimensional magnetic resonance fingerprinting of the human brain." In: *Magnetic Resonance in Medicine* 84.5 (2020), pp. 2606–2615. ISSN: 1522-2594. DOI: https://doi.org/10.1002/mrm.28301.

[113] Refik Soyak, Ebru Navruz, Eda Ozgu Ersoy, Gastao Cruz, Claudia Prieto, Andrew P. King, Devrim Unay, and Ilkay Oksuz. "Channel Attention Networks for Robust MR Fingerprinting Matching." In: *arXiv:2012.01241 [cs, eess]* (Dec. 2020).

[114] Hongli Fan, Pan Su, Judy Huang, Peiying Liu, and Hanzhang Lu. "Multi-band MR fingerprinting (MRF) ASL imaging using artificial-neural-network trained with high-fidelity experimental data." In: *Magnetic Resonance in Medicine* 85.4 (2021), pp. 1974–1985. ISSN: 1522-2594. DOI: https://doi.org/10.1002/mrm.28560.

[115] Maxim Zaitsev, Julian. Maclaren, and Michael Herbst. "Motion Artefacts in MRI: a Complex Problem with Many Partial Solutions." In: *Journal of magnetic resonance imaging : JMRI* 42.4 (Oct. 2015), pp. 887–901. ISSN: 1053-1807. DOI: 10.1002/jmri.24850.

[116] Hayit Greenspan, Bram van Ginneken, and Ronald M. Summers. "Guest Editorial Deep Learning in Medical Imaging: Overview and Future Promise of an Exciting New Technique." In: *IEEE Transactions on Medical Imaging* 35.5 (May 2016), pp. 1153–1159. ISSN: 1558-254X. DOI: 10.1109/TMI.2016.2553401.

[117] Mojtaba F. Fathi, Isaac Perez-Raya, Ahmadreza Baghaie, Philipp Berg, Gabor Janiga, Amirhossein Arzani, and Roshan M. D'Souza. "Super-resolution and denoising of 4D-Flow MRI using physics-Informed deep neural nets." In: *Computer Methods and Programs in Biomedicine* 197 (Dec. 2020), p. 105729. ISSN: 1872-7565. DOI: 10.1016/j.cmpb.2020.105729.

[118] Tomer Weiss, Ortal Senouf, Sanketh Vedula, Oleg Michailovich, Michael Zibulevsky, and Alex Bronstein. "PILOT: Physics-Informed Learned Optimized Trajectories for Accelerated MRI." In: *MELBA* (Apr. 2021), pp. 1–23.

[119] A. Loktyushin, K. Herz, N. Dang, F. Glang, A. Deshmane, S. Weinmüller, A. Doerfler, B. Schölkopf, K. Scheffler, and M. Zaiss. "MRzero - Automated discovery of MRI sequences using supervised learning." In: *Magnetic Resonance in Medicine* 86.2 (Aug. 2021), pp. 709–724. ISSN: 0740-3194. DOI: 10.1002/mrm.28727.

[120] Shanshan Wang, Huitao Cheng, Leslie Ying, Taohui Xiao, Ziwen Ke, Hairong Zheng, and Dong Liang. "DeepcomplexMRI: Exploiting deep residual network for fast parallel MR imaging with complex convolution." In: *Magnetic Resonance Imaging* 68 (May 2020), pp. 136–147. ISSN: 1873-5894. DOI: 10.1016/j.mri.2020.02.002.

[121] Alexander Selvikvåg Lundervold and Arvid Lundervold. "An overview of deep learning in medical imaging focusing on MRI." In: *Zeitschrift für Medizinische Physik*. Special Issue: Deep Learning in Medical Physics 29.2 (May 2019), pp. 102–127. ISSN: 0939-3889. DOI: 10.1016/j.zemedi.2018.11.002.

[122] Sean C. L. Deoni, Brian K. Rutt, Tarunya Arun, and et. al. "Gleaning multicomponent T1 and T2 information from steady-state imaging data." In: *Magnetic Resonance in Medicine* 60.6 (Dec. 2008), pp. 1372–1387. ISSN: 1522-2594. DOI: 10.1002/mrm.21704.

[123] Sunli Tang, Carlos Fernandez-Granda, Sylvain Lannuzel, Brett Bernstein, Riccardo Lattanzi, Martijn Cloos, Florian Knoll, and Jakob Assländer. "Multicompartment magnetic resonance fingerprinting." In: *Inverse Problems* 34.9 (July 2018), p. 094005. ISSN: 0266-5611. DOI: 10.1088/1361-6420/aad1c3.

[124] Martijn Nagtegaal, Peter Koken, Thomas Amthor, and Mariya Doneva. "Fast multi-component analysis using a joint sparsity constraint for MR fingerprinting." In: *Magnetic Resonance in Medicine* 83.2 (2020), pp. 521–534. ISSN: 1522-2594. DOI: https://doi.org/10.1002/mrm.27947.

[125] Alice C. Yu, Chaitra Badve, Lee E. Ponsky, Shivani Pahwa, Sara Dastmalchian, Matthew Rogers, Yun Jiang, Seunghee Margevicius, Mark Schluchter, William Tabayoyong, et al. "Development of a Combined MR Fingerprinting and Diffusion Examination for Prostate Cancer." In: *Radiology* 283.3 (Feb. 2017), pp. 729–738. ISSN: 0033-8419. DOI: 10.1148/radiol.2017161599.

[126] Eva M. Serrao, Dimitri A. Kessler, Bruno Carmo, Lucian Beer, Kevin M. Brindle, Guido Buonincontri, Ferdia A. Gallagher, Fiona J. Gilbert, Edmund Godfrey, Martin J. Graves, et al. "Magnetic resonance fingerprinting of the pancreas at 1.5 T and 3.0 T." In: *Scientific Reports* 10.1 (Oct. 2020), p. 17563. ISSN: 2045-2322. DOI: 10.1038/s41598-020-74462-6.